**Automated Vehicle (AV) Deployment Across Scales:**

**From Production Vehicle Evaluation to Network Impacts and Control**

By

Yang Li

A dissertation submitted in partial fulfillment of

the requirements for the degree of

Doctor of Philosophy

(Civil and Environmental Engineering)

at the

UNIVERSITY OF WISCONSIN-MADISON

2026

Date of final oral examination: 05/01/2026

The dissertation is approved by the following members of the Final Examination Committee:

Xiaopeng (Shaw) Li, Professor, Civil and Environmental Engineering, UW-Madison
Soyoung (Sue) Ahn, Professor, Civil and Environmental Engineering, UW-Madison
Sikai (Sky) Chen, Assistant Professor, Mechanical Engineering, UW-Madison
Pei-Sung Lin, Center for Urban Transportation Research, University of South Florida

## DEDICATION

I dedicate this dissertation to my beloved husband, baby, parents, and sister, whose continuous love, support, and encouragement made this achievement possible. Without them, I could not have earned my Doctor of Philosophy degree.

## ACKNOWLEDGMENTS

I would like to express my deepest gratitude to my advisor, Professor Xiaopeng Li, for his guidance, support, and encouragement throughout my Ph.D. study. His high standards for research and strong passion for academic work have had a deep influence on me. He has taught me how to think critically, work carefully, and approach research problems with both rigor and creativity. I am truly grateful for his mentorship, which has made my Ph.D. journey a meaningful and rewarding experience.

I would also like to thank my dissertation committee members. I am sincerely grateful to Professor Sue Ahn for her valuable comments and suggestions on my paper and dissertation. Her feedback helped me improve the clarity and quality of my work. I am also deeply grateful to Professor Sikai Chen for his helpful advice and thoughtful suggestions, which helped me strengthen the academic quality of my research. I would like to thank Dr. Pei-Sung Lin for his valuable feedback, practical insights, and support during my dissertation process.

Finally, I am thankful to the Department of Civil and Environmental Engineering at the University of Wisconsin–Madison for providing a supportive academic environment. I also want to thank all members of the CATS Lab. I feel very fortunate to have worked with such a kind, talented, and supportive group of people. I will always cherish the discussions, collaboration, and time we shared over the past years.

## ABSTRACT

Despite rapid progress in market growth and supportive policy momentum, automated vehicle (AV) deployment still faces critical challenges across multiple scales, including uncertain technical readiness of production AVs, unclear network-level benefits, and limited strategies for active network-level control. This dissertation addresses these challenges through three interconnected studies that examine AV deployment across vehicle, network, and control scales.

The first part conducts an empirical evaluation of AV driving features in 6 production vehicles under diverse real-world conditions. The results reveal that the performance of these features is not uniformly reliable and depends strongly on sensing technology and driving environment. Camera-only features are sensitive to low visibility and unclear markings, while radar-based features remain more stable across lighting conditions. Recommendations are provided for vehicle manufacturers and infrastructure stakeholders to improve the performance of AV driving features.

The second part conducts a cross-network simulation study of 12 urban networks under pure AV and pure HV regimes, examining how 5 network features moderate AV impacts on operational, environmental, and surrogate safety performance. The results show that AV impacts vary systematically with network features rather than appearing uniformly. AV fuel benefits are stronger in high-demand, high-density, and highly signalized networks, while AV–HV surrogate safety differences are more favorable in longer, more continuous networks. These findings highlight the need for a network-aware perspective in AV deployment and evaluation.

The third part develops a macroscopic control framework that uses AVs as mobile controllers for network-level traffic management. An Area Transmission Model (ArTM) is proposed as a macroscopic extension of the Cell Transmission Model (CTM) based on the

macroscopic fundamental diagram (MFD), combined with a rolling-horizon optimal control strategy that provides area-level Variable Speed Advisories (VSAs). The framework is validated on 2 real-world urban networks in Madison and Boston, demonstrating improved network mobility and reduced energy consumption.

Together, these studies provide a multiscale perspective on AV deployment by linking vehicle capabilities, network conditions, and active control strategies in urban traffic systems.

**KEYWORDS**

Automated Vehicles,

Production Vehicle Evaluation,

Connected and Automated Driving Features,

Network Features,

Cross-Network Simulation;

Macroscopic Fundamental Diagram,

Area Transmission Model,

Variable Speed Advisory,

Network-Level Control.

# TABLE OF CONTENTS

# LIST OF TABLES

# LIST OF FIGURES

# 1 INTRODUCTION

## 1.1 Background

For many years, automated vehicles (AVs) were largely viewed as a future-oriented technology, with their widespread deployment often discussed as a long-term possibility. However, recent advances in sensing, computing, and vehicle automation have moved AVs closer to real-world applications and market adoption. The global AV market was worth approximately 68 billion dollars in 2024 and is projected to reach more than 214 billion dollars by 2030, growing at a compound annual rate of around 20 percent (Grand View Research, 2024). In the United States alone, AVs have driven more than 145 million miles on public roads as of May 2025, with Waymo completing over 250 thousand paid rides per week (AVIA, 2025; Waymo, 2025).

The policy side for AVs is moving at a similar pace. By 2024, more than thirty countries had published AV testing or deployment rules. UN Regulation No. 157, the first binding international AV regulation, has been adopted by over 50 countries since coming into force in 2021 (UNECE, 2021). In April 2025, the National Highway Traffic Safety Administration (NHTSA) released a new AV framework designed to remove barriers and enable deployment (NHTSA, 2025), and 26 U.S. states have now enacted AV deployment statutes, covering 56 percent of the U.S. population (AVIA, 2025). Together, the market, operations, and policy signals indicate that the AV era has begun.

Despite this rapid progress, the deployment of AVs faces critical challenges that span multiple scales, from individual vehicle capabilities to network-level traffic operations and active traffic control. Three challenges are particularly important and remain only partially addressed in existing literature.

The first challenge concerns the technical readiness of AV features/functions. Although manufacturers frequently report positive performance results, most of these evaluations are conducted in controlled environments such as closed tracks or limited test routes. The actual performance of those AV features in production vehicles, including adaptive cruise control, lane keeping, and traffic light detection, has not been systematically verified under diverse real-world conditions (Boggs et al., 2020). Existing studies often focus on isolated features or single vehicle models (J. Wang et al., 2020), leaving open the question of how production AVs perform across different vehicles, sensing modalities, and environmental conditions. Without this evidence, vehicle-level readiness for broader deployment remains uncertain.

The second challenge concerns the network-level impacts of AVs. Existing studies on AV impacts often focus on isolated corridors, single intersections, or homogeneous network settings (Mahdinia et al., 2021; Stogios et al., 2019), making it difficult to generalize the findings across different urban environments. AV performance depends not only on the vehicle itself but also on the network in which it operates, including demand levels, road geometry, intersection density, signalization, and connectivity. Whether AV benefits are consistent across networks, and which network features amplify or dampen these benefits, remains insufficiently understood. This gap limits the ability to provide network-aware AV deployment guidance.

The third challenge concerns the active use of AVs in network-level traffic control. Most existing studies treat AVs as passive participants in traffic, focusing on how they respond to surrounding vehicles or follow predefined behaviors (Talebpour & Mahmassani, 2016). The potential of AVs to actively shape network-level traffic flow, by leveraging their communication and control capabilities, has received comparatively less attention. Although several studies have explored AV-based control at the corridor level or for specific bottlenecks (M. Wang et al., 2015),

scalable control frameworks that operate at the network level remain limited. As a result, the path from passive AV operation to active network-level AV control is not yet well established.

Taken together, these three challenges show that AV deployment is not a single-scale problem. It spans vehicle-level readiness, network-level performance, and control-level intervention, and addressing it requires research that connects these scales rather than treating them in isolation. This motivates the present dissertation, which examines AV deployment across these three scales and aims to support more reliable evaluation and more targeted deployment of AVs in real-world urban systems.

## 1.2 Research Objectives and Scope of Work

Given the critical challenges identified above, this dissertation aims to support the reliable evaluation and deployment of AVs across vehicles, network, and control scales. Three specific research objectives are pursued:

(i) Empirically evaluate the real-world performance of AV driving features in production vehicles through field tests under diverse driving conditions.

(ii) Analyze how network features shape AV impacts through a cross-network simulation study, providing a network-aware perspective for AV deployment.

(iii) Develop a macroscopic control framework that uses AVs as mobile controllers to actively improve network-level traffic performance.

The scope of this dissertation is focused on urban road networks. Vehicle-level evaluation is limited to production AVs currently available on the consumer market, while network-level and control-level studies are conducted through simulation rather than field deployment. In this dissertation, connected and automated vehicles (CAVs) are treated as a subcategory of AVs, referring to AVs equipped with connectivity capabilities that enable information exchange with

other vehicles, infrastructure, or traffic management systems. Therefore, the terms AV and CAV are sometimes used interchangeably when the discussion broadly concerns AV deployment, while CAV is used more specifically in contexts where connectivity is essential to the proposed control framework.

## 1.3 Contributions

Through this dissertation, the following contributions are made:

(i) An empirical evaluation framework is developed and applied to production vehicles from 6 major brands, covering 6 AV driving features. The evaluation identifies key environmental and operational factors that affect AV driving features performance under real-world driving conditions, providing practical insights for vehicle manufacturers and government agencies responsible for infrastructure planning and development.

(ii) A reproducible cross-network simulation framework is established across 12 urban networks. This framework identifies how 5 network features moderate the impacts of AVs on operational, environmental, and surrogate safety performance, and translates these findings into a network-aware perspective for AV deployment.

(iii) An Area Transmission Model (ArTM) is proposed as a macroscopic extension of the Cell Transmission Model (CTM), grounded in the macroscopic fundamental diagram (MFD). The model is integrated with a rolling-horizon optimal control strategy that uses AVs as mobile controllers through area-level Variable Speed Advisories (VSAs) to jointly minimize travel delay and energy consumption. The proposed ArTM-VSA framework is validated on two real-world urban networks, Madison and Boston, demonstrating its scalability and effectiveness for city-level urban traffic management.

## 1.4 Dissertation Overview

This dissertation is organized as follows. Chapter 2 reviews the relevant studies on AV technical readiness, network-level impacts of AVs, and urban mobility applications enabled by AVs. Chapter 3 presents an empirical evaluation of AV driving features in production vehicles under real-world driving conditions. Chapter 4 conducts a cross-network simulation analysis to examine how network features shape AV impacts across diverse urban networks. Chapter 5 develops a macroscopic control framework that uses AVs as mobile controllers to actively improve network-level traffic performance through area-level VSAs. Chapter 6 concludes the dissertation and discusses directions for future research.

# 2 LITERATURE REVIEW

## 2.1 Technical Readiness

AV driving features offer substantial advantages and hold the potential to fundamentally reshape transportation systems and societal norms. Common AV driving features available in production vehicles can be broadly categorized into the following types: Adaptive Cruise Control (ACC), Lane Markings Detection, Static Message Sign Detection, Traffic Light Awareness, and Full Self-Driving (FSD)(Jia et al., 2022; Z. Li, Bao, et al., 2025; Pillai et al., 2023; Sun et al., 2022; Q. Wang et al., 2022; L. Yu & Wang, 2022; Zhao et al., 2019). These technologies promise a range of benefits, including enhanced road safety (Trubia et al., 2017), improved traffic flow and congestion management (T. Zhang & Gao, 2020), reduced emissions through more efficient driving patterns (Miller & Heard, 2016), increased mobility for individuals unable to drive due to age or disability (Harper et al., 2016), and more efficient use of urban infrastructure and spaces (Fayyaz et al., 2022).

Although an increasing number of production vehicles now come equipped with AV driving features, their performance in the real-world environment remains insufficiently validated. Manufacturers often claim that these features can reliably function across a wide range of scenarios, including heavy traffic, poor weather, and complex road geometries. However, reports from researchers and transportation agencies have highlighted notable limitations under such scenarios. For example, studies have shown that ACC systems can contribute to traffic congestion due to string instability (Shi & Li, 2021a) and may also struggle to detect cut-in vehicles promptly (Chen et al., 2021), often reacting with a delay that reflects unreliable performance in dynamic traffic environments. Additional evaluations, such as those from the Federal Highway Administration (FHWA), reveal that ACC performance significantly degrades in adverse weather, such as rain,

snow, fog, or road spray, resulting in unexpected disengagements (Neumeister & Pape, 2019), and may cause side-impact crashes (Ding et al., 2025). Recently, Dongchedi conducted safety tests on 36 vehicle models equipped with AV driving features. The test scenarios included highway situations such as lead vehicles suddenly disappearing, temporary road construction, and wild boar crossing, as well as typical urban driving risks like avoiding a broken-down vehicle and a child suddenly running across the road. The results indicate that current mainstream intelligent driving assistance systems still struggle to effectively handle complex and high-risk traffic scenarios, particularly under extreme highway conditions and in situations involving the sudden crossing of children (Dongchedi, 2025).

One potential reason for this performance gap is that manufacturer-led testing is typically conducted in controlled environments, such as closed tracks or simulators, where variables are limited. In contrast, real-world driving presents a wide range of unpredictable challenges, including sensor impairment from adverse weather, deteriorated road infrastructure, and erratic human behavior of other transportation entities. These complexities make it significantly more challenging to ensure the consistent and reliable operation of AV driving features. Therefore, it is essential to evaluate the environmental adaptability of these AV driving features and identify the factors that influence their performance. Gaining such insights can help stakeholders, including vehicle manufacturers and transportation agencies, refine vehicle technologies and guide infrastructure improvements, ultimately supporting the safer and more effective deployment of connected and automated driving systems.

Although some research has addressed the infrastructural implications of AV driving features adoption, many of these studies base their recommendations on policy analysis (American Planning Association, 2024; Saeed et al., 2021; Tafidis et al., 2021; Y. Wang et al., 2025),

stakeholder surveys (Federal Highway Administration, 2021; McDonald & Rodier, 2015; Nitsche et al., 2014; Tengilimoglu et al., 2023; P. Wang et al., 2022), or literature reviews (Hallmark et al., 2019; Khoury et al., 2019; Liu et al., 2019; Manivasakan et al., 2021; Othman, 2021), rather than on empirical testing of AV driving features in production vehicles. As a result, the recommendations emerging from these studies may not accurately reflect the functional realities or limitations of existing systems. Without validation through real-world testing, proposed infrastructure improvements risk being misaligned with the actual needs of current vehicles, thereby reducing their practical value and effectiveness.

## 2.2 Network Feature Impact

In urban traffic systems, network features, including both structural and operating features, systematically shape network-level operational efficiency, environmental performance, and exposure to traffic conflicts. On the structural side, network connectivity and topology (Choi & Ewing, 2021; Marshall & Garrick, 2011; Wong et al., 2021), road and intersection density (Loder et al., 2019; Taillanter et al., 2024; S. Wang et al., 2020), the spatial distribution and control intensity of signalized intersections (Akandwanaho & Nakamura, 2020a; Ardekani et al., 1992), and network scale (Choi & Ewing, 2021; Loder et al., 2019; Zlatkovic et al., 2019) all exert systematic effects on network-level travel speeds and delay, and further shape the spatial propagation and diffusion patterns of congestion (Akandwanaho & Nakamura, 2020a; Ardekani et al., 1992; Wong et al., 2021; Zlatkovic et al., 2019); road network density additionally influences travel distance and detour behavior (S. Wang et al., 2020). On the operating side, traffic demand levels and loading conditions determine the operating environment under which these structural features function, thereby moderating network-level performance in speed, delay, and congestion propagation (Daganzo & Geroliminis, 2008; Loder et al., 2019; Taillanter et al., 2024).

Mechanistically, higher connectivity and redundant path options enable detouring and flow redistribution (Allen et al., 2024); density and scale shape the distribution and disturbance intensity of bottlenecks (Daganzo & Geroliminis, 2008; He & Zeng, 2024); and signal control intensity and coordination level modulate efficiency through stop-and-go cycles, queue spillback, and spatial heterogeneity (L. Zhang et al., 2013).

This line of research has converged on a relatively consistent evidence base. Empirical and analytical/theoretical work, including studies within the MFD framework, has quantified the sensitivity of efficiency and congestion propagation to network structure and loading conditions (Ardekani et al., 1992; Daganzo & Geroliminis, 2008; Loder et al., 2019), while microscopic and network simulation studies have varied topology, density, and signal control under controlled conditions to test the impact of these variations on network operations across demand levels (Essamlali et al., 2025; Wong et al., 2021; Zlatkovic et al., 2019). Together, these studies indicate that connectivity, density, signal control intensity, network scale, and the demand conditions that interact with them systematically shape speed, delay, congestion propagation, and, in some cases, broader network-level efficiency and safety outcomes (Loder et al., 2019; Marshall & Garrick, 2011; Wong et al., 2021; Zlatkovic et al., 2019). This body of work establishes the methodological and conceptual foundation for cross-city and cross-scale comparisons of feature–performance relationships.

However, most of the above feature–performance relationships have been established under a behavioral regime dominated by human-driven vehicles (HVs) (Taillanter et al., 2024). As autonomous vehicles (AVs) and AV–HV mixed traffic gradually emerge, the longitudinal car-following, acceleration/deceleration response, and interaction with traffic signals of vehicles may all undergo systematic changes (Hu et al., 2023; Le et al., 2015; Z. Li, Bao, et al., 2025; Rosca et

al., 2025; Shi & Li, 2021b; Y. Wang et al., 2023). Importantly, these behavioral differences do not act uniformly across all performance dimensions: recent simulation studies have shown that AV-related improvements in operational efficiency and emissions do not necessarily coincide with reductions in conflict risk (Morando et al., 2018; Papadoulis et al., 2019). Consequently, the effect of a given network feature under the AV regime may differ from that under the HV regime in magnitude, shape, and in some cases direction.

In terms of behavioral representation in simulation, existing AV studies still represent AV–HV behavioral differences relatively coarsely. When incorporating AVs into microscopic simulation, researchers typically calibrate a single set of car-following parameters for each vehicle class based on empirical data or the literature (Hu et al., 2023; Q. Lu et al., 2020; Morando et al., 2018; Sadid & Antoniou, 2024; Shi & Li, 2021b), and apply the same parameter set uniformly to both road segments and intersections. Yet empirical studies indicate that AV–HV behavioral differences take distinct forms in steady-state car-following on road segments (Hu et al., 2023) and in signal interactions near intersections, and behavior at intersections may further vary across different turning movements (Y. Wang et al., 2023); the growing availability of AV and HV signal/sign interaction trajectory data has also opened the door to more granular behavioral characterization (Z. Li, Bao, et al., 2025; Z. Li, Zhang, et al., 2025). Applying a single car-following parameter set across segments and intersections cannot capture these differences, and may lead to under- or over-estimation of AV impacts in network-level evaluations. How to more granularly represent AV–HV differences at the vehicle–signal interaction level within microscopic simulation, therefore, remains an open question.

In terms of study scope, existing AV research rarely compares feature–performance relationships directly across the HV and AV regimes. Most AV studies have instead focused on

vehicle-level behavior itself or on scenario-specific or aggregate performance gains: at the vehicle level, researchers study AV car-following characteristics and modeling (Hu et al., 2023; Shi & Li, 2021b); at the system level, studies examine aggregate efficiency under different AV market penetration rates (Q. Lu et al., 2020; Rosca et al., 2025), or evaluate specific control strategies for mixed traffic (Lin et al., 2023; S. Wang et al., 2023). Even in studies that report HV and AV performance separately within the same simulation setting (Q. Lu et al., 2020; Morando et al., 2018; Sadid & Antoniou, 2024), the reporting typically focuses on whether AVs perform better or worse overall, with few studies going further to directly compare how the magnitude, or direction, of network-feature effects changes between AV and HV under the same network and demand. Moreover, these AV simulation studies are largely confined to a single urban network or a typical corridor, limiting the generalization of how network features moderate AV impacts across network types. As a result, whether AVs simply replicate the HV feature–performance relationships, or instead lead to substantive changes on specific network features, remains an open question.

## 2.3 Urban Mobility Applications

Urban traffic congestion has become a persistent and growing challenge for cities worldwide, resulting in substantial increases in travel time, energy consumption, and pollutant emissions (Desai et al., 2023; González-Aliste et al., 2023; J. Lu et al., 2021; M. Zhang et al., 2023). Meanwhile, the rapid development of CAVs is expected to fundamentally reshape urban transportation systems, offering new opportunities for mitigating congestion and improving network efficiency (Rahman & Thill, 2023; Ramezani & Ye, 2019; Seuwou et al., 2020). By enabling vehicle-to-vehicle and vehicle-to-infrastructure communication, CAVs allow traffic flows to be coordinated at a level of precision not achievable with HVs, facilitating more effective routing, speed regulation, and utilization of roadway capacity. When strategically deployed and

controlled, CAVs have the potential to move beyond passive participation in traffic and serve as active mobile traffic control agents, supporting more efficient and sustainable urban traffic management systems.

When CAVs are leveraged as mobile traffic controllers, existing studies can be broadly classified into microscopic and macroscopic control perspectives. Microscopic control approaches explicitly model individual vehicle dynamics and kinematics while incorporating detailed network information, such as road geometry, lane configurations, and signal timing, to optimize vehicle trajectories and route choices. The majority of prior studies adopt this microscopic viewpoint ((Mirbakhsh et al., 2023; Wan et al., 2024; C. Yu et al., 2019)(Levin et al., 2017; Zhou et al., 2024; Zhu and Ukkusuri, 2015; Chen et al., 2022; )). For example, Wang et al. (2020) proposed a control strategy that addresses intersection conflict resolution, multi-objective optimization within road segments, and the management of heterogeneous decision-making behaviors. Then validated through simulation in a network consisting of 6 intersections. Chu et al. (2020) proposed a Dynamic Lane Reversal-Traffic Scheduling Management scheme to determine the optimal timetable and routes for CAVs. Qian et al. (2021) proposed a method for optimizing the departure times, routes, trajectories, and intersection signal timings for CAVs, aimed at minimizing the total travel time within the network. This method was validated within a network containing 26 intersections. While such approaches can capture fine-grained traffic interactions and provide high behavioral fidelity, their reliance on detailed modeling and high-dimensional state spaces often leads to substantial computational burdens. As a result, these methods are typically evaluated on small-scale networks with a limited number of intersections, which constrains their scalability and limits their applicability to large urban traffic networks.

In contrast to microscopic approaches, a growing body of research adopts a macroscopic control perspective for urban traffic management. Rather than modeling individual road segments or intersections in detail, these studies partition the urban network into aggregated regions and characterize traffic dynamics using area-wide average variables. Within this framework, the MFD has been introduced to describe the aggregate relationship between network vehicle accumulation (veh or veh/km) and network performance measures, such as production (veh·km) or circulating flow (veh/h), at the urban scale (Daganzo, 2005, 2007; Daganzo & Geroliminis, 2008).

The MFD provides a holistic understanding of urban traffic dynamics, enabling the development of more effective traffic management and planning strategies that consider the city-wide implications of traffic interventions. Some scholars have proposed perimeter control methods based on MFD (Aboudolas & Geroliminis, 2013; Geroliminis et al., 2013). The fundamental idea of this method is to divide a heterogeneous network into several homogeneous areas, and then implement perimeter control on the traffic flowing between the boundaries of these areas, to achieve the maximum overall throughput and to minimize congestion throughout the system (Aboudolas & Geroliminis, 2013). Kouvelas et al. (2017) divided an entire area into multiple areas and proposed a traffic transfer modeling method based on the MFD. This model describes the relationship between traffic transfers and traffic accumulation. Additionally, they introduced an adaptive optimization scheme for perimeter control in heterogeneous traffic networks. Simulation experiments in large urban networks demonstrated that the proposed scheme could achieve better congestion distribution, improve overall delays and outflow.

Scholars have also proposed various actuation methods based on perimeter control, including signal timing plans (De Jong et al., 2013; Hajiahmadi et al., 2013), proportional-integral control (Ingole et al., 2020), iterative learning control (Y. Ren et al., 2020), model-free adaptive control

driven by data strategies (Lei et al., 2020), and adaptive boundary feedback control (Haddad et al., 2021). The perimeter control has also been applied in emerging transportation areas (Yang et al., 2018). Despite its demonstrated effectiveness, this approach faces several practical challenges. For instance, assuming homogeneity within each region and applying control only at area boundaries may oversimplify localized traffic dynamics. This can lead to artificial boundary queues that distort the internal traffic states and reduce the method's effectiveness in real-world heterogeneous networks. In addition, the formation of boundary queues negatively affects the spatial homogeneity of the network, undermining the assumptions required for this method (Sirmatel & Yildirimoglu, 2023).

In addition to the perimeter control, speed control strategies are also common actuation methods, such as Variable Speed Limits (VSL) (Khondaker & Kattan, 2015). VSL can enhance traffic safety by homogenizing speeds (Abdel-Aty et al., 2006). Additionally, VSL can prevent or delay traffic disruptions by reducing or postponing the flow of vehicles toward potential active bottleneck locations (Hegyi et al., 2003). Sirmatel and Yildirimoglu (2023) proposed a variable speed control strategy that adjusts the average speed in the outer region to mitigate congestion in the inner region, assuming each region follows an MFD. While the approach offers useful insights, it is developed under simplifying assumptions, such as a two-region setup, homogeneous traffic conditions, and an accumulation-based MFD model. It also does not explicitly account for factors such as driver compliance with advised speeds or localized disturbances arising from on-street/off-street parking and access to local destinations, which may limit its applicability in more complex urban settings.

# 3 TECHNICAL READINESS EVALUATION

This chapter focuses on the vehicle level by empirically evaluating what current production AVs can actually do under real-world driving conditions. While manufacturers frequently report positive performance results, most of these evaluations are conducted in controlled environments such as closed tracks. The actual performance of connected and automated driving features (CADFs) in everyday driving conditions, therefore, remains largely unverified.

This chapter addresses that gap by empirically testing CADFs in 6 production vehicles, including Toyota, Hyundai, Ford, Audi, Honda, and Tesla. The evaluation covers key features such as ACC, Collision Avoidance Assist, Lane Markings Detection, Static Message Sign Detection, Traffic Light Awareness, and FSD, tested under diverse real-world conditions, including varying lighting and lane visibility. The results reveal substantial variability in performance across vehicles and scenarios, highlighting the influence of environmental and operational factors. Based on these findings, the chapter provides recommendations for automakers and public stakeholders to improve CADF reliability and supports future improvements in both vehicle technology and infrastructure.

The remainder of this chapter is organized as follows. Section 3.1 outlines the test vehicles, features, and scenarios, along with the test procedure and data collection methods. Section 3.2 presents the results of the tested CADFs and provides initial observations on performance patterns across vehicles and conditions. Section 3.3 offers recommendations for vehicle manufacturers and government authorities responsible for infrastructure development. Section 3.4 concludes the chapter and summarizes the key findings.

## 3.1 Test Method

### 3.1.1 Test Vehicles, Features and Scenarios

This study evaluates production vehicles from 6 of the most popular automotive brands in the United States, including the Toyota Corolla, Hyundai Santa Fe, Ford Bronco, Audi Q5, Honda Accord, and Tesla Model Y, each equipped with various CADFs designed to perceive and interact with environmental elements to support driving tasks. The selection of these 6 models was made to ensure representative coverage of major vehicle categories and technology maturity levels in the U.S. market. The Toyota Corolla and Honda Accord represent high-volume mid-size sedans that have remained among the nation's best-selling passenger cars for over a decade. The Hyundai Santa Fe and Ford Bronco capture the compact and mid-size SUV segments, which continue to dominate U.S. vehicle sales. The Audi Q5 represents the premium market, offering advanced driver-assistance features typical of luxury vehicles. Finally, the Tesla Model Y, the best-selling electric vehicle in the United States since 2022, exemplifies the growing prevalence of camera-based automation systems. Collectively, these models provide a representative snapshot of the technological diversity and market penetration of CADFs across today's U.S. vehicle fleet.

The test vehicles were sourced from rental services; therefore, it is important to note that some models may not include the full suite of CADFs offered by their respective manufacturers. The specific CADFs evaluated for each vehicle are detailed in TABLE 3.1. As shown in the table, Collision Avoidance and Lane Marking Detection are the most prevalent functions, indicating their maturity and standardization in current production vehicles. ACC and Static Message Sign Detection appear in several models, reflecting brand-specific implementations of advanced driver-assistance packages. In contrast, Traffic Light Awareness and FSD capabilities are limited to a few models, as they rely on specialized connectivity and high-level sensor-fusion algorithms that remain less widely adopted. To comprehensively assess performance, tests were conducted under a range of environmental conditions, including variations in lighting (daytime vs. nighttime), lane

marking visibility (clear vs. degraded), road geometry (straight vs. curved), and traffic sign readability (optimal vs. obstructed, faded, or dirty).

**TABLE 3.1 Test vehicles and features list.**

| Vehicle Features |  Toyota Corolla |  Hyundai Santa Fe |  Ford Bronco |  Audi Q5 |  Honda Accord |  Tesla Model Y |
|---|---|---|---|---|---|---|
| Adaptive Cruise Control | × | √ | × | √ | × | × |
| Collision Avoidance Assist | √ | √ | √ | √ | × | √ |
| Lane Markings Detection | √ | √ | √ | √ | √ | √ |
| Static Message Sign Detection | √ | × | × | × | √ | √ |
| Traffic Light Awareness | × | × | × | √ | × | √ |
| Full Self-driving | × | × | × | × | × | √ |

### 3.1.2 Test Procedure and Data Collection Methods

All tests were conducted in two locations, as shown in Figure 3.1: Tampa, Florida, one of the southernmost cities in the United States, and Madison, Wisconsin, one of the northernmost cities. During the evaluation process, a test driver operated each vehicle and repeated each scenario multiple times. Most vehicles were tested ten times per scenario. For vehicles that showed strong performance under adverse conditions, additional trials were conducted to verify consistency and identify any potential inaccuracies. During each test trial, an external observer was seated in the front passenger seat to directly monitor the vehicle dashboard and determine whether the tested feature was successfully activated. All tested CADFs provided in-vehicle notifications (visual and/or auditory) upon activation. For safety-related features such as collision avoidance, a trial was recorded as False if no activation message appeared within a safe distance before a potential conflict. For other perception-based features, such as static message sign detection, the observer recorded the detection distance once the feature was activated; if the vehicle passed the sign

without detection, the trial was recorded as False. Since all test vehicles were rentals, the study could not access internal system logs, as vehicle modifications were not permitted.

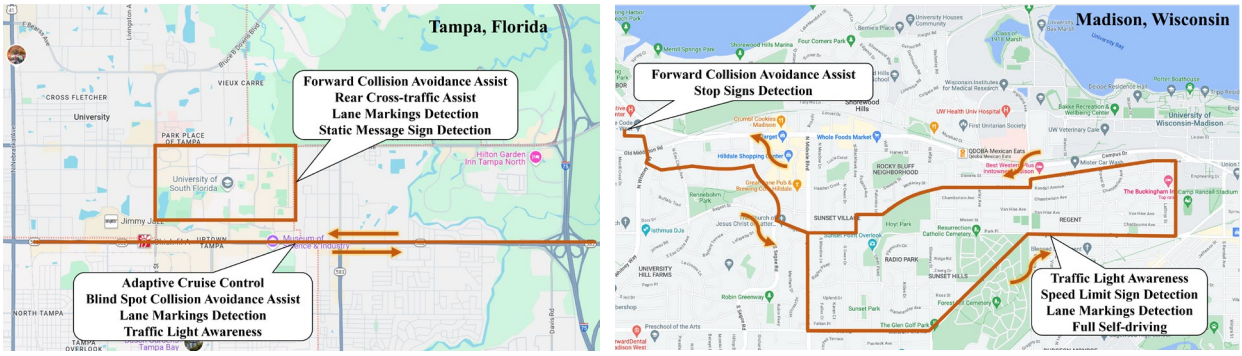


**Figure 3.1. Test locations.**

## 3.2 Test Results and Discussion

### 3.2.1 Adaptive Cruise Control (ACC)

The ACC system uses onboard sensors such as cameras or Radar to detect vehicles ahead, automatically adjusting acceleration and braking to maintain a safe following distance. This feature enhances driver comfort by reducing the need for constant manual input, improves traffic flow through more consistent speeds, increases road safety by helping to prevent rear-end collisions, and optimizes fuel efficiency through smoother vehicle operation.

ACC is one of the more advanced CADFs and is typically available only on premium production vehicles. Among the 6 vehicles tested in this study, only the Hyundai Santa Fe and Audi Q5 were equipped with ACC. Testing was conducted under both daytime and nighttime conditions. Figure 3.2 illustrates examples of the test vehicles following a lead vehicle. TABLE 3.2 summarizes the ACC testing results for both vehicles in different lighting conditions. A test was considered successful if the vehicle accurately detected the lead vehicle and maintained appropriate following behavior; otherwise, the trial was recorded as a failure.

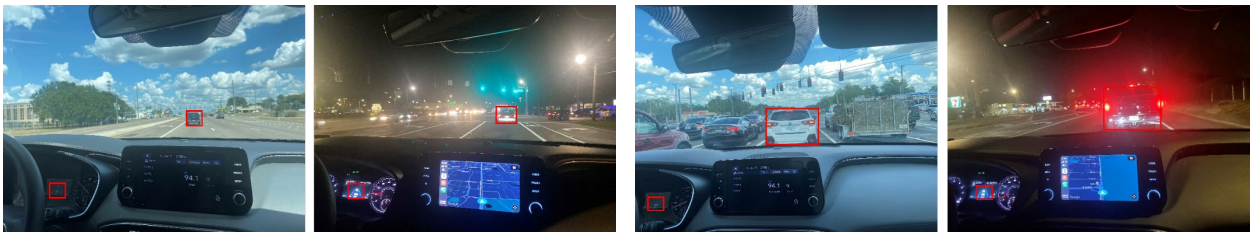

(a) Detecting and successfully following the lead vehicle (b) Following and stopping behind the lead vehicle

**Figure 3.2. Illustrations of test vehicle detection and following behavior.**

**TABLE 3.2 ACC testing results during daytime and nighttime conditions.**

| Vehicle | Successful Follows/Tests | |
|---|---|---|
| | Daytime | Nighttime |
| Hyundai Santa Fe | 7/10 | 6/10 |
| Audi Q5 | 8/10 | 7/10 |

Additionally, it was observed that when the lead vehicle exited the lane, the Audi Q5 quickly accelerated to the preset speed limit. This acceleration was noticeably abrupt, which may raise safety concerns and suggests a need for further calibration to ensure smoother transitions.

### 3.2.2 Collision Avoidance Assist

Collision Avoidance Assist systems use onboard sensors such as cameras and Radar to detect nearby vehicles, cyclists, and pedestrians. When a potential collision is identified, the system can automatically initiate corrective actions, such as braking or steering adjustments, to help avoid or mitigate the impact. These technologies play a critical role in enhancing road safety by reducing the frequency and severity of accidents, thereby protecting both vehicle occupants and other road users. Common Collision Avoidance Assist features include Forward Collision Avoidance Assist, Blind Spot Collision Avoidance Assist, and Rear Cross-Traffic Assist. This study evaluates the collision avoidance performance of 5 production vehicles: Toyota Corolla, Hyundai Santa Fe, Ford Bronco, Audi Q5, and Tesla Model Y, each equipped with at least one of these Collision Avoidance Assist features.

#### 3.2.2.1 Forward Collision Avoidance Assist

Forward Collision Avoidance Assist utilizes sensor fusion, combining cameras and Radar to detect obstacles in front of the vehicle. When an obstacle is detected, it provides visual and auditory warnings to the driver and may also engage in braking assistance or apply direct braking to help the driver avoid or mitigate the effects of a collision.

This study evaluates the Forward Collision Avoidance Assist functionality of four production vehicles from different manufacturers: the Toyota Corolla, the Hyundai Santa Fe, the Ford Bronco, and the Tesla Model Y. Figure 3.3 illustrates the testing scenarios, and TABLE 3.3 summarizes the corresponding results. The evaluation focuses on the impact of lighting conditions (daytime vs. nighttime) and vehicle speed on the system's performance. For safety reasons, all tests were conducted in a closed parking lot. A test was considered successful when the vehicle detected the obstacle (another vehicle or a pedestrian) and issued either a visual or auditory warning.

The results indicate that all vehicles demonstrated better obstacle detection performance during the daytime compared to nighttime. In addition, most vehicles were more effective at detecting other vehicles than pedestrians, which may be attributed to the larger physical profile of vehicles, making them easier to detect.

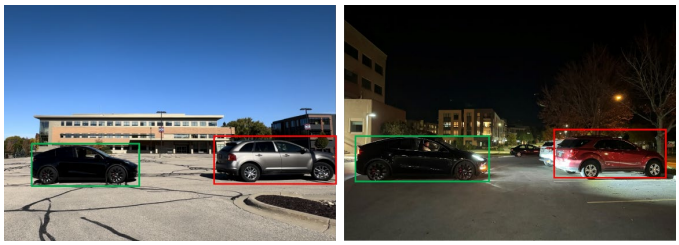

**Figure 3.3. Illustrations of Forward Collision Avoidance Assist testing scenarios (daytime and nighttime). The green box indicates the test vehicle, while the red box marks the object vehicle for which collision avoidance is required.**

**TABLE 3.3 Forward Collision Avoidance Assist testing results during daytime and nighttime.**

| Vehicles | Successful Detections/Tests | | | |
|---|---|---|---|---|
| | Daytime | | Nighttime | |
| | Vehicle | Pedestrian | Vehicle | Pedestrian |
| Toyota Corolla | 9/10 | 9/10 | 0/10 | 0/10 |
| Hyundai Santa Fe | 9/10 | 9/10 | 7/10 | 6/10 |
| Ford bronco | 7/10 | 6/10 | 7/10 | 5/10 |
| Tesla Model Y | 10/10 | 9/10 | 9/10 | 7/10 |

**TABLE 3.4 Forward Collision Avoidance Assist in detecting distance results.**

| Speed (mph) | Distance (ft) | | | | | | Successful Detections/Tests |
|---|---|---|---|---|---|---|---|
| | 1 | 2 | 3 | 4 | 5 | Average | |
| 15 | 31 | 40 | 28 | 39 | 32 | 34 | 7/10 |
| 20 | 51 | 61 | 53 | 61 | 55 | 56 | 6/10 |
| 25 | 71 | 62 | 65 | 65 | 71 | 67 | 5/10 |

Additional tests were conducted at varying speeds to investigate the effect of speed on detection performance further. The results presented in TABLE 3.4 show that detection distances generally increased with vehicle speed, likely due to the system's need to maintain a longer safe stopping distance. However, despite the increase in detection range, overall detection reliability tended to decline at higher speeds, suggesting that performance degrades as vehicle dynamics become more demanding.

3.2.2.2 Blind Spot Collision Avoidance Assist

Blind Spot Collision Avoidance Assist utilizes either Radar alone or a combination of the front view camera and rear corner Radar to detect approaching vehicles in blind spots. Upon detecting an approaching vehicle, these systems provide visual and auditory warnings to the driver and may also offer collision avoidance assistance. This study evaluates the performance of this feature in production vehicles from three different manufacturers: Hyundai Santa Fe, Ford Bronco, and Audi Q5. Testing was conducted under both daytime and nighttime conditions. Figure 3.4

illustrates examples of the testing scenarios used in this evaluation. TABLE 3.5 presents the test results for both daytime and nighttime conditions. When the test vehicle detects an approaching vehicle and triggers a visual alert, the detection is considered successful. The results show that the performance is similar during the day and at night. This may be due to the Radar used in this feature, which is not affected by lighting conditions.

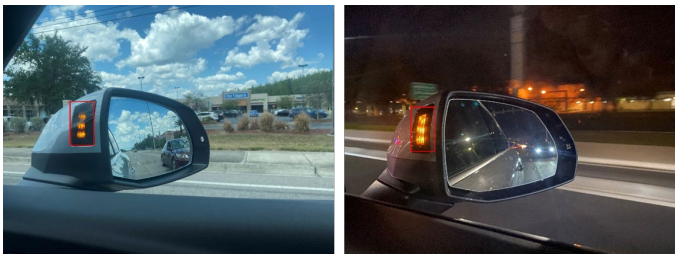

(a) Daytime (b) Nighttime

**Figure 3.4. Illustrations of Blind Spot Collision Avoidance Assist warning during daytime and nighttime.**

**TABLE 3.5 Blind Spot Collision Avoidance Assist testing results during daytime and nighttime.**

| Vehicles | Successful Detections/Tests | |
|---|---|---|
| | Daytime | Nighttime |
| Hyundai Santa Fe | 8/10 | 8/10 |
| Ford bronco | 8/10 | 8/10 |
| Audi Q5 | 8/10 | 7/10 |

3.2.2.3 Rear Cross-traffic Assist

Rear Cross Traffic Assist is engineered to detect vehicles approaching from both the left and right sides while the test vehicle is in reverse. It provides a warning to the driver in case of an impending collision, using both a visual message and an audible alert. Additionally, the system assists in braking to help prevent a collision. Rear corner radar is used to detect approaching vehicles from both the left and right sides.

**TABLE 3.6 Rear Cross-traffic Assist testing results during daytime and nighttime.**

| Vehicles | Successful Detections/Tests | |
|---|---|---|
| | Daytime | Nighttime |
| Hyundai Santa Fe | 8/10 | 7/10 |
| Ford bronco | 7/10 | 8/10 |
| Audi Q5 | 9/10 | 7/10 |

This study evaluates the Rear Cross-Traffic Assist functionality of three production vehicles: the Hyundai Santa Fe, the Ford Bronco, and the Audi Q5. Testing was conducted under both daytime and nighttime conditions. Figure 3.5 provides illustrations of the test scenarios, and the results are summarized in TABLE 3.6. All three vehicles demonstrated consistent performance across lighting conditions, with only minor variations that may be attributed to random factors. The consistent results are likely due to the radar-based nature of the system, which is generally unaffected by changes in lighting. It is also important to note that this feature does not activate when vehicles approach directly from behind the test vehicle.

(a) Daytime vehicle testing (b) Nighttime vehicle testing

**Figure 3.5. Illustrations of Rear Cross-Traffic Assist testing (outside-vehicle view and in-vehicle view). The green box indicates the test vehicle, while the red box marks the object vehicle for which collision avoidance is required.**

### 3.2.3 Lane Markings Detection

Lane Markings Detection systems rely on onboard cameras to identify lane boundaries, enabling vehicle control features such as Lane Tracing Assist and Lane Departure Alert. These

systems help maintain vehicle position within the lane, reduce unintended lane departures, and contribute to overall driving safety. As one of the most basic CADFs, all 6 vehicles evaluated in this study were equipped with lane markings detection capabilities.

The evaluation considered a variety of conditions, including clear and unclear lane markings, straight and curved roads, and both daytime and nighttime driving. Additionally, the study assessed system performance in more complex scenarios, such as merging and diverging lanes, as well as combinations of multiple adverse conditions. Figure 3.6 illustrates examples of these scenarios. TABLE 3.7 summarizes the detection results for each vehicle under seven distinct test scenarios: (1) clear, straight lane markings during daytime; (2) unclear, straight lane markings during daytime; (3) clear, curved lane markings during daytime; (4) clear, straight lane markings at nighttime; (5) merging, clear lanes during daytime; (6) diverging, clear lanes during daytime; and (7) unclear, straight lane markings at nighttime. To ensure a fair comparison across vehicles and scenarios, the test vehicle was driven at a consistent speed through each scenario. A detection was considered successful when the vehicle's display screen visibly showed the lane markings while passing through the test area; otherwise, it was recorded as a failure.

**TABLE 3.7 Lane Markings Detection testing results in different scenarios.**

| Scenario # | Successful Detections/Tests | Toyota Corolla | Hyundai Santa Fe | Ford Bronco | Audi Q5 | Honda Accord | Tesla Model Y |
|---|---|---|---|---|---|---|---|
| 1 | Clear, straight lane markings during the daytime | 9/10 | 9/10 | 9/10 | 9/10 | 10/10 | 10/10 |
| 2 | Unclear, straight lane markings during the daytime | 4/10 | 6/10 | 5/10 | 5/10 | 5/10 | 10/10 |
| 3 | Clear, curved lane markings during the daytime | 5/10 | 7/10 | 5/10 | 7/10 | 6/10 | 10/10 |
| 4 | Clear, straight lane markings at nighttime | 6/10 | 6/10 | 8/10 | 4/10 | 9/10 | 10/10 |
| 5 | Merging, clear lanes during the daytime | 5/10 | 7/10 | 6/10 | 6/10 | 7/10 | 10/10 |
| 6 | Diverging, clear lanes during the daytime | 5/10 | 6/10 | 5/10 | 7/10 | 6/10 | 10/10 |
| 7 | Straight, unclear lane at nighttime | 3/10 | 4/10 | 4/10 | 3/10 | 5/10 | 10/10 |

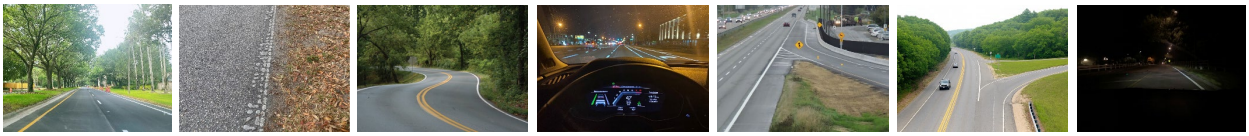

(a) (b) (c) (d) (e) (f) (g)

**Figure 3.6. Illustrations of different scenarios of lane markings: (a) Clear lane markings; (b) unclear lane markings; (c) curve lane markings; (d) lane markings at nighttime; (e) merging lanes; (f) diverging lanes; (g) unclear lane at nighttime.**

For Scenario 1, it is observed that almost all vehicles are capable of successfully detecting lanes during the daytime when lane markings are clear and straight. A comparison between Scenario 1 and Scenario 2 reveals a notable decline in detection performance for the first 5 vehicles (see TABLE 3.7) when faced with unclear lane markings. This observation underscores the critical dependency of lane detection systems on the clarity of lane markings. Meanwhile, the Tesla Model Y demonstrates the ability to successfully detect lanes regardless of the clarity of the lane markings.

Similarly, when comparing the test results from Scenario 1 with Scenario 3, it is evident that for the first 5 vehicles, the detection performance of curved lane markings is significantly inferior to that of straight lane markings, particularly during sharp turns or at higher speeds, where the detection becomes even more challenging. Tesla Model Y, however, does not show a diminished test result with curved lane markings.

In Scenario 4, test results indicate that the detection performance of the first 5 vehicles is somewhat impacted by nighttime conditions. For the Tesla Model Y, poor nighttime lighting does not affect the test outcomes.

Scenarios 5 and 6 present challenges somewhat similar to those encountered in Scenario 3, with merging and diverging lanes ultimately falling under the category of curved lanes. These similarities lead to a similar decrease in detection accuracy for the first 5 vehicles, as well as

increased difficulty in detection at higher speeds. This suggests inherent challenges that vehicles face in handling complex lane configurations and dynamic changes in road structures. Nonetheless, the Tesla Model Y continues to perform well in both scenarios.

These test results may be because the first 5 vehicles utilize front cameras (Audi, 2023; Bronco, 2022; Honda, 2022; Hyundai, 2022; Toyota, 2022) for Lane Markings Detection, where the clarity, geometric shape, and intensity of lighting can significantly impact the effectiveness of detection. In contrast, the Tesla Model Y is capable of successfully detecting lanes under any challenging driving conditions, regardless of the visibility of lane markings. This proficiency is likely due to the Tesla Model Y's approach of supplementing camera-based detection with onboard map data (Tesla, 2024). The integration of map data enriches the lane detection process with an additional layer of information, enabling the vehicle to maintain lane detection capabilities even in challenging driving conditions.

### 3.2.4 Static Message Sign Detection

Static Message Sign Detection systems utilize cameras to enable vehicles to "see" and recognize various informational road signs. By accurately interpreting signs, these systems assist drivers in understanding their driving environment, navigating complex traffic scenarios, and adapting to changing road conditions, thus contributing to safer driving practices.

This study evaluates the detection performance of stop signs, speed limit signs, and yield signs across different scenarios for the selected production vehicles. To ensure safety, all tests were conducted on the closed road.

#### 3.2.4.1 Stop Signs

A stop sign instructs drivers to come to a complete stop at intersections or crossings. It serves to regulate traffic flow, ensure safety, and prevent accidents by clearly indicating where

drivers must yield to other road users or pedestrians. This study evaluates stop sign detection performance in two production vehicles equipped with this feature: the Toyota Corolla and Tesla Model Y.


(a) (b) (c) (d) (e) (f)

**Figure 3.7. Illustrations of stop signs in different scenarios: (a) Normal; (b) moderate obstruction; (c) severe obstruction; (d) at nighttime; (e) moderately fading; (f) severely fading.**

**TABLE 3.8 Stop sign testing results in different scenarios.**

| Scenario # | Successful Detections/Tests | Toyota Corolla | Tesla Model Y |
|---|---|---|---|
| 1 | Normal stop sign | 8/10 | 10/10 |
| 2 | Moderate obstruction | 6/10 | 9/10 |
| 3 | Severe obstruction | 2/10 | 6/10 |
| 4 | Nighttime | 3/10 | 10/10 |
| 5 | Moderately fading | 8/10 | 9/10 |
| 6 | Severely fading | 2/10 | 5/10 |

**TABLE 3.9 Stop sign detection distance results for different speeds.**

| Vehicle | | Toyota Corolla | | | Tesla Model Y | | |
|---|---|---|---|---|---|---|---|
| Speed (mph) | | 5 | 15 | 25 | 5 | 15 | 25 |
| Distance (ft) | 1 | 41 | 107 | 21 | 140 | 95 | 75 |
| | 2 | 35 | 114 | 26 | 135 | 99 | 72 |
| | 3 | 40 | 96 | 30 | 155 | 96 | 60 |
| | 4 | 52 | 111 | 24 | 160 | 105 | 73 |
| | 5 | 40 | 107 | 19 | 154 | 90 | 55 |
| | 6 | 39 | 110 | 20 | 153 | 109 | 52 |
| | 7 | 38 | 115 | 22 | 166 | 95 | 60 |
| | 8 | 40 | 92 | 31 | 142 | 101 | 75 |
| | 9 | 52 | 108 | 25 | 145 | 112 | 73 |
| | 10 | 45 | 105 | 20 | 144 | 102 | 66 |
| | Average | 42 | 107 | 24 | 149 | 100 | 66 |

Vehicle detection performance can be influenced by several factors, including sign obstruction, fading, nighttime visibility, and vehicle speed. Figure 3.7 illustrates stop signs under different test scenarios, while TABLE 3.8 and TABLE 3.9 present the detection results. The data show that as the degree of obstruction increases, both vehicles experience greater difficulty in detecting stop signs. Additionally, the Tesla Model Y demonstrates superior detection performance compared to the Toyota Corolla under nighttime conditions. For both vehicles, detection accuracy decreases as the stop sign fades more, likely due to reduced visual contrast. These results may be attributed to the fact that both vehicles rely on camera-based detection, with the Tesla Model Y using a more advanced camera system that performs better in low-light environments.

Tests were conducted at varying speeds to investigate the effect of vehicle speed on detection performance. For the Tesla Model Y, higher speeds resulted in shorter detection distances, suggesting that the system reacts closer to the stop sign at faster speeds. In contrast, the Toyota Corolla did not exhibit a consistent relationship between speed and detection distance. Notably, the Corolla performed best at 15 miles per hour, detecting stop signs from a greater distance than at higher speeds. These findings suggest that detection algorithms and sensor configurations may be optimized differently across vehicle models, leading to unique performance characteristics under varying operating conditions.

#### 3.2.4.2 Yield Signs

A yield sign instructs drivers to give the right of way to other vehicles or pedestrians. Accurate detection of yield signs supports compliance with traffic regulations and promotes safe vehicle navigation. Among the vehicles tested in this study, only the Toyota Corolla was equipped with a yield sign detection feature. This evaluation investigates the impact of obstructions,

nighttime conditions, dirt on the sign surface, and varying vehicle speeds on the Corolla's ability to detect yield signs. Figure 3.8 illustrates yield signs in different scenarios.


(a) (b) (c) (d) (e)

**Figure 3.8. Illustrations of yield signs in different scenarios: (a) Normal; (b) moderate obstruction; (c) severe obstruction; (d) at nighttime; (e) dirty sign.**

**TABLE 3.10 Yield sign testing results in different scenarios.**

| Scenario # | Successful Detections/Tests | Toyota Corolla |
|---|---|---|
| 1 | Normal yield sign | 4/10 |
| 2 | Moderate obstruction | 4/10 |
| 3 | Severe obstruction | 2/10 |
| 4 | Nighttime | 2/10 |
| 5 | Dirty sign | 3/10 |

**TABLE 3.11 Yield sign detection distance results for different speeds.**

| Speed (mph) | Distance (ft) | | | | | Successful Detections/Tests |
|---|---|---|---|---|---|---|
| | 1 | 2 | 3 | 4 | Average | |
| 5 | 121 | 128 | 126 | 123 | 124.5 | 4/10 |
| 15 | 74 | 218 | 217 | 169 | 169.5 | 4/10 |
| 25 | 188 | 188 | 194 | 183 | 188.3 | 6/10 |

The test results are presented in TABLE 3.10 and TABLE 3.11. TABLE 3.10 shows that the vehicle's detection performance for moderately obstructed yield signs is comparable to that of unobstructed signs. However, when the signs are severely obstructed, the detection performance significantly declines. Compared to daytime, vehicles exhibit a decline in detection performance at night. Additionally, the detection performance also slightly decreases when the yield signs are

dirty. These results are attributed to the Toyota Corolla's use of camera-based detection systems, which are affected by obstructions, reduced visibility at night, and dirt on the sign surfaces. Test results at different speeds show that the higher the vehicle speed, the greater the distance at which yield signs are detected, presenting a stark contrast to the detection results for stop signs. This discrepancy may be due to differences in the detection algorithms used for identifying yield signs and stop signs.

3.2.4.3 Speed Limit Signs

Speed limit signs indicate the maximum legal speed at which vehicles can safely travel on a particular section of road. The ability of a vehicle to accurately detect speed limit signs is essential for maintaining legal speeds and enhancing road safety.


(a) (b) (c) (d) (e) (f) (g) (h)

**Figure 3.9. Illustrations of speed limit signs in different scenarios: (a) Normal; (b) at nighttime; (c) moderately obstructing the number "5"; (d) severely obstructing the number "5"; (e) moderately obstructing the number "2"; (f) severely obstructing the number "2"; (g) moderately obstructing the number "25"; (h) severely obstructing the number "25".**

**TABLE 3.12 Speed limit sign testing results during daytime and nighttime.**

| Vehicles | Successful Detections/Tests | |
|---|---|---|
| | Daytime | Nighttime |
| Toyota Corolla | 10/10 | 7/10 |
| Honda Accord | 9/10 | 6/10 |
| Tesla Model Y | 115/120 | 118/120 |

This study evaluates the speed limit sign detection performance of three production vehicles: the Toyota Corolla, the Honda Accord, and the Tesla Model Y. Testing was conducted

under both daytime and nighttime conditions, with illustrative examples shown in Figure 3.9 (a-b). The results are summarized in TABLE 3.12. The findings reveal that detection performance declines at night for both the Toyota Corolla and Honda Accord, suggesting a reduction in the effectiveness of their camera-based systems under low-light conditions. In contrast, the Tesla Model Y maintains consistent detection performance regardless of lighting and, in some cases, even performs better at night. This superior performance is likely attributable to the vehicle's specialized camera hardware, which is optimized for low-light environments (Tesla, 2024).

Additionally, we examined the performance of the tested vehicles in detecting speed limit signs under various obstruction conditions, as such conditions frequently occur in real-world driving environments and may challenge the reliability of vision-based recognition systems. The tested scenarios are shown in Figure 3.9 (c-h), and the test results are shown in TABLE 3.13. The results indicate that moderate obstructions do not significantly impact the vehicle's detection performance, while severe obstructions greatly diminish it. Notably, when severely obstructed, vehicles occasionally misidentify speed limit signs for 25 mph as 20 mph. This is because the vehicle uses cameras to detect signs, and the effectiveness of camera detection can be affected by obstructions.

**TABLE 3.13 Speed limit sign obstructed detection results.**

| Scenarios | Detection Results | Successful Detections/Tests |
|---|---|---|
| Moderately obstructing the number "5" | 25 mph | 10/10 |
| Severely obstructing the number "5" | 20/25 mph | 4 (20 mph) /2 (25 mph)/10 |
| Moderately obstructing the number "2" | 25 mph | 10/10 |
| Severely obstructing the number "2" | 25 mph | 4/10 |
| Moderately obstructing the number "25" | 25 mph | 10/10 |
| Severely obstructing the number "25" | Cannot detect the sign | 0/10 |

### 3.2.5 Traffic Light Awareness

Vehicles' ability to detect traffic light status assists drivers in safely navigating traffic signal-controlled intersections. Some advanced production vehicles are equipped with this capability. As dynamic signals with changing colors, traffic lights present challenges for detection systems, and thus, this feature is not yet widely adopted. This study evaluates the Traffic Light Awareness performance of two production vehicles: Tesla Model Y and Audi Q5. Figure 3.10 and Figure 3.11 respectively illustrate traffic light testing for Tesla and Audi during daytime and nighttime conditions.

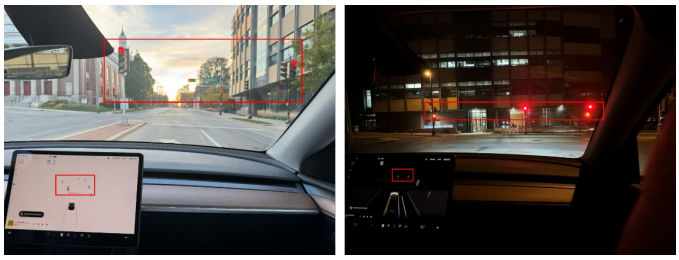

(a) Daytime (b) Nighttime

**Figure 3.10. Illustrations of Tesla traffic light testing during the daytime and nighttime.**

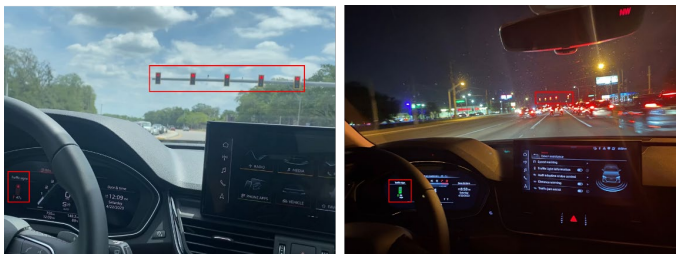

(a) Daytime (b) Nighttime

**Figure 3.11. Illustrations of Audi traffic light testing during the daytime and nighttime.**

**TABLE 3.14 Traffic light testing results during daytime and nighttime.**

| Vehicles | Successful Show the Phase/Tests | |
|---|---|---|
| | Daytime | Nighttime |
| Tesla Model Y (perception-based) | 82/85 | 81/85 |
| Audi Q5 (connectivity-based) | 5/10 | 5/10 |

Note: For the Audi Q5, even if the phase can be recognized correctly, the red-light countdown still has an error of a few seconds.

The first one is the Tesla Model Y, which relies on perception-based (sensor detection) technology. This vehicle uses camera-based detection technology to visually detect the status of traffic lights and make decisions based on the data it gathers. The second vehicle is the Audi Q5, which uses connectivity-based technologies. This vehicle is equipped with vehicle-to-infrastructure (V2I) technologies, which can communicate with the traffic management system via onboard 4G LTE to receive real-time traffic light data.

This study conducts tests for these two vehicles during both daytime and nighttime. Nighttime driving scenarios are characterized by the unique interplay of light sources, such as the glare from streetlights, intermittent beams from other vehicles' headlights, and the flickering of production billboards and signs. These factors can influence the vehicles' ability to recognize traffic lights that rely on perception-based technology, as they create a dynamic and sometimes challenging environment. TABLE 3.14 shows the traffic light testing results of these two vehicles during the daytime and nighttime.

The test results reveal that the Tesla Model Y experienced a higher number of instances where it could not accurately recognize the correct phase of traffic lights at night. This indicates a slight reduction in the Tesla Model Y's capability to detect traffic lights under nighttime conditions. This decrease in detection performance may be attributed to interference from other light sources in the nighttime environment affecting the vehicle's camera, resulting in a diminished capacity for the camera to interpret traffic signals correctly.

The Audi Q5 performs the same during the daytime and nighttime. While Audi recognizes and shows the upcoming traffic lights, the display of traffic light phases is often inaccurate. The accuracy of the red-light countdown always shows an error of around 4 seconds or more. This may result from V2I technologies delay or inaccuracy. In addition, the speed recommendations

provided by the Audi Q5 system usually align with the existing speed limits on the road. This does not assess whether Audi Q5 can generate real-time speed recommendations based on the distance to traffic lights and the remaining green light duration, a functionality Audi claims their vehicles can achieve (Audi Newsroom, 2024). Furthermore, in some cases, the countdown experiences unexpected fluctuations. That may be because some intersections dynamically adjust traffic light timing based on current traffic flow conditions, causing the countdown of red-light duration to change dynamically according to real-time traffic situations.

The Traffic Light Awareness feature's maturity and effectiveness in production vehicles remain in the developmental stage. Further enhancements and improvements may be necessary to increase the accuracy and reliability of traffic light detection, ensuring it meets the high standards required for safe and efficient navigation.

### 3.2.6 Full Self-driving (FSD)

Tesla Model Y's FSD (Beta), also known as Autosteer on City Streets. It handles a variety of driving scenarios, including intersections, turns, roundabouts, and highway entrances/exits. It maintains appropriate speed and following distance relative to the preceding vehicle and responds effectively to traffic lights, stop signs, speed limit signs, pedestrians, cyclists, and other vehicles on the road. The system employs data from multiple cameras to construct a real-time model of the surrounding environment, ensuring safe navigation (Tesla, 2024).

Figure 3.12 shows an example of FSD testing during the daytime and nighttime. TABLE 3.15shows the Tesla Model Y FSD road testing results. From the results, it is evident that Tesla Model Y's FSD functionality exhibits good performance in recognizing traffic lights, traffic signs, lane markings, and following cars, both during the day and at night. However, its ability to detect pedestrians is relatively lacking, particularly with poorer detection effectiveness at night.

Additionally, the testing process also finds misidentified cases, such as interpreting two pedestrians walking side by side as a cyclist.

(a) Daytime (b) Nighttime

**Figure 3.12. Illustrations of FSD testing during the daytime and nighttime.**

In addition, during the test, the FSD system exhibited behaviors akin to an assertive, albeit less experienced, human driver. This included rapid and uneven acceleration, quick turning, and sudden braking. Drivers using the system should exercise constant vigilance. During the testing process, a near-collision incident occurred when the test Tesla Model Y was making a left turn at an intersection. At that moment, an oncoming car hesitated, and the test Tesla Model Y mistakenly perceived it as stationary. Fortunately, the quick reaction of the human driver averted a collision.

**TABLE 3.15 Tesla Model Y FSD road testing results.**

| Scenarios | Successful Shows/Tests | |
|---|---|---|
| | Daytime | Nighttime |
| Traffic light | 85/85 | 81/85 |
| Stop sign | 54/55 | 55/55 |
| Speed limit sign | 115/120 | 118/120 |
| Car following | 58/58 | 40/40 |
| Pedestrian | 22/24 | 15/19 |
| Lane markings (mile) | 38/38 | 38/38 |

### 3.2.7 Summary of the Test Results and Suggestions

Through testing the automated driving functions of existing production vehicles, we identified the factors that may impact their performance. For ACC, low nighttime visibility can

negatively affect vehicle performance. Additionally, when the front vehicle of the test vehicle exits the lane, the sudden acceleration behavior of the test vehicle may be unsafe or uncomfortable. To address these issues, vehicle manufacturers should consider using sensors that perform well in low-visibility conditions, such as infrared cameras, to assist in detecting the lead vehicle. They should also enhance the ACC algorithm to improve the success rate of following and develop a smooth driving mode for when the front vehicle exits the lane, enhancing driving comfort and safety.

For the Collision Avoidance Assist systems, Forward Collision Avoidance Assist systems rely on sensor fusion, combining cameras and Radar to detect objects, the performance is generally better during the day than at night, and these systems tend to perform better for vehicle collision avoidance than for pedestrian collision avoidance. In contrast, systems that primarily rely on Radar, sometimes in combination with cameras, for Blind Spot and Rear Cross-Traffic Collision Avoidance Assist demonstrate strong performance both during the day and at night. The warning distance for Forward Collision Avoidance Assist systems also increases with vehicle speed. To enhance the performance of Forward Collision Avoidance Assist, vehicle manufacturers should consider using cameras that perform well at night, improving the algorithm's effectiveness, and enhancing pedestrian collision avoidance. Additionally, incorporating advanced sensor fusion technologies could further improve the system's overall reliability and safety across different scenarios.

For Lane Markings Detection, unclear lane markings, curved roads, poor nighttime lighting, merging, and diverging lanes can all affect a vehicle's detection performance. To address these issues, vehicle manufacturers could introduce onboard map data to significantly bolster lane detection performance. Integrating thermal imaging or infrared technology into vehicle camera

systems could also provide a complementary detection method for nighttime driving. From an infrastructure standpoint, regular maintenance and the use of high-contrast, reflective, or illuminated materials for lane markings would greatly aid detection, such as employing durable thermoplastic resistant to weather and traffic wear. Incorporating advanced lighting solutions, such as LED or intelligent lighting systems, strategically placed streetlights can enhance visibility and detection in low-light conditions. Increasing the density of lane markings on curves, using wider or more reflective markings, would make it easier for vehicle sensors to detect them. Curve-specific signs, utilizing illuminated or reflective materials, could provide advanced warning to drivers and autonomous driving systems, extending the time for lane-keeping adjustments. Additionally, distinctive lane marking patterns should be used for merging and diverging lanes. From a traffic technology perspective, implementing V2I communication could provide real-time data about road conditions and upcoming lane changes, enabling vehicles to better predict and navigate various scenarios. By implementing these improvements, the overall safety and efficiency of autonomous and assisted driving systems can be enhanced, addressing current limitations in lane detection under diverse road and environmental conditions.

In terms of Static Message Sign Detection, obstruction, fading, dirt, and nighttime conditions can affect a vehicle's detection performance. The distance at which different vehicles detect stop signs/yield signs varies at different speeds, without a consistent trend of increasing or decreasing. Obstructing parts of speed limit signs may result in incorrect speed readings. Detection performance for stop signs and speed limit signs is generally better than for yield signs. Addressing these factors requires targeted vehicles and infrastructure improvements tailored to each specific challenge. From a vehicle improvement perspective, effective algorithm enhancements may help vehicles detect signs impacted by obstruction, fading, dirt, and nighttime conditions. Additionally,

improving sensor technology could enhance detection in challenging conditions, such as using higher-resolution cameras, more sensitive Radar, or thermal imaging systems. High-definition digital maps can provide vehicles with redundant sign information, helping maintain compliance even when physical signs are missed or degraded. From an infrastructure perspective, ensuring reliable traffic sign detection requires a combination of physical design, maintenance, and technological augmentation. Signs should be placed in unobstructed locations visible to both human drivers and vehicle sensors. Regular inspections and maintenance are essential to remove vegetation or infrastructure that blocks visibility, while establishing clear zones around signs can prevent future obstructions. To maintain long-term legibility, signs should be made from durable, fade-resistant materials with UV-protective coatings. Routine cleaning, especially in areas prone to dust or pollution, and the use of hydrophobic or dirt-repellent coatings can further preserve clarity. At night, retroreflective materials and supplemental lighting such as ground-mounted or overhead fixtures can enhance visibility, while LED-illuminated signs can offer consistent detectability regardless of ambient lighting. In addition to physical enhancements, digital infrastructure plays a key role in supporting traffic sign recognition. Roadside communication units, using V2I communication, can transmit real-time regulatory information, such as speed limits or stop sign presence, directly to connected vehicles. Integrating these digital technologies with well-maintained physical signage creates a more robust and resilient system, improving safety and operational effectiveness for both automated and human drivers.

For Traffic Light Awareness, ambient nighttime light sources can affect the performance of perception-based vehicles in detecting traffic signals. To address this, regarding vehicle improvements, using advanced camera systems with better low-light performance can enhance detection capabilities. Further, improving the algorithms for signal detection and recognition can

enhance performance, especially in complex lighting conditions. From the infrastructure perspective, enhancing the illumination of traffic lights can ensure they stand out more distinctly against the nighttime environment. Employing LED lights with consistent luminosity and minimal diffusion can make traffic lights more visible to detection systems without increasing glare. Additionally, implementing anti-reflective coatings on traffic light housing, as well as using retroreflective backplates, can help reduce interference from other light sources. For vehicles using connectivity technology, the interaction performance between production vehicles and traffic lights is found to be suboptimal. Issues such as incorrect phase displays, delays, inaccurate speed recommendations, and fluctuating red light countdowns indicate that the connectivity technology in use is still in the developmental stages. To enhance connectivity-based technology for accurate traffic light detection, joint improvements in both vehicles and infrastructure are essential. Enhancing data transmission reliability through robust communication protocols, such as 5G cellular networks, can significantly improve the speed and reliability of traffic light information transmitted to vehicles. Improving interoperability between different vehicles is also crucial. Expanding the coverage of V2I-enabled infrastructure to more intersections will enhance the benefits of improved traffic efficiency and safety on a larger scale. Lastly, facilitating regular software updates for vehicle systems ensures compatibility with the latest V2I technologies and standards, allowing vehicles to remain equipped with the most current traffic light detection functionalities.

For FSD, the feature demonstrates excellent performance in recognizing traffic lights, traffic signs, lane markings, and following vehicles during both daytime and nighttime. However, its ability to detect pedestrians is relatively lacking, particularly with poorer detection effectiveness at night. Additionally, the testing process revealed some misinterpretations, such as perceiving two

pedestrians walking side by side were mistaken as a person riding a bicycle. The vehicle also behaved like an aggressive young driver, exhibiting rapid and uneven acceleration, quick turning, and sudden braking. Therefore, Tesla should conduct further research to enhance FSD's performance, focusing on improving pedestrian detection, particularly under low-light conditions. Refining the detection algorithms to better differentiate between various objects, such as distinguishing between pedestrians and cyclists, can reduce false interpretations. Additionally, adjusting the vehicle's driving algorithms to exhibit more cautious and smooth driving behavior, especially during turning or braking, can improve overall safety and comfort. By focusing on these areas, Tesla can enhance the performance of FSD, particularly in pedestrian detection, while also making the driving experience safer and more comfortable.

## 3.3 Recommendation

Building upon the test results of CADFs in current production vehicles, we recognize that these evaluations reflect the current stage of technological readiness. As CAV technology continues to evolve and the penetration rate of CAVs increases, new demands may arise for both infrastructure and vehicle technologies. To support this transition, it is critical to identify forward-looking recommendations that address these emerging needs.

### 3.3.1 Early Stage of the CAV Technology

In the early stages of CAV technology development, when the prevalence of CAVs on the road is low and CAV technology levels are limited, infrastructure should prioritize supporting all road users, including both CAVs and HVs (FHWA, 2023). Large-scale modifications to existing infrastructure are not anticipated (Sanusi et al., 2022). The MUTCD (FHWA, 2023) emphasizes that the uniform and consistent application of traffic control devices significantly improves the ability of CAV technologies to interpret and respond accurately. It recommends using standardized

devices across similar roadway types, conducting timely maintenance and replacement of aging or damaged devices, ensuring temporary or emergency controls adhere to uniform standards, and removing outdated or unnecessary devices to minimize confusion. Additionally, good road conditions are also crucial during the early stages of CAV development. However, according to a recent infrastructure report by the American Society of Civil Engineers (ASCE), approximately 43% of public roadways in the United States are in poor or mediocre condition (Saeed et al., 2021). The effective operation of a collision avoidance system requires an adequate road friction coefficient (Nitsche et al., 2014). Road conditions, such as potholes, fractures, or even ruts, can affect a vehicle's electrical stability, particularly when the vehicle is attempting to avoid roadside obstructions (Binshuang et al., 2019). Improved design and maintenance of drainage infrastructure (such as culverts, channels, and gullies) is important for early CAV development (Johnson, 2017).

Additionally, from the perspective of vehicle technology development, this stage should focus on developing automated driving features aimed at enhancing driving efficiency and safety. Beyond the already tested features, potential developments could include functionality for vehicles to detect road and pavement signs (Coyner & Bittner, 2021) and assistance features for approaching work zones (T. Ren et al., 2020). Further improvements might involve developing features to assist with adverse weather conditions (B. Zhu et al., 2023), detecting and avoiding obstacles such as fallen trees or debris (Haris & Hou, 2020), and providing emergency response assistance, etc. To improve detection performance, employing better sensors (Gouda & El-Basyouny, 2022) or utilizing sensor fusion technology (Khatab et al., 2021; Kmiotek & Ruichek, 2008) can enhance vehicle perception capabilities. Developing improved algorithms (He et al., 2024; Kuang et al., 2024; Tang et al., 2025; B. Zhu et al., 2023; Zhuang et al., 2025), enhancing V2I technology (Fei et al., 2024; Malinverno et al., 2018; Rakha et al., 2016), and ensuring robust

communication between vehicles and infrastructure are also crucial steps in advancing CAV technology.

### 3.3.2 Prevailing Mixture of CAVs and HVs

As CAV technology evolves, dedicated infrastructure will be necessary to achieve its intended benefits, such as improving road capacity, enhancing safety, and reducing fuel consumption. At the same time, traditional infrastructure familiar to human drivers should be maintained in good condition. For example, transition zones between highways and urban networks (Farah et al., 2018), CAV-exclusive lanes (Glancy et al., 2016; Ma & Wang, 2019; McDonald & Rodier, 2015), and digital infrastructure supporting wireless technology (Sanusi et al., 2022) should be established. Revising and strengthening bridge and pavement design standards to accommodate changes in load characteristics due to CAV operations, particularly for autonomous truck platooning, will be important (Liu et al., 2019). Unified, readable emergency signage should be set up, and digital roadside communication devices should be established to replace static facilities, providing real-time data (Liu et al., 2019). Parking facilities should be designed, with the top floors designated for CAV-compliant parking and the remaining floors reserved for conventional parking spaces (Liu et al., 2019). At this stage, different levels of automation may require different infrastructure, which should be considered accordingly (Farah et al., 2018).

As CAV technology evolves, this phase should focus on enhancing vehicle platooning (Q. Li et al., 2024; Martinez-Diaz et al., 2021), improving sensor fusion capabilities (Ravindran et al., 2022), and developing more advanced vehicle-to-everything (V2X) communication systems (Lakshminarasimhan & Knoll, 2020). Vehicle platooning, which allows multiple CAVs to travel closely together, requires precise vehicle-to-vehicle (V2V) communication and coordination to

enhance road capacity, safety, and fuel efficiency. The development of advanced sensor fusion technologies will improve the CAVs' ability to perceive and interpret their surroundings, while robust V2X communication systems will facilitate real-time interaction between CAVs and infrastructure, enhancing traffic flow and safety.

### 3.3.3 Mature Stage of the CAV Technology

At the mature stage of CAV technology, when HVs are nearly nonexistent, more advanced infrastructure features can be deployed to maximize the benefits of CAV. Simultaneously, it may be possible to reduce or eliminate some existing infrastructure components. For example, single communication beacons could replace numerous traffic signals (Duarte & Ratti, 2018; Johnson, 2017), and parking lot layouts could be streamlined and unified (Liu et al., 2019), offering pick-up and drop-off zones for shared vehicle users (Yigitcanlar et al., 2019). Additionally, lane assignments could be controlled through communication rather than road markings, which would allow for narrower lanes and increased road capacity (Farah et al., 2018). Service stations could be constructed to provide safe shelters for malfunctioning CAV vehicles (Begg, 2014). Roundabouts and other collision avoidance devices, such as speed bumps, could be reduced.

In this mature phase, the vehicle would realize full driving automation (Level 5), eliminating the need for people to drive vehicles themselves. At this stage, robust artificial intelligence (AI) will be essential for controlling autonomous vehicles (Di & Shi, 2021). The AI systems should be highly sophisticated and capable of real-time decision-making, obstacle detection, and navigation. Continuous learning and adaptation will be crucial for improving performance and handling novel situations. To ensure safety, autonomous vehicles should be equipped with redundant systems, including backup sensors, computing units, and communication systems. These redundant systems will help prevent system failures and ensure safe operation even

if a component malfunctions. Autonomous vehicles should also utilize dynamic mapping technologies to provide up-to-date information about road conditions, traffic, and obstacles. These maps should be continuously updated through cloud-based services to reflect real-time changes in the driving environment.

## 3.4 Chapter Summary

This chapter evaluated existing automated driving features in production vehicles across various scenarios, identifying factors that influence their performance. The features tested included ACC, Collision Avoidance Assist, Lane Markings Detection, Static Message Sign Detection, Traffic Light Awareness, and FSD. The study highlighted the critical impact of environmental conditions on these systems, revealing significant variations in effectiveness under different scenarios.

Most production vehicles rely on cameras and radars to perceive their surroundings; however, low visibility conditions significantly hinder the effectiveness of vision-based systems. In addition, current V2I technologies remain in an early stage of deployment and are not yet fully mature. Integrating up-to-date digital maps can partially compensate for environmental perception limitations by providing contextual information. Nonetheless, technologies still require further enhancement to ensure reliable operation in complex and challenging environments. Moreover, the results reveal considerable heterogeneity in CADF performance across different manufacturers and vehicle models. These differences likely stem from variations in sensor configurations (e.g., mono camera vs. sensor fusion), algorithm design, system calibration, and integration strategies. Recognizing such heterogeneity is essential for regulators, infrastructure planners, and consumers, as it impacts the evaluation of system capabilities and the design of appropriate supporting infrastructure and policies. Therefore, improving perception and communication technologies,

while also accounting for brand-specific performance variability, is critical for advancing the robustness, safety, and scalability of autonomous vehicle systems under diverse real-world conditions.

There are several limitations that should be acknowledged. First, the use of rental vehicles means that not all test vehicles represented the highest trim levels available for their respective models. As a result, some advanced connected and automated driving features may not have been present or activated, limiting the scope of features evaluated. In addition, internal system logs were not accessible to the research team, which restricted the ability to trace detailed sensor fusion processes or algorithmic decision-making within the CADFs. Consequently, the analysis primarily focused on observable outputs rather than internal operational mechanisms, which may limit the interpretability of certain performance variations. In future studies, we plan to integrate external data-logging devices—such as LiDAR, radar, and video-based sensing systems—to capture continuous measurements of system response behavior (e.g., relative speed, headway distance, and activation timing). Such detailed data will enable more quantitative evaluation of feature reliability and failure modes, particularly for longitudinal control functions such as ACC. Furthermore, the test results are specific to the selected vehicles and scenarios, which may affect the generalizability of the findings. The scope of testing presented in this chapter is also constrained and should not be interpreted as exhaustive or as a definitive assessment of vehicle performance. For example, achieving lane detection success in 4 out of 10 trials does not directly imply a 40% accuracy rate, as this study focuses on identifying influencing factors rather than producing statistically validated metrics. The results are intended to provide qualitative insights into the conditions that may affect CADF performance. Moreover, smartphones were used to capture images during testing. While care was taken to select images that best represented real-world conditions, the automatic lighting

compensation features of smartphones may have introduced discrepancies, particularly under low-light or nighttime settings. Therefore, the images presented in this chapter may not fully reflect the actual visual conditions encountered during testing. Finally, future studies could incorporate a more quantitative definition of obstruction and degradation conditions to enhance experimental rigor. For example, partial occlusions could be designed at specific levels (e.g., 10%, 30%, and 50%) to systematically examine system performance under varying degrees of visibility loss. Similarly, controlled variations in the clarity of signs or lane markings could be used to evaluate perception robustness. While such quantitative control was not feasible on public roadways in this study, it could be implemented under test-track conditions or through augmented or mixed reality (AR/MR) environments. These approaches would enable more precise replication and analysis of challenging real-world conditions.

Despite these limitations, this study serves as a foundation for identifying key environmental and operational factors that influence vehicle performance. Future research can build on these findings by conducting more detailed, quantitative evaluations. For example, testing the retroreflectivity of lane markings and static message signs may help determine infrastructure requirements for reliable CAV operation. Similarly, measuring system performance across varying ambient light levels, camera glare conditions, and adverse weather such as rain, snow, and fog could reveal the sensitivity of different sensing modalities. These future directions, including the investigation of glare effects from headlights, sunlight reflections, and other visual interferences, will contribute to the continued development and refinement of connected and automated driving technologies.

# 4 NETWORK FEATURE IMPACT ASSESSMENT

Chapter 3 examined what current production AVs can actually do under real-world driving conditions, providing an assessment of AV performance at the vehicle level under specific driving scenarios. However, real road networks are far more complex than isolated driving scenarios. Urban networks differ widely in demand levels, road geometry, intersection density, signalization, and connectivity, and these differences shape how vehicles interact and how driving behavior aggregates into network-level outcomes. Even as AV technology matures, its benefits may not transfer uniformly across networks. This raises a broader question: across diverse urban networks, are AV impacts consistent, and which network features make those impacts more or less pronounced?

To answer this question, this chapter conducts a cross-network simulation study of 12 urban networks in Simulation of Urban Mobility (SUMO) under pure AV and pure HV regimes, with movement-specific parameterization for vehicle-signal interactions. Five network features, demand intensity, road length, road density, street connectivity, and signalized intersection percentage, are examined against operational, environmental, and surrogate safety performance measures. Feature-performance relationships are evaluated using correlation analysis and trend analysis. The results show that AV impacts are network-dependent rather than uniform, with different network features moderating different aspects of AV performance. These findings highlight the need for a network-aware perspective in AV deployment and evaluation, so that assessment reflects network context rather than average performance alone.

The remainder of this chapter is organized as follows. Section 4.1 introduces the network features and performance measures, covering the selection and extraction of candidate features and the computation of performance measures. Section 4.2 describes the study networks and

simulation setup, including network selection, simulation settings, and AV/HV parameterization. Section 4.3 presents the cross-network results, including correlation and trend analyses. Section 4.4 concludes the chapter.

## 4.1 Network Features and Performance Measures

### 4.1.1 Selection and Extraction of Network Features

To study how network features shape AV impacts, we first need to characterize networks according to their features. An initial set of ten candidate features was considered, and final feature selection was guided by three principles. First, theoretical grounding: each retained feature was required to have a plausible mechanistic link to network-level traffic operations, ensuring that observed feature–performance associations could be interpreted within an established traffic engineering framework. Second, physical interpretability: each feature was required to be directly computable from network topology or demand data and to carry a clear, unambiguous physical meaning, facilitating comparison across heterogeneous networks. Third, limited collinearity: where two or more candidate features were highly correlated ($|\rho| > 0.7$) and conceptually redundant, only one representative feature was retained. Variables with substantial conceptual or statistical overlap were not retained simultaneously, particularly among size-related, signalization-related, and connectivity-related measures. The final feature set included four structural features, signalized intersection percentage, road density, street connectivity, and road length, and one operational feature, demand intensity. Figure 4.1 illustrates both the candidate feature correlation structure and the feature screening process that led to this final set.

The final retention and operational definition of the features were tailored to the objectives of the present study and standardized to support consistent cross-network comparison. The retained features were defined as follows:

- **Demand intensity**: the total loaded traffic demand divided by the 1 h simulation period and the total vehicle-accessible road length (veh/h/km), representing the level of traffic demand loaded onto the network infrastructure.
- **Signalized intersection percentage:** the percentage of signalized intersections among all intersections in the vehicle-accessible subgraph, representing the degree to which signal control governs junction operations across the network.
- **Road density**: the total vehicle-accessible road length normalized by the network area (km/km²), representing the spatial concentration of road infrastructure.
- **Street connectivity:** the ratio of the number of undirected links to the number of nodes in the vehicle-accessible subgraph (links/nodes), representing the topological structure of the network.
- **Road length:** the total length of all vehicle-accessible road segments in the network (km), representing the overall network scale.

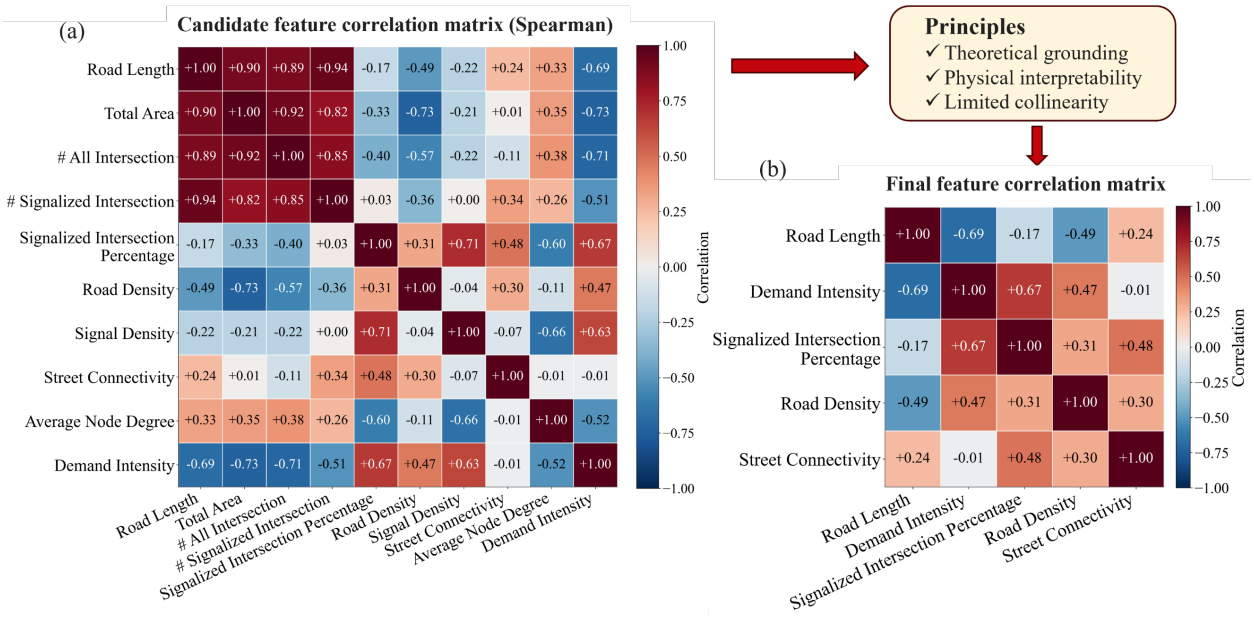


**Figure 4.1. Feature screening process and Spearman correlation structure of the candidate and final network features.**

To ensure comparability across heterogeneous SUMO networks, all features were extracted using a unified preprocessing procedure. Internal connectors and internal junctions were excluded because they primarily reflect simulation-specific coding details rather than meaningful road network structure. All road-based measures were computed on vehicle-accessible edges only, with one representative lane used per edge when summing road length to avoid double-counting multilane facilities. Network area was defined as the convex hull of junction coordinates, including dead-end nodes but excluding internal junctions, rather than a rectangular bounding box, because this better represents the spatial footprint of irregularly shaped networks. Road density was computed as vehicle-accessible road length divided by this convex hull area. Street connectivity was computed on the vehicle-accessible subgraph, with nodes defined as the unique endpoints of retained edges and bidirectional edges deduplicated to obtain undirected link counts. Together, these choices ensured that the extracted features reflected the effective vehicle-oriented structure of each network rather than artifacts of network coding or lane-level representation.

Based on these definitions and extraction rules, the retained network features provide a consistent structural and operational description of the study networks. Section 4.1.2 next defines the network-level performance measures used to evaluate how these features relate to traffic efficiency, fuel consumption, and surrogate safety outcomes.

### 4.1.2 Computation and Aggregation of Performance Measures

To capture efficiency, environmental, and surrogate safety dimensions of traffic performance, 5 network-level performance measures were derived from the simulation outputs. All measures were computed over the effective 50-minute analysis window, consistent with the simulation settings described in Section 4.2.2. For each network and scenario, vehicle–timestep observations, including speed and trajectory information, were extracted from the floating car data

(FCD) output files, fuel consumption records were extracted from the emission output files, and conflict records were extracted from the surrogate safety measure (SSM) output files. These outputs were then aggregated to the network level, and the reported value for each network–scenario combination represents the mean across 5 runs with different random seeds. The 5 retained performance measures were Average Travel Speed, Average Delay, Fuel Consumption Intensity, Low-Time-To-Collision (TTC) event rate, and Low-Post-Encroachment Time (PET) event rate.

Efficiency was characterized by two measures derived from the FCD output. Average Travel Speed was computed as the time-mean speed across all vehicle–timestep observations recorded in the FCD output:

$$\bar{v} = \frac{1}{N_{obs}} \sum_{i=1}^{N_{obs}} v_i$$

where $v_i$ is the instantaneous speed of the $i$-th vehicle–timestep observation and $N_{obs}$ is the total number of such observations during the analysis window.

Average Delay was computed as the cumulative difference between actual travel time and estimated free-flow travel time, averaged across all vehicles observed during the analysis window:

$$\overline{Delay} = \frac{1}{N_{veh}} \sum_{i=1}^{N_{obs}} \delta_i$$

where $\delta_i = \max\left(\Delta t - \frac{s_i}{v_{ff,i}}, 0\right)$ is the delay incurred at observation $i$, $\Delta t$ is the simulation time step, $s_i = v_i \cdot \Delta t$ is the distance traveled during that step, $v_{ff,i}$ is the lane-level free-flow speed approximated as the maximum observed speed on the corresponding lane, and $N_{veh}$ is the number of unique vehicles observed during the analysis window.

Environmental performance was characterized by Fuel Consumption Intensity derived from the emission output, defined as total fuel consumption normalized by vehicle kilometers traveled (VKT):

$$I_{fuel} = \frac{F_{tot}}{VKT} = \frac{\frac{1}{1000}\sum_{i=1}^{N_{obs}} f_i \cdot \Delta t}{VKT}$$

$$VKT = \frac{1}{1000}\sum_{i=1}^{N_{obs}} v_i \cdot \Delta t$$

where $f_i$ is the instantaneous fuel consumption rate (mg/s) at observation $i$. Both the numerator and denominator are divided by 1000 to convert cumulative fuel consumption from milligrams to grams and cumulative travel distance from meters to kilometers, respectively. The resulting unit is g/veh-km. Fuel consumption was modeled using the HBEFA4/PC_petrol_Euro-4 emission model in SUMO and was applied identically to both AV and HV scenarios. Differences in fuel consumption intensity between AV and HV, therefore, reflect differences in vehicle speed profiles and acceleration–deceleration behavior rather than differences in the fuel consumption model itself.

Safety performance was characterized by two surrogate safety measures derived from the SSM output. The Low-TTC Events rate was defined as the number of conflict events with a minimum time-to-collision below 1.5 s, normalized by network exposure:

$$R_{TTC} = \frac{N_{TTC<1.5}}{VKT}$$

where $N_{TTC<1.5}$ is the total number of observed TTC events with TTC less than 1.5 s. Only events in which the recorded speed at the moment of minimum TTC was at or above 1.0 m/s were retained, to reduce false positives arising from near-stationary vehicles.

The Low-PET Events rate was defined as the number of conflict events with a post-encroachment time below 5.0 s, normalized by the number of intersections in the network:

$$R_{PET} = \frac{N_{PET<5.0}}{N_{int}}$$

where $N_{PET<5.0}$ is the total number of observed PET events with PET less than 5.0 s, $N_{int}$ denotes the number of valid intersections in the vehicle-accessible subgraph, excluding internal junctions and dead-end nodes, consistent with the feature extraction procedure described in Section 4.1.1. The TTC threshold of 1.5 s and the PET threshold of 5.0 s follow widely adopted conventions in the surrogate safety literature (Gettman et al., 2008). Prior to computing both metrics, mirror duplicates in the SSM output, conflict records in which the ego and foe vehicle identifiers are swapped but the event is otherwise identical, were removed by retaining only one record per unique vehicle pair and event signature, defined by the rounded event time, position, and conflict value.

## 4.2 Study Networks and Simulation Design

### 4.2.1 Selection of Study Networks

The study sample consisted of 12 urban traffic simulation networks selected from two sources. The first comprised publicly available SUMO scenarios obtained from peer-reviewed studies or the official SUMO scenario repository, each with documented construction details and calibrated demand inputs. The second consisted of two networks constructed by the research team (NparkSt and UGAcampus), built from OpenStreetMap base data and manually refined using field-collected traffic counts to represent the geometry and operational conditions of their real-world counterparts. Combining these two source types helped balance source credibility with variation in network form and operating context.

**TABLE 4.1 Selected networks and their feature values.**

| Network | City / Country | Road Length (km) | Demand Intensity (veh/h/km) | Signalized Intersection Percentage (signalized / all) | Road Density (km/km²) | Street Connectivity (links/nodes) |
|---|---|---|---|---|---|---|
| NParkSt | Madison / USA | 1.62 | 1792.28 | 100.00% | 17.54 | 1.05 |
| UGAcampus | Athens / USA | 4.19 | 415.71 | 4.00% | 17.87 | 1.12 |
| Bologna_Pasubio (Bieker et al., 2014) | Bologna / Italy | 17.11 | 528.99 | 46.88% | 10.19 | 1.28 |
| Bologna_Acosta (Bieker et al., 2014) | Bologna / Italy | 22.04 | 401.12 | 26.67% | 11.10 | 1.34 |
| MoST (Codecá & Härri, 2017) | Monaco | 39.48 | 23.71 | 0.82% | 1.03 | 0.94 |
| TAVF (David & Plötz, 2020) | Hamburg / Germany | 45.54 | 469.05 | 33.96% | 5.96 | 1.13 |
| InTAS (Lobo et al., 2020) | Ingolstadt / Germany | 110.56 | 112.61 | 3.94% | 1.31 | 0.87 |
| HaTS (Ostendorf et al., 2025) | Hanover / Germany | 112.82 | 69.31 | 6.76% | 8.48 | 1.19 |
| Dublin_Urban (Guériau & Dusparic, 2020) | Dublin / Ireland | 483.34 | 64.05 | 20.74% | 14.67 | 1.28 |
| Ingolstadt (Harth et al., 2021) | Ingolstadt / Germany | 652.40 | 34.91 | 1.46% | 8.86 | 0.98 |
| LuST (Codecá et al., 2015) | Luxembourg City / Luxembourg | 929.29 | 27.34 | 10.52% | 8.41 | 1.38 |
| Nagoya (Higuchi et al., 2024) | Nagoya / Japan | 1494.45 | 76.79 | 47.20% | 2.83 | 1.20 |

Network inclusion was governed by three criteria. First, representativeness: each network had to represent an urban road system; scenarios limited to freeways or closed-loop ring roads were excluded. The full set was also required to span diverse geographic contexts so that the analysis would not be dominated by region-specific features. Second, comparability: each network had to include, at a minimum, a network file (which encodes both road topology and signal control

logic) and a demand file; scenarios providing signal timing in a separate additional file were also accepted. Networks without signalized intersections were excluded, as signal control provides a critical context in which behavioral differences between AVs and HVs can emerge. Third, heterogeneity across network features: the final set needed to span a wide range of values across all 5 network features to support meaningful cross-network feature–performance analysis.

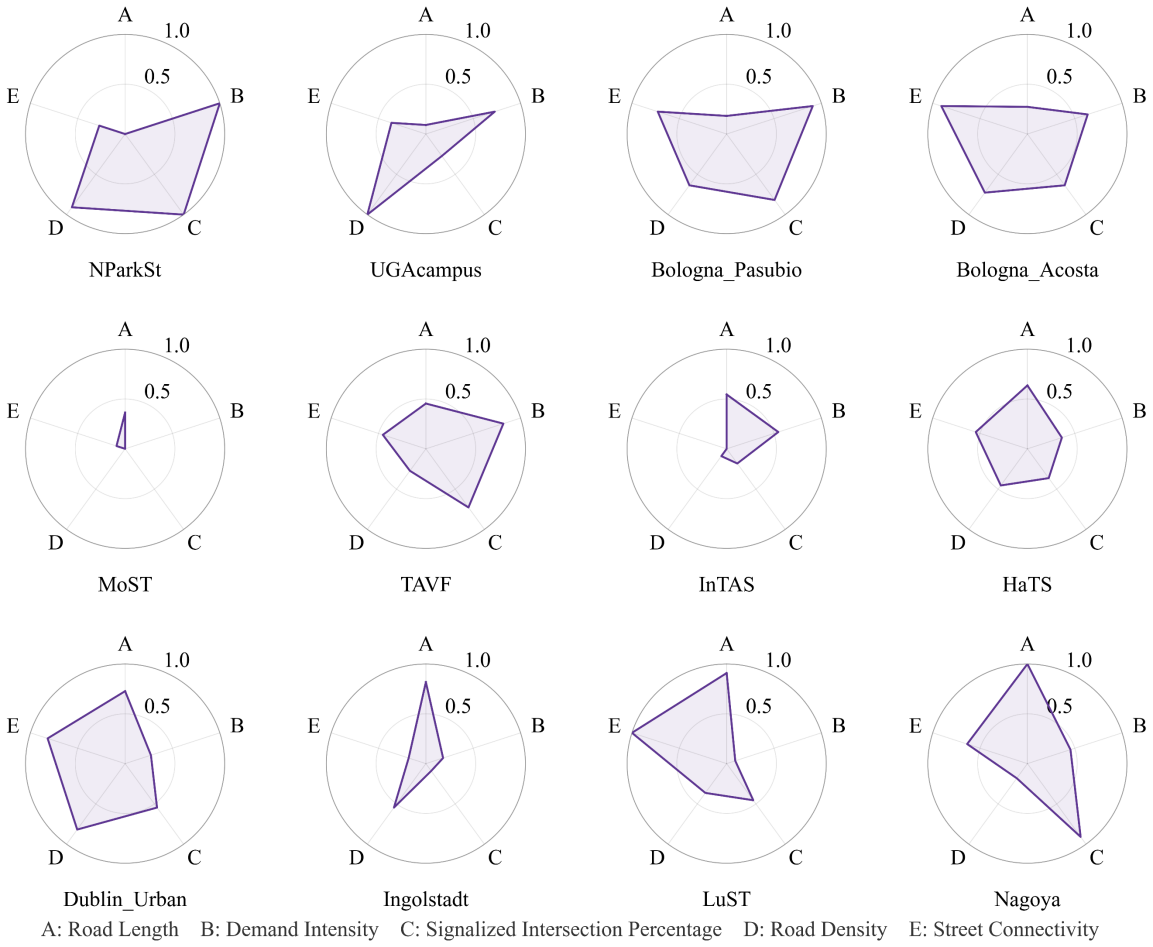


**Figure 4.2. Rank-based profiles of the 12 study networks across 5 features (A-E).**

The 12 selected networks span North America (2), Europe (9), and Asia (1), with total road length ranging from 1.6 km (NparkSt) to approximately 1,494 km (Nagoya), covering nearly three orders of magnitude (TABLE 4.1). To facilitate visual comparison across networks, the 5 feature values for each network are displayed as rank-based radar charts (Figure 4.2). Demand intensity

ranges from 23.7 to 1,792.3 veh/h/km, signalized intersection percentage from less than 1% to 100%, road density from 1.03 to 17.87 km/km², and street connectivity from 0.87 to 1.38. This heterogeneity is essential for the cross-network analysis that follows, as insufficient variation across features would limit the ability to detect meaningful feature–performance associations or assess whether they differ between HV and AV.

### 4.2.2 Simulation Settings

All simulations were conducted in SUMO (version 1.25.0) under a consistent configuration to ensure cross-network comparability. Each simulation covered a 1 h morning peak period, including an initial 10 min warm-up period. The warm-up period was excluded from subsequent analysis to minimize initialization effects. Accordingly, all reported performance measures were calculated over an effective 50 min analysis period.

To preserve empirical loading conditions, each network was simulated using its original observed morning-peak demand, without rescaling or synthetic substitution. The simulation time step was fixed at 0.1 s for all networks and scenarios. For each network, two scenarios were simulated: pure HV and pure AV. Within each network, the HV and AV scenarios shared the same network, demand input, simulation duration, temporal resolution, and seed set, so that differences between HV and AV can be attributed to behavioral parameterization rather than to scenario construction.

Each network was simulated using the same set of 5 seeds under both the HV and AV scenarios, and the reported results were obtained by averaging across the 5 runs for each scenario. For each run, vehicle-level outputs were first aggregated to the network level, and the final value for each network and scenario was then calculated as the mean across the 5 seeds. This design reduced stochastic variability and provided a consistent basis for comparing AV and HV

performance across networks. The definitions and aggregation methods for individual performance measures are provided in Section 4.1.2.

### 4.2.3 Vehicle Behavior Logic

Building on the selected study networks described in Section 4.2.1, this section specifies how vehicle behavior was represented within those networks during simulation. In each simulation network, vehicle behavior followed the logic shown in Figure 4.3. Initially, the vehicle follows the leading vehicle if no traffic signal is detected within a specified distance ($D^{lookahead} = 100\,m$, fixed in SUMO). When a traffic signal is detected within $D^{lookahead}$ and a leading vehicle is present between the vehicle and the signal, the vehicle continues to follow the leading vehicle. Otherwise, its behavior is determined by the signal indication and intended movement, with signal indications classified as red/yellow, green arrow, or green circle. Green arrows correspond to protected movements, whereas green circles permit straight-through and right-turn movements and require yielding for permissive left turns. The logic is as follows:

- If the traffic signal is red or yellow:
    - If the vehicle plans to turn right and the signal displays a red or yellow circle, the vehicle makes a permitted right turn after yielding to cross traffic.
    - Otherwise, the vehicle stops before the signal.
- If the traffic signal displays a green arrow:
    - If the vehicle plans to go straight, the vehicle proceeds straight through the intersection.
    - If the vehicle plans to turn right, the vehicle makes a protected right turn.
    - If the vehicle plans to turn left, the vehicle makes a protected left turn.
- If the traffic signal displays a green circle:

- If the vehicle plans to go straight, the vehicle proceeds straight through the intersection.
- If the vehicle plans to turn right, the vehicle makes a permitted right turn at green.
- If the vehicle plans to turn left, the vehicle makes a permitted left turn at green after yielding to cross traffic.

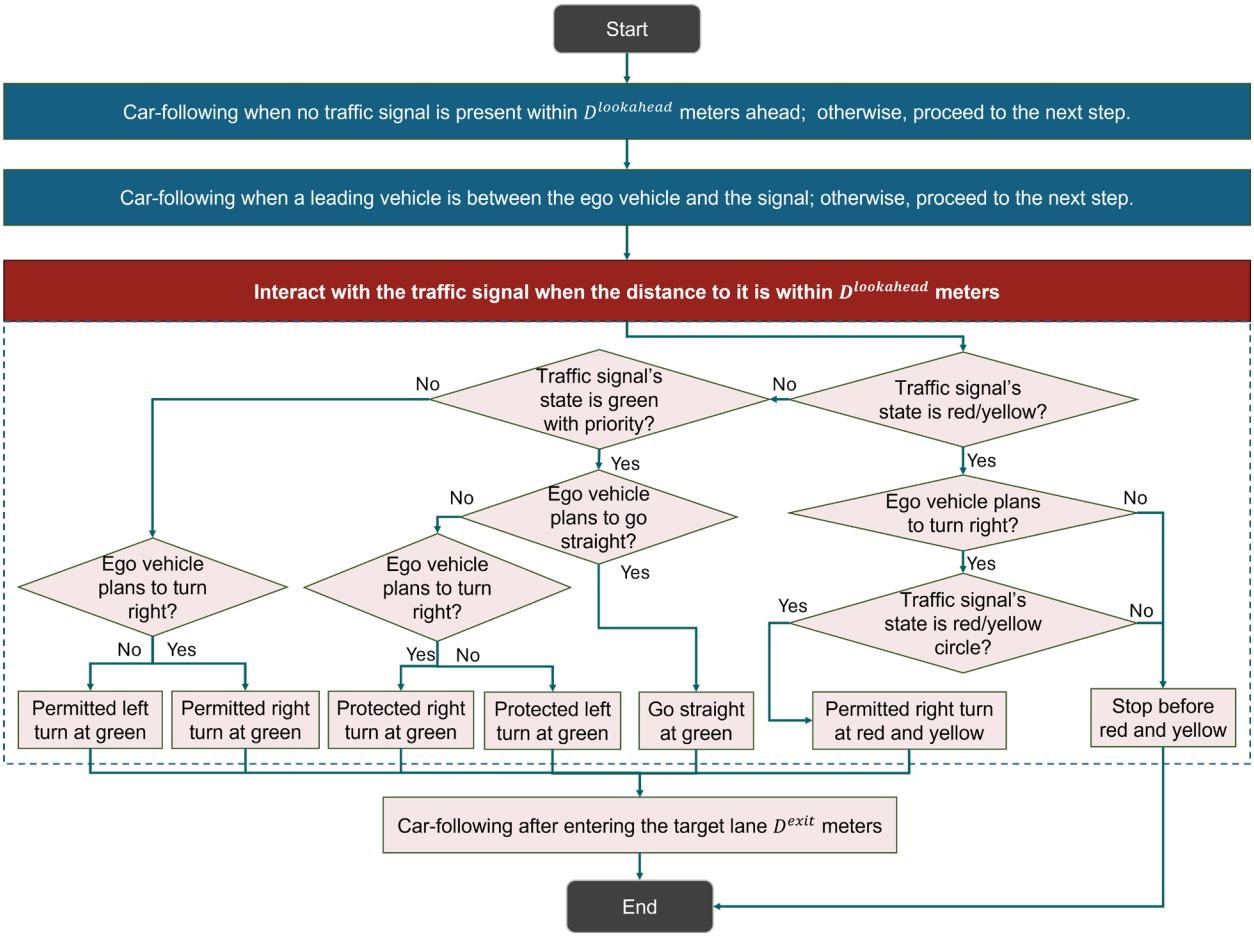


**Figure 4.3. Vehicle behavior in SUMO.**

Both AV and HV scenarios followed the same behavioral logic, except that, in the HV scenario, protected and permitted right-turn movements shared the same parameter set in the Right

Turn at Green model. After entering the target lane, the vehicle resumes car-following behavior at $D^{exit} = 5\ m$ beyond the stop line.

Longitudinal behavior in the car-following model was governed by the Intelligent Driver Model (IDM) in both AV and HV scenarios. The corresponding IDM parameters, together with the signal-interaction parameters for each movement type, differed by driving regime and are detailed in Section 4.2.4.

Lane-changing behavior was governed by SUMO's default LC2013 model in both scenarios, with no regime-specific modifications. Together with the shared behavior logic described above, this design ensures that any observed differences in network-level performance can be attributed primarily to differences in car-following and signal-response parameters rather than to differences in behavioral architecture or simulation structure.

### 4.2.4 AV and HV Parameterization

AV and HV scenarios followed the same behavioral logic described in Section 4.2.3 but differed in the parameter values used in the car-following model and signal-interaction mode. The parameterization, therefore, consisted of two components: IDM parameters governing longitudinal behavior when vehicles operated in the car-following model outside the signal-interaction range, and movement-specific parameters governing vehicle responses in signal-interaction mode from the point at which a signalized intersection was detected within $D^{lookahead}$ until the vehicle had moved $D^{exit}$ beyond the stop line.

When vehicles operated in the car-following model outside the signal-interaction range, longitudinal behavior was represented using the IDM. The AV and HV IDM parameters adopted in this study were taken from Jang et al. (2023), who calibrated the model using car-following data derived from the Waymo Open Dataset. TABLE 4.2 lists the adopted IDM parameters for AV and

HV in the car-following model outside the signal-interaction range. The calibrated AV parameters indicate more conservative longitudinal behavior than the HV parameters, including a larger minimum gap, a longer desired time headway, and a lower comfortable deceleration.

**TABLE 4.2 IDM parameters for AV and HV in the car-following model.**

| Parameter | Maximum acceleration ($m/s^2$) | Comfortable deceleration ($m/s^2$) | Minimum gap ($m$) | Desired time headway ($s$) | Desired speed ($m/s$) |
|---|---|---|---|---|---|
| AV | 1.68 | 0.88 | 6.04 | 1.41 | 12.49 |
| HV | 1.93 | 1.14 | 3.76 | 0.99 | 12.06 |

When vehicles operated in signal-interaction mode, movement-specific parameters were assigned for the signal-response behaviors defined in Section 4.2.3, including stop before red and yellow, go straight at green, protected turns, and permitted turns. These parameters were not recalibrated in the present study; instead, they were directly adopted from calibration results previously developed by the research team (Z. Li et al., 2026). In that calibration study, the AV signal-interaction parameters were calculated using processed Waymo Open Dataset trajectories reported in Li et al. (2025), whereas the HV signal-interaction parameters were calculated using the field dataset reported in Li, Zhang, et al. (2025). Unlike more conservative AV behavior in the car-following model, the calibrated signal-interaction parameters imply tighter temporal spacing for AVs during several green-phase intersection maneuvers. Shorter desired time headways and, in some cases, smaller minimum gaps indicate that AVs were parameterized to pass through signalized intersections in a more temporally compact manner than HVs for several green-phase maneuvers. This contrast highlights that AV and HV differed not only in car-following conservativeness but also in temporal spacing during selected signalized-intersection maneuvers. TABLE 4.3 summarizes the AV signal-interaction parameters by movement type, and TABLE 4.4 summarizes the corresponding HV parameters.

The present study used these previously calibrated parameter sets as fixed behavioral inputs rather than re-estimating them for the current network sample. This treatment was adopted because the objective of this study was to evaluate network-level performance differences across heterogeneous networks rather than to recalibrate microscopic behavioral models. Using previously calibrated, data-grounded parameter values allowed the analysis to focus on feature–performance relationships across heterogeneous networks while maintaining the same realistic behavioral representation for both HV and AV.

**TABLE 4.3 AV signal-interaction parameters by movement type.**

| Parameter \ Model | Stop before Red and Yellow | Go Straight at Green | Protected Left at Green | Protected Right Turn at Green | Permitted Right Turn at Green | Permitted Right Turn at Red and Yellow | Permitted Left Turn at Green |
|---|---|---|---|---|---|---|---|
| Maximum acceleration m/$s^2$ | 4.77 | 1.25 | 1.42 | 2.14 | 1.84 | 1.25 | 1.53 |
| Comfortable deceleration m/$s^2$ | 4.00 | 6.00 | 8.50 | 7.50 | 0.67 | 2.50 | 1.97 |
| Emergency braking deceleration m/$s^2$ | 7.50 | / | / | / | / | 2.5 | / |
| Minimum gap (m) | 2.50 | 2.21 | 0.55 | 0.55 | 1.11 | 1.75 | 1.97 |
| Desired time headway s | 1.63 | 1.09 | 0.55 | 0.89 | 1.78 | 1.75 | 0.75 |
| Desired speed m/s | 10.55 | 20.00 | / | / | / | / | / |
| Desired speed on entry lane m/s | / | / | 10.50 | 6.08 | 5.59 | 7.50 | 6.20 |
| Desired speed on exit lane m/s | / | / | 14.50 | 8.50 | 22.00 | 12.50 | 13.50 |
| Desired speed when entering junction m/s | / | / | 8.17 | 6.25 | 5.54 | 12.50 | 9.87 |
| Desired speed when exiting junction m/s | / | / | 14.50 | 6.51 | 6.02 | 12.50 | 11.61 |
| Base impatience | / | / | / | / | 0.50 | 0.25 | 0.20 |

**TABLE 4.4 HV signal-interaction parameters by movement type.**

| Parameter \ Model | Stop before Red and Yellow | Go Straight at Green | Protected Left at Green | Right Turn at Green | Permitted Right Turn at Red and Yellow | Permitted Left Turn at Green |
|---|---|---|---|---|---|---|
| Maximum acceleration m/$s^2$ | 0.37 | 1.26 | 1.32 | 1.42 | 1.04 | 1.82 |
| Comfortable deceleration m/$s^2$ | 2.31 | 3.06 | 1.10 | 0.67 | 5.00 | 0.57 |
| Emergency braking deceleration m/$s^2$ | 1.85 | / | / | / | 7.00 | / |
| Minimum gap (m) | 2.41 | 5.97 | 1.92 | 2.00 | 1.00 | 2.00 |
| Desired time headway s | 2.55 | 2.26 | 2.00 | 2.67 | 1.50 | 5.10 |
| Desired speed m/s | 12.61 | 17.30 | / | / | / | / |
| Desired speed on entry lane m/s | / | / | 5.72 | 4.22 | 12.00 | 8.00 |
| Desired speed on exit lane m/s | / | / | 11.00 | 10.00 | 12.00 | 10.00 |
| Desired speed when entering junction m/s | / | / | 5.73 | 4.67 | 10.00 | 10.00 |
| Desired speed when exiting junction m/s | / | / | 11.00 | 10.00 | 10.00 | 10.00 |
| Base impatience | / | / | / | / | 0.20 | 0.20 |

## 4.3 Cross-Network Results and Analysis

This section presents the cross-network analysis of AV and HV performance and examines its associations with network features. It first compares overall AV and HV performance across the 12 study networks, then evaluates pairwise feature–performance associations using Spearman rank correlations. Finally, trend analysis is subsequently used to explore potential nonlinear trends that may not be fully captured by monotonic correlations alone.

### 4.3.1 Descriptive Comparison of AV and HV Performance

Before examining how AV–HV performance differences vary with network features, this section provides a descriptive overview of the overall performance differences between HV and AV across the 12 study networks. Improvement-oriented differences are defined such that positive values consistently indicate better AV performance: AV−HV for average travel speed, and

HV−AV for average delay, fuel consumption intensity, low TTC events, and low PET events. Figure 4.4 presents the cross-network distribution of these differences, and TABLE 4.5 reports the corresponding statistics. In the figure, networks are ordered by ascending road length, and panel-specific x-axis ranges are used to improve readability.

For efficiency and environmental outcomes, AV consistently outperformed HV across most study networks. Average travel speed was higher under AV in all 12 networks, and average delay was lower in 11 of 12. Fuel consumption intensity followed a similar pattern, with AV exhibiting lower values in 10 of 12 networks. Across all three outcomes, the magnitude of the AV advantage varied substantially across networks, indicating that the efficiency and environmental gains associated with AV deployment were not uniform across the study networks.

**TABLE 4.5 Summary statistics of AV–HV descriptive differences.**

| Outcome | Mean AV | Mean HV | AV Better (n/12) | Range of Differences |
|---|---|---|---|---|
| Average Travel Speed (m/s) | 5.57 | 4.39 | 12/12 | 0.25 to 2.12 |
| Average Delay (s/veh) | 197.96 | 250.84 | 11/12 | -2.22 to 134.62 |
| Fuel Consumption Intensity (g/veh-km) | 122.82 | 154.73 | 10/12 | -12.32 to 78.91 |
| Low TTC Events (#/veh-km) | 0.1 | 0.01 | 1/12 | -0.15748 to 0.00001 |
| Low PET Events (#/junction) | 1.73 | 1.12 | 0/12 | -2.19325 to -0.00216 |

The surrogate safety outcomes showed the opposite overall tendency. Low TTC event frequency was higher under AV than HV in 11 of 12 networks, with the single exception showing only a negligible difference. Low PET event frequency was likewise higher under AV across the study networks. This near-universal pattern of elevated surrogate safety exposure under AV stood in clear contrast to the efficiency and environmental improvements, indicating that the effects of

AV deployment were not consistent across performance dimensions. The cross-network variability observed across all performance dimensions motivates the subsequent investigation of whether specific network feature characteristics systematically condition the direction and magnitude of the AV–HV performance differential.

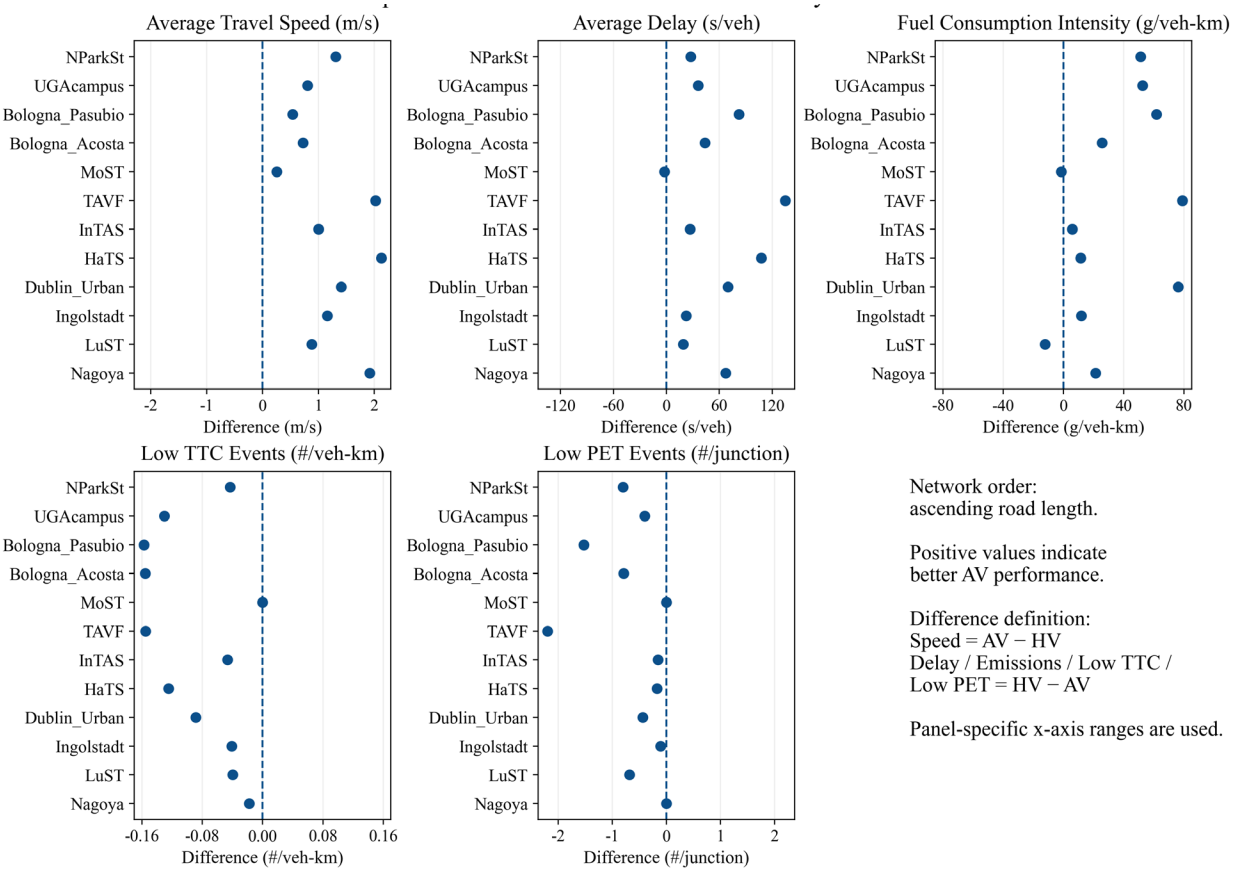


**Figure 4.4. Improvement-oriented AV–HV performance differences across 12 networks.**

### 4.3.2 Correlation Analysis between Network Features and Performance Measures

This section examines the pairwise Spearman correlations between network features and performance measures under the AV and HV regimes. Figure 4.5(a) and (b) present the baseline feature–performance correlations for each HV and AV separately, while Figure 4.5(c) shows shifts in association strength ($\Delta\rho = \rho_{AV} - \rho_{HV}$). To assess whether the relative AV effect is itself feature-dependent, Figure 4.5(d) relates network features to raw AV–HV performance differences;

for delay, fuel consumption intensity, and surrogate safety outcomes, negative coefficients indicate that higher feature values are associated with larger relative AV improvements. Overall, this analysis evaluates whether feature–performance associations remain directionally consistent across HV and AV, whether their strength changes under AV, and whether the relative AV effect varies systematically with network features.

As shown in Figure 4.5(a) and (b), the broad feature–performance patterns are similar under AV and HV. Demand intensity is the feature most strongly and consistently associated with performance under both HV and AV: it is negatively correlated with average travel speed and positively correlated with fuel consumption intensity, low TTC events, and low PET events, consistent with the MFD framework in which network performance deteriorates as loading increases (Geroliminis & Daganzo, 2008). Road density shows a broadly similar pattern, with denser networks associated with lower speed and higher fuel consumption intensity and surrogate safety event frequencies, in line with evidence linking denser or more interruption-prone networks to reduced travel efficiency (Akandwanaho & Nakamura, 2020b; Wong et al., 2021). Road length exhibits the opposite tendency: longer networks are associated with higher speed and lower fuel consumption intensity and surrogate safety event frequencies, consistent with the view that larger-scale networks better support continuous progression (Akandwanaho & Nakamura, 2020b; HCM, 2022). Signalized intersection percentage shows directionally consistent associations across several outcomes, with more highly signalized networks tending to have lower speed and higher fuel consumption intensity and surrogate safety event frequencies, extending intersection-level evidence on stop-and-go effects to the network scale (Pandian et al., 2009). Street connectivity shows comparatively weaker and less consistent associations across all 5 measures.

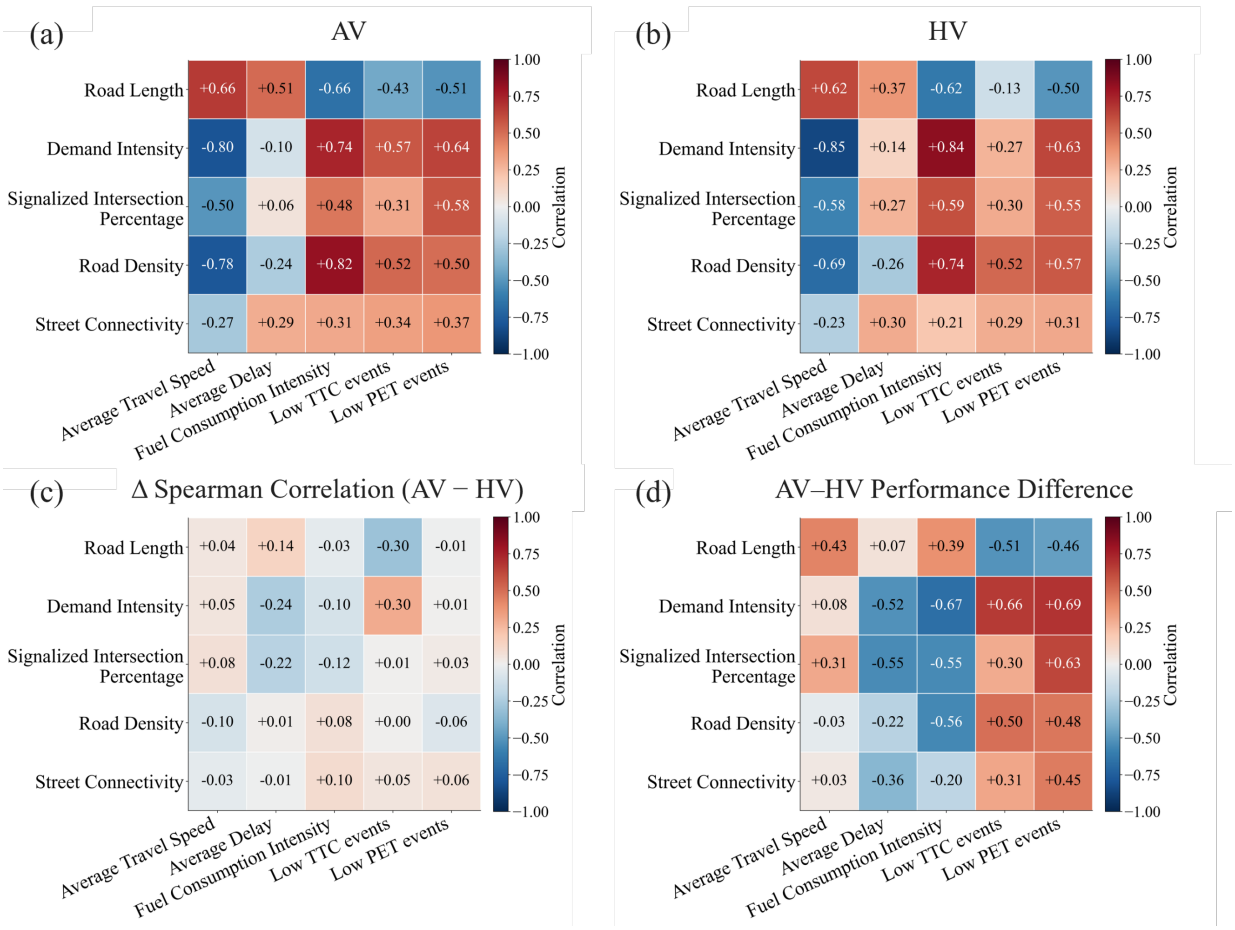


**Figure 4.5. Spearman correlations between network features and performance measures under AV and HV regimes, cross-regime changes in feature–performance association strength, and correlations between network features and AV–HV performance differences.**

Although these overall patterns are broadly similar across HV and AV, Figure 4.5(c) shows that the strength of several associations shifts under AV, particularly for surrogate safety outcomes. The clearest changes involve low TTC events. The positive correlation between demand intensity and low TTC events strengthens from +0.27 under HV to +0.57 under AV ($\Delta\rho = +0.30$), indicating that TTC-related risk becomes substantially more sensitive to traffic loading under AV. At the same time, the negative correlation between road length and low TTC events also becomes stronger under AV ($\Delta\rho = -0.30$), suggesting that the mitigating effect of larger network scale on

TTC risk is more pronounced under AV. Signalized intersection percentage also shows regime-dependent changes, with its positive association with average delay weakening under AV ($\Delta\rho$ = −0.22), alongside a modest weakening of its association with fuel consumption intensity. For road density and street connectivity, cross-regime changes in correlation strength are comparatively modest, suggesting that their associations with performance are more stable across HV and AV. Taken together, these shifts indicate that AV does not simply reproduce the same feature–performance relationships observed under HV, but exhibits different sensitivities to the same network feature set; the safety implications of AV deployment in particular appear more feature-dependent than those of HV, and cannot be assessed independently of the network context.

Figure 4.5(d) further shows that the relative AV effect is itself feature-dependent. Demand intensity, road density, and signalized intersection percentage all exhibit the same directional pattern: higher values of these features are associated with lower AV–HV differences in fuel consumption intensity but higher AV–HV differences in surrogate safety outcomes. For demand intensity, the correlations are −0.67 for fuel consumption intensity and +0.66 and +0.69 for low TTC and low PET, respectively. Road density shows a similar structure (−0.56 for fuel consumption intensity, +0.50 and +0.48 for low TTC and low PET). Signalized intersection percentage follows the same directional pattern, with negative correlations for fuel consumption intensity and delay ($\rho$ = −0.55 for both) and positive correlations for low TTC and low PET ($\rho$ = +0.30 and +0.63). Taken together, these results indicate that network conditions associated with larger relative AV gains in fuel consumption intensity also tend to be associated with less favorable relative AV surrogate safety outcomes. This pattern holds consistently across the three loading- and density-related features, but is reversed for network scale. Road length shows the opposite tendency. It is positively correlated with the AV–HV differences in average travel speed and fuel

consumption intensity ($\rho = +0.43$ and $+0.39$, respectively), but negatively correlated with the AV–HV differences in low TTC and low PET ($\rho = -0.51$ and $-0.46$, respectively). This suggests that longer networks are associated with a more favorable relative AV effect for speed and surrogate safety, but a weaker relative AV advantage for fuel consumption intensity.

Overall, no single network context makes AV uniformly superior across all performance dimensions. Instead, the relative AV effect varies systematically with network features, underscoring the need to evaluate AV impacts at the network scale rather than only at the vehicle or corridor level. This feature-dependent divergence provides the empirical basis for the subsequent trend analyses.

### 4.3.3 Trend Analysis between Network Features and Performance Measures

This subsection applies trend analysis to examine how performance responses vary across network features under AV and HV regimes, complementing and extending the Spearman correlation analysis in Section 4.3.2. While Spearman coefficients capture the direction and strength of monotonic associations, they cannot reveal threshold effects, non-monotonic relationships, or divergences in curve shape between HV and AV across the feature range. The analysis, therefore, moves beyond average performance comparisons to examine whether AV and HV share similar response directions, whether AV responds more rapidly or more gradually, whether its curves are smoother, and whether AV–HV differences are systematically amplified within specific feature ranges. In this sense, the analysis moves from a comparison of association strength to a comparison of response curves.

The smoothed curves were plotted separately for AV and HV for each feature–outcome pair (Figures 4.6–4.10). Because only 12 networks are included and feature values are highly unevenly distributed across networks, demand intensity, for example, spans approximately 24 to

1792 veh/h/km, the horizontal axis was defined as each network's rank on the corresponding feature (1 to 12, ascending). This treatment mitigates the leverage of extreme values and yields a more stable representation of cross-network trends. The rank axis indicates relative ordering only and does not imply equal spacing in the original feature values. The smoothing parameter was set to 0.75 to emphasize broad trends over local noise. Shaded bands represent 90% bootstrap confidence intervals based on 1000 resamples, reflecting estimation uncertainty under the small-sample setting. The Spearman coefficients annotated in each panel were computed in the same manner as in Section 4.3.2 and are included for reference; the primary analytical focus here is on trend-shape comparison rather than formal significance testing of differences in curve shape.

Before turning to individual feature–performance trends, it is worth noting that the AV–HV trend differences examined here reflect a coherent behavioral basis in the underlying parameter configuration. The AV regime does not operate uniformly more conservatively or more aggressively across all driving contexts. On links, AV adopts lower maximum acceleration and comfortable deceleration, a larger minimum gap, and a longer desired time headway, reflecting a car-following strategy oriented toward flow stability and oscillation suppression. Near signalized intersections, by contrast, AV uses smaller minimum gaps, shorter time headways, and higher approach, departure, and crossing speeds across multiple movement types, indicating more regular, compact, and efficient operations in the intersection. The feature-conditioned performance differences examined below should therefore be understood as the network-level expression of this context-dependent behavioral reconfiguration: stabilizing along links while becoming more compact and throughput-oriented at nodes.

In the figures, red solid lines and blue dashed lines denote trend fits for AV and HV, respectively, with red square and blue hollow circle markers indicating raw observed values.

Within-network AV–HV differences are visualized through gray vertical segments connecting the two observations. Given the limited sample size, fitted curves near the rank extremes are more strongly influenced by individual observations, resulting in wider confidence bands. The emphasis is therefore placed on overall cross-network trend patterns, curve shape, and the relative positions of the AV and HV curves, rather than on fine-grained local fluctuations.

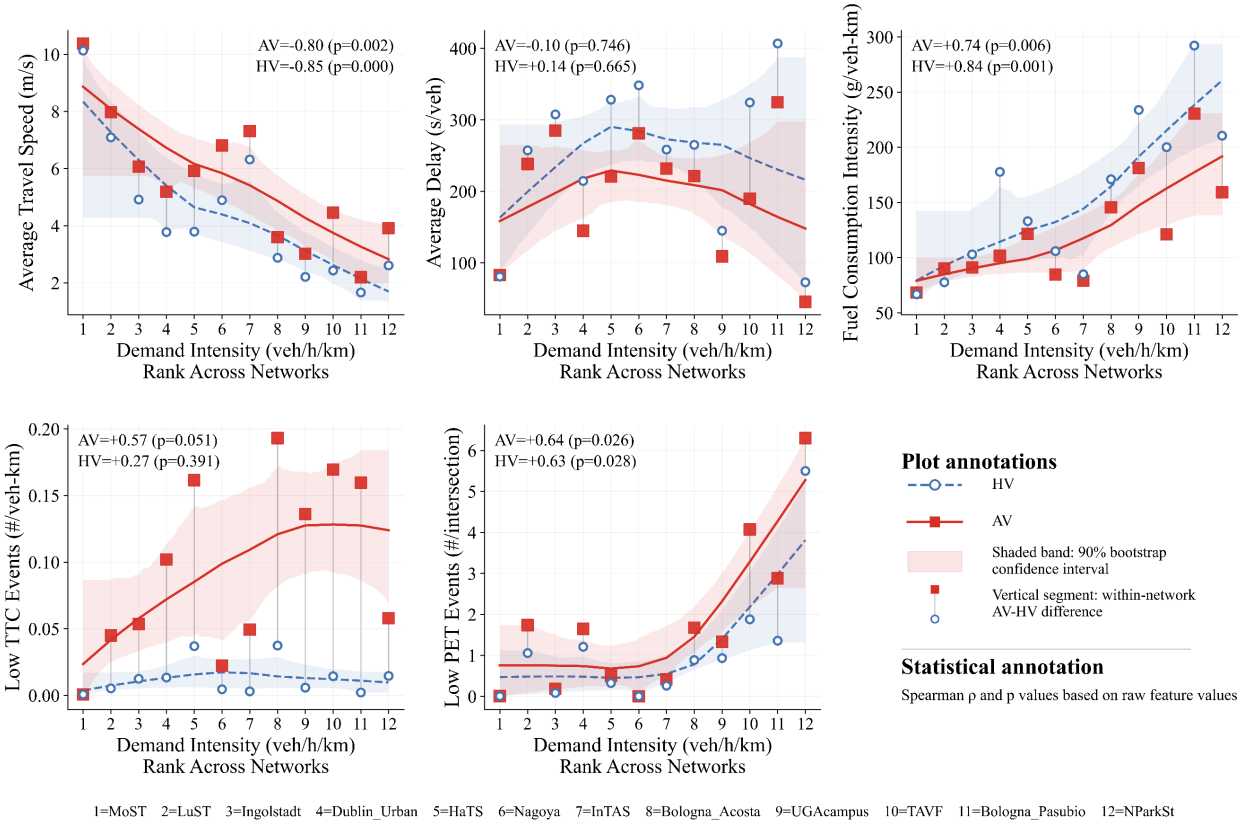


**Figure 4.6. Feature–performance trends across demand intensity under AV and HV.**

Figure 4.6 presents the trends between demand intensity and the 5 performance outcomes. As established in Section 4.3.2, demand intensity shows the strongest and most consistent feature–performance associations under HV and AV; the focus here is on how the response curves of AV and HV diverge across the demand range.

For average travel speed, both curves decline monotonically with increasing demand intensity, with the AV curve positioned systematically above HV across the full range, indicating a generally higher speed level under AV across the demand range. The two curves follow similar slopes, suggesting that demand-induced speed suppression operates with comparable intensity under HV and AV. Average delay exhibits a non-monotonic, hump-shaped response under both AV and HV, consistent with the near-zero Spearman coefficients reported in Section 4.3.2. The two curves follow similar trends, though the AV curve falls slightly below HV at the high-demand end, suggesting a possible delay advantage under the highest loading conditions; given the wide confidence bands in that interval, however, this tendency should be treated as exploratory rather than conclusive.

Of the 5 performance outcomes, fuel consumption intensity shows the most pronounced AV–HV curve difference across the demand range. The AV curve lies systematically below HV across the entire demand range, and the gap between the two curves widens at higher demand levels. This pattern is consistent with AV's more conservative longitudinal car-following behavior on links, larger minimum gaps and longer desired time headways reduce the amplitude of acceleration and deceleration cycles. In higher-demand networks where flow disturbances are more frequent, this oscillation-suppressing effect becomes relatively more effective, producing a progressively larger fuel consumption advantage over HV as demand intensity increases.

The surrogate safety outcomes, however, exhibit a qualitatively different pattern of regime divergence and therefore warrant separate discussion, because the behavioral mechanisms underlying low TTC and low PET events differ fundamentally. For low TTC events, the HV curve remains largely flat across the demand range, while the AV curve rises steeply from the mid-to-high demand interval and substantially exceeds HV at the upper end, with the gap between the two

curves widening markedly with demand. This pattern corroborates the $\Delta\rho = +0.30$ identified in Section 4.3.2, indicating that AV's TTC-related surrogate safety exposure is substantially more sensitive to network loading than that of HV. Although AV adopts larger desired gaps, its more regular and stable car-following state reduces the stochastic spacing variability between vehicles, causing spatiotemporal proximity events to breach the TTC threshold more frequently, an effect that intensifies as demand increases. For low PET events, the AV curve is uniformly elevated above HV across the full demand range, with the two curves rising approximately in parallel, a pattern that contrasts with the demand-driven divergence observed for low TTC events. The relatively stable AV–HV gap across the demand range for low PET suggests that its elevation is not primarily mediated by loading level. Unlike TTC, the increase in low PET events reflects AV's more compact intersection-level behavior, smaller minimum gaps, shorter time headways, and higher approach and crossing speeds near signalized intersections, which reduces spatiotemporal margins at conflict points and generates more frequent surrogate conflict exposure. This mechanism operates independently of car-following in the road segment, explaining why the demand-response shape for low PET differs from that of low TTC.

Taken together, the demand intensity trends reveal three distinct regime-specific contrasts: AV maintains a systematic speed advantage and a progressively widening fuel consumption benefit as demand increases; AV's TTC surrogate safety exposure is markedly more demand-sensitive than HV's, with the gap expanding sharply at high loading levels; and AV's PET exposure consistently exceeds HV's across all demand levels, driven by intersection-level behavioral differences rather than car-following in road segment. These contrasts collectively point to a demand-mediated divergence in which efficiency and environmental gains under AV coexist with elevated surrogate safety exposure, a pattern that intensifies as network loading increases.

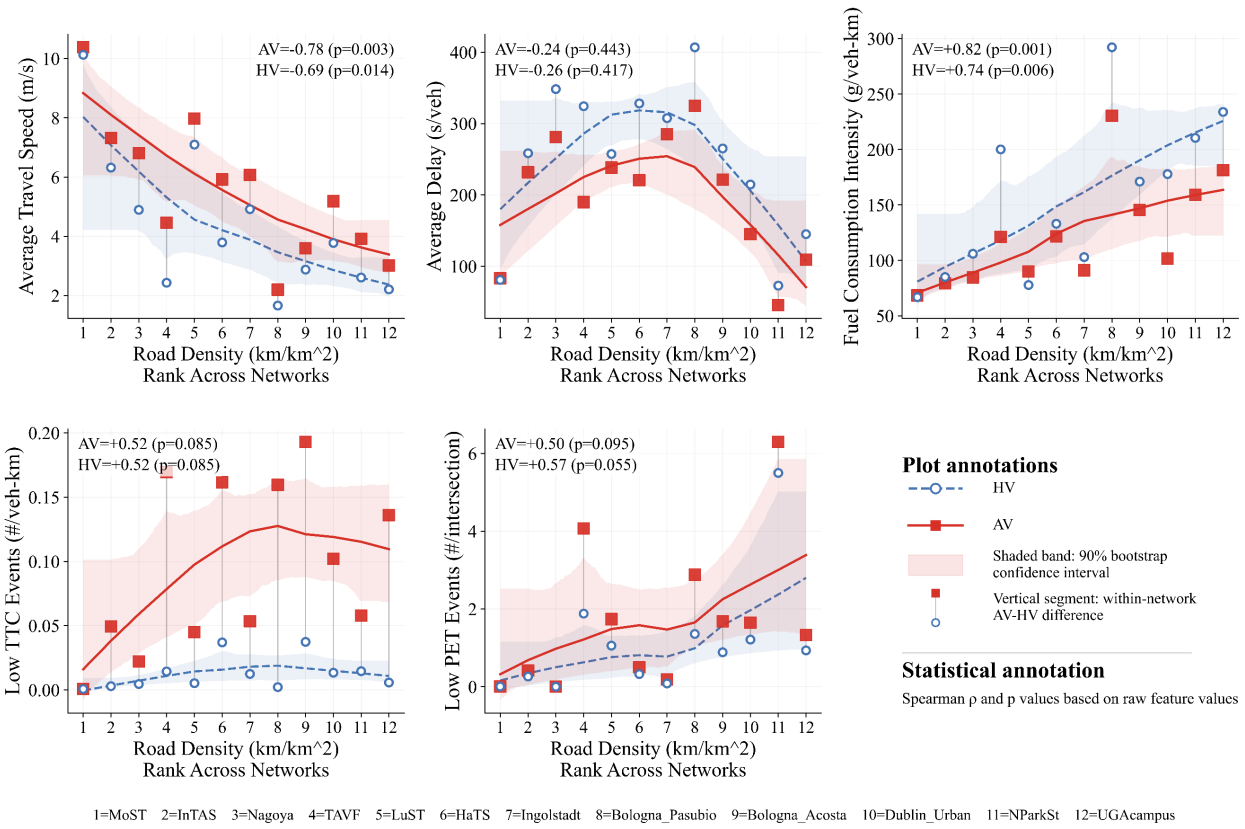


**Figure 4.7. Feature–performance trends across road density under AV and HV.**

Figure 4.7 presents the trends between road density and the 5 performance measures. Overall, road density exhibits a feature–performance direction and AV–HV divergence pattern similar to those of demand intensity.

Average travel speed declines monotonically under HV and AV, with the AV curve remaining consistently above the HV curve across the full density range. The inter-regime gap remains stable across density levels, indicating a persistent speed advantage under AV. Average delay follows an inverted-U pattern under both HV and AV, increasing at low-to-moderate density and declining at the high-density end, with the AV curve falling slightly below HV in the upper range. However, the Spearman correlations are not statistically significant (AV: $\rho = -0.24$, $p = 0.443$; HV: $\rho = -0.26$, $p = 0.417$), so this pattern is treated as exploratory. A plausible interpretation involves two competing mechanisms. At low-to-moderate density, more frequent intersections and

signal interactions introduce stop-and-go movements and queueing, which increase per-vehicle delay. At higher density, networks tend to be more spatially compact with shorter average trip lengths, which can partly offset this effect since average delay is measured per vehicle rather than per vehicle-kilometer. The similar curve shapes under AV and HV further suggest that this pattern is primarily shaped by network characteristics rather than driving regime.

Fuel consumption intensity shows the clearest AV–HV curve difference across the road density range. The AV curve lies systematically below the HV curve across the full density range, with the gap widening at higher density levels, so the fuel consumption advantage of AVs becomes more pronounced in denser networks. Such a pattern accords with AVs' more conservative longitudinal car-following behavior on links: more frequent intersection-induced disturbances in high-density networks create greater scope for the acceleration-smoothing effect of AVs to translate into larger environmental gains.

Low-TTC and low-PET events exhibit distinct response characteristics. For low-TTC events, the Spearman correlation coefficients for AV and HV are identical (both $\rho = +0.52$), and the two curves share the same overall positive direction, yet the AV curve remains consistently above the HV curve across the full density range. Unlike the demand intensity pattern, where the AV–HV gap widens progressively through the mid-to-high demand range, here the gap opens primarily at low-to-moderate density levels and subsequently stabilizes, without further notable divergence at the high-density end. Road density appears to elevate AV exposure to near-conflict TTC events while shaping a gap that emerges earlier and then remains elevated, rather than continuing to widen through the upper range as it does under demand intensity. For low-PET events, the AV curve likewise lies above the HV curve throughout, with both rising as road density increases. Although the Spearman coefficient for HV ($\rho = +0.57$) is marginally higher than that

for AV (ρ = +0.50), the difference is too small to support a firm interpretation in this small sample. The AV–HV separation in low PET remains elevated, but its rate of separation does not continue to increase in the way observed under demand intensity.

Overall, the road density trends mirror those observed under demand intensity in the efficiency and environmental dimensions, particularly in the widening fuel consumption advantage of AVs at higher density levels. By contrast, in the surrogate safety dimension, the TTC gap under road density emerges earlier and then remains elevated, rather than widening progressively through the upper range as observed under demand intensity. A similar pattern applies to low PET: the AV curve remains above the HV curve throughout, but the inter-regime separation does not continue to widen at the high-density end.

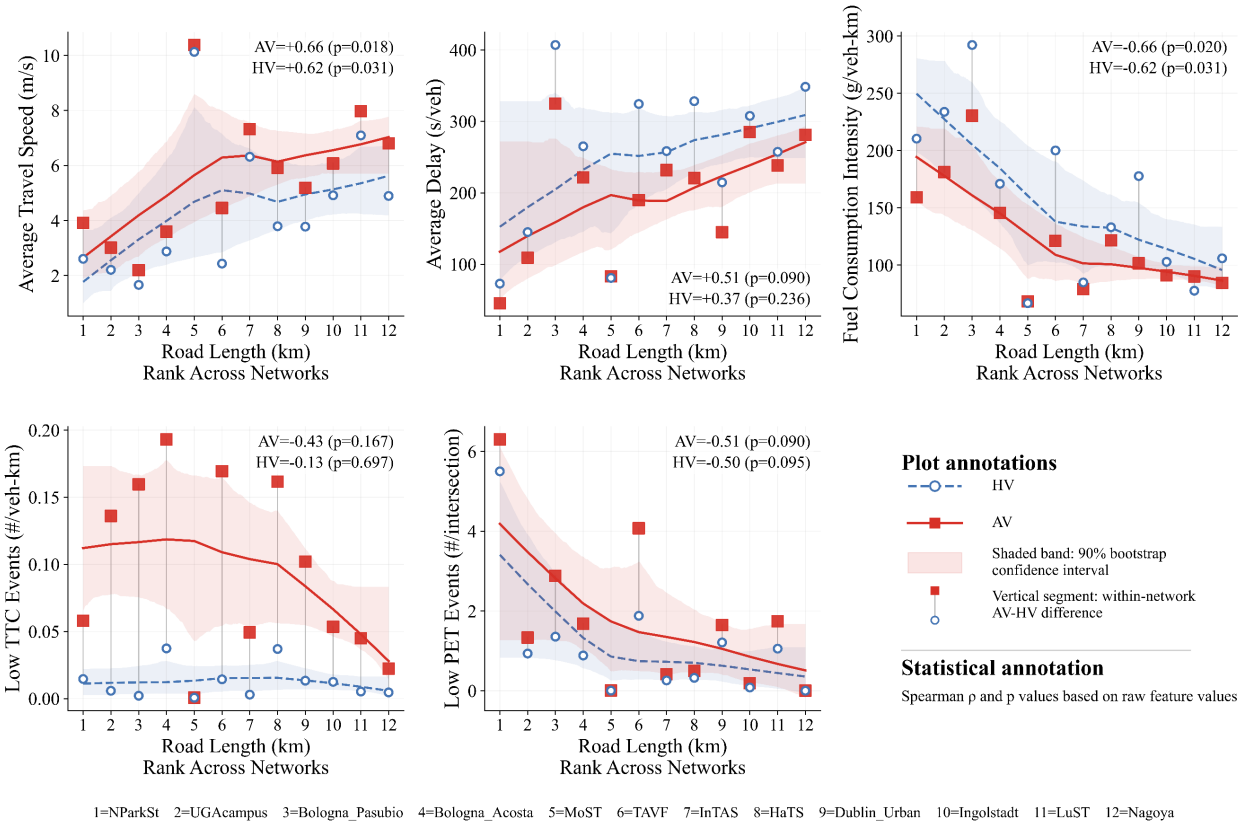


**Figure 4.8. Feature–performance trends across road length under AV and HV.**

Figure 4.8 presents the trends between road length and the 5 performance outcomes. Overall, the AV–HV response pattern under road length differs from those observed under demand intensity and road density. Its most notable role lies not in further enlarging AV's environmental advantage, but in reshaping the inter-regime gap in surrogate safety outcomes.

Average travel speed increases under HV and AV as road length becomes larger, with the AV curve generally remaining above HV across the full range. This shows that increasing road length does not change the direction of AV's speed advantage. The two curves follow similar shapes, indicating that the speed-improving effect of longer networks is broadly comparable under HV and AV. Average delay rises overall with road length under HV and AV, while the AV curve remains generally below HV across the range, indicating a persistent delay advantage under AV. However, uncertainty is greater at the short-length end, so this difference should be interpreted cautiously.

Fuel consumption intensity shows a different AV–HV separation pattern from that observed under demand intensity and road density. Although the AV curve remains below HV throughout, the gap is larger in shorter networks and gradually narrows as road length increases. This indicates that AV's environmental advantage is stronger in shorter networks, but is not further amplified by longer network length. The mechanism still lies in road segment acceleration smoothing, but longer and more continuous operating conditions also allow HV to benefit from smoother flow, reducing the environmental contrast between HV and AV.

Low TTC and low PET both decline as road length increases, but their inter-regime divergence patterns differ. For low TTC events, the HV curve remains low and changes only gradually, whereas the AV curve starts from a much higher level in shorter networks and declines steadily with road length. As a result, the AV–HV gap progressively narrows. This indicates that

longer networks weaken AV's relative disadvantage in TTC exposure. Because low TTC mainly reflects spatiotemporal proximity during link-based car-following, the result suggests that longer networks help reduce the frequent TTC triggering associated with AV's regular and continuous following state. For low PET events, both AV and HV curves also decline with road length, and their Spearman coefficients are nearly identical (AV = −0.51, HV = −0.50). The AV curve is higher than HV in shorter networks, but the two curves gradually converge across the mid-to-high length range. This indicates that longer networks also reduce AV's additional exposure in intersection-based surrogate safety, although the convergence is more gradual than for TTC. Because low PET is mainly shaped by compact behavior near conflict points, longer networks do not remove this tendency in the intersection, but they do weaken its cumulative expression at the network level.

Taken together, the road length trends reveal two main AV–HV contrasts. First, AV's fuel consumption advantage is more pronounced in shorter networks, but does not continue to widen as road length increases. Second, the inter-regime gap in surrogate safety, especially for low TTC, narrows steadily with increasing road length. Overall, longer networks appear more effective in alleviating AV's surrogate safety disadvantage, whereas shorter networks make its environmental benefit more visible.

Figure 4.9 presents the trends between signalized intersection percentage and the 5 performance outcomes. Overall, the AV–HV response differences under signalized intersection percentages are reflected mainly in flatter operational and environmental responses, together with stronger sensitivity in node-related surrogate safety exposure. This feature is particularly important because the present study incorporates detailed movement-specific behavioral parameters for signal-interaction scenarios, allowing the behavioral differences between AV and HV under signal control to be captured more directly.

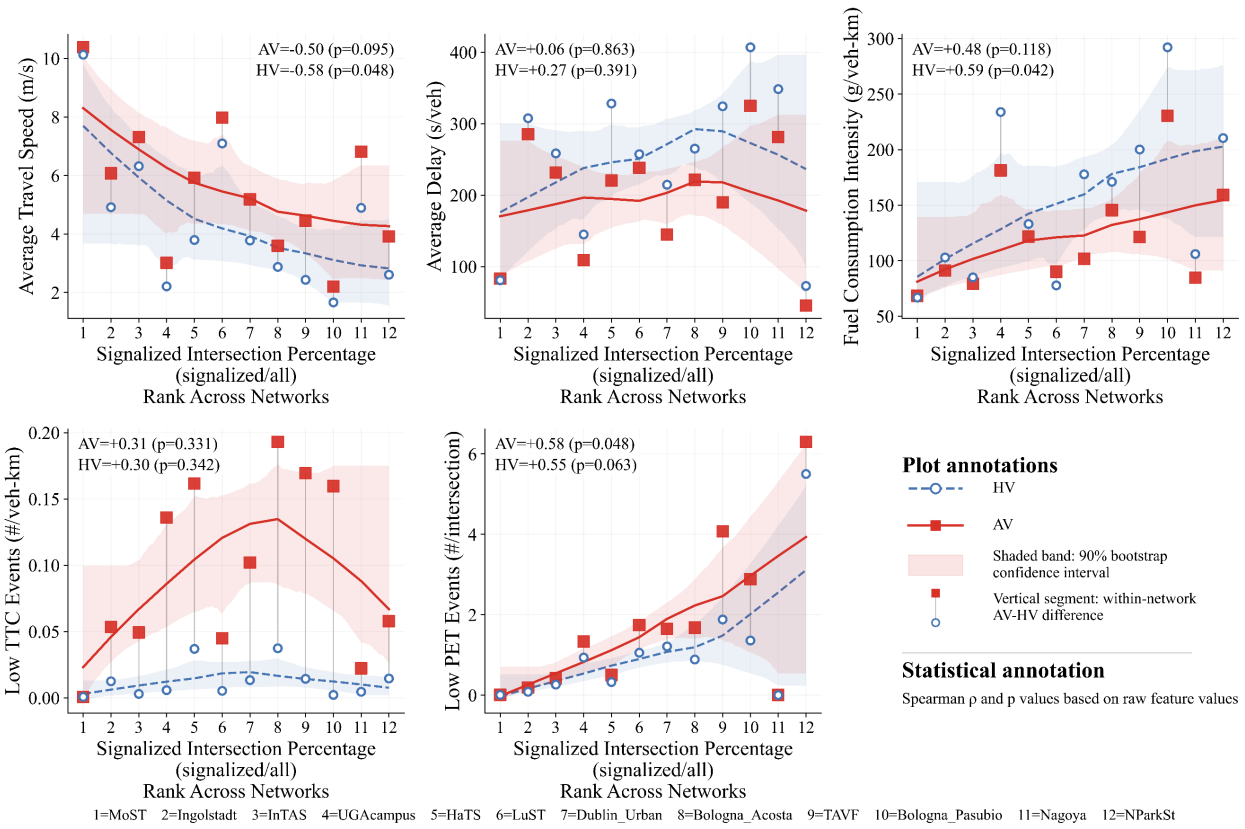


**Figure 4.9. Feature–performance trends across signalized intersection percentage under AV and HV.**

Average travel speed declines under both AV and HV as signalized intersection percentage increases. The AV curve remains generally above HV across the full range and is flatter than the HV curve, indicating that a higher level of signalization does not alter the direction of AV's speed advantage, but instead is associated with a smoother deterioration pattern in speed. This flatter response is also consistent with the slightly weaker negative association under AV than under HV ($\rho = -0.50$ vs. $-0.58$). This likely reflects more regular and efficient AV movement near signalized intersections, where smaller minimum spacing, shorter headways, and higher entry and crossing speeds help maintain more continuous operations under frequent signal interruptions. Average delay also follows a non-monotonic pattern under HV and AV, but the AV curve is flatter overall and remains below HV across most of the range. In the low-to-mid signalization range, delay rises

more clearly under HV, whereas the AV response is more restrained, suggesting that AV is less sensitive to operational deterioration as signalized intersection percentage increases. This interpretation is also in line with the near-flat Spearman coefficient under AV ($\rho = +0.06$), compared with the somewhat stronger positive tendency under HV ($\rho = +0.27$). Given the wide confidence bands at the upper end, however, this should be treated as a trend-level observation.

Fuel consumption intensity shows a clear AV–HV separation pattern. The AV curve remains below HV throughout the full range, and its rate of increase is flatter, indicating a smoother fuel-consumption response under AV as signalized intersection percentage rises. The same tendency is reflected in the weaker positive association under AV than under HV ($\rho = +0.48$ vs. $+0.59$). As in the demand intensity and road density results, this pattern can still be linked to AV's more conservative and stable longitudinal control on links, here expressed more clearly through its greater ability to smooth speed fluctuations under frequent signal interruptions. A higher level of signalization does not weaken AV's environmental advantage, but instead is associated with a flatter fuel-consumption curve.

Low TTC and low PET show different response patterns. For low TTC events, the AV curve stays well above HV throughout the range, while the HV curve remains close to zero and shows little variation with signalization. The AV curve first rises from the low to the mid-to-high signalization range and then turns downward, reaching its peak around the mid-to-high range before declining toward the upper end. This indicates that AV's exposure to low-TTC events does not increase monotonically with signalization but instead follows a clear non-monotonic pattern. A plausible interpretation involves two opposing effects. In the low-to-moderate signalization range, more signal-controlled intersections lead to more frequent stop-and-go movements and closer car-following behavior under AV, which increases low-TTC events. In the high

signalization range, however, AV speeds drop noticeably (as seen in the speed panel), and since TTC depends on the relative speed between vehicles, lower travel speeds reduce the chance of triggering low-TTC events even when vehicles remain close.

For low PET events, both curves rise as signalized intersection percentage increases, but the AV curve remains above HV and rises more rapidly in the high-signalization range. Since PET is primarily shaped by movement behavior near conflict points, this pattern is consistent with AV's smaller minimum gaps, shorter headways, and higher entry and crossing speeds in signal-interaction scenarios. A higher signalized intersection percentage implies more frequent interactions at the intersection, and AVs' more compact and efficient movement execution correspondingly reduces spatiotemporal margins near conflict points, thereby increasing PET exposure.

Taken together, the AV–HV differences under signalized intersection percentage are reflected mainly in two ways. First, as the level of signalization increases, the AV response curves for speed, delay, and fuel consumption remain flatter overall, indicating stronger operational smoothing under frequent signal interruptions. Second, AV shows a faster increase than HV in low PET as the signalized intersection percentage rises. Overall, a higher signalized intersection percentage is associated with greater stability under AV in the operational and environmental dimensions, but also with a stronger tendency to amplify surrogate safety exposure in node-interaction settings.

Figure 4.10 presents the trends between street connectivity and the 5 performance outcomes. Overall, the AV–HV differences under street connectivity are weaker than those observed for the preceding features, and all Spearman coefficients are non-significant. This suggests that the effect of street connectivity is limited overall and is expressed more through

differences in curve shape and local fluctuation amplitude than through clear and progressively widening inter-regime separation.

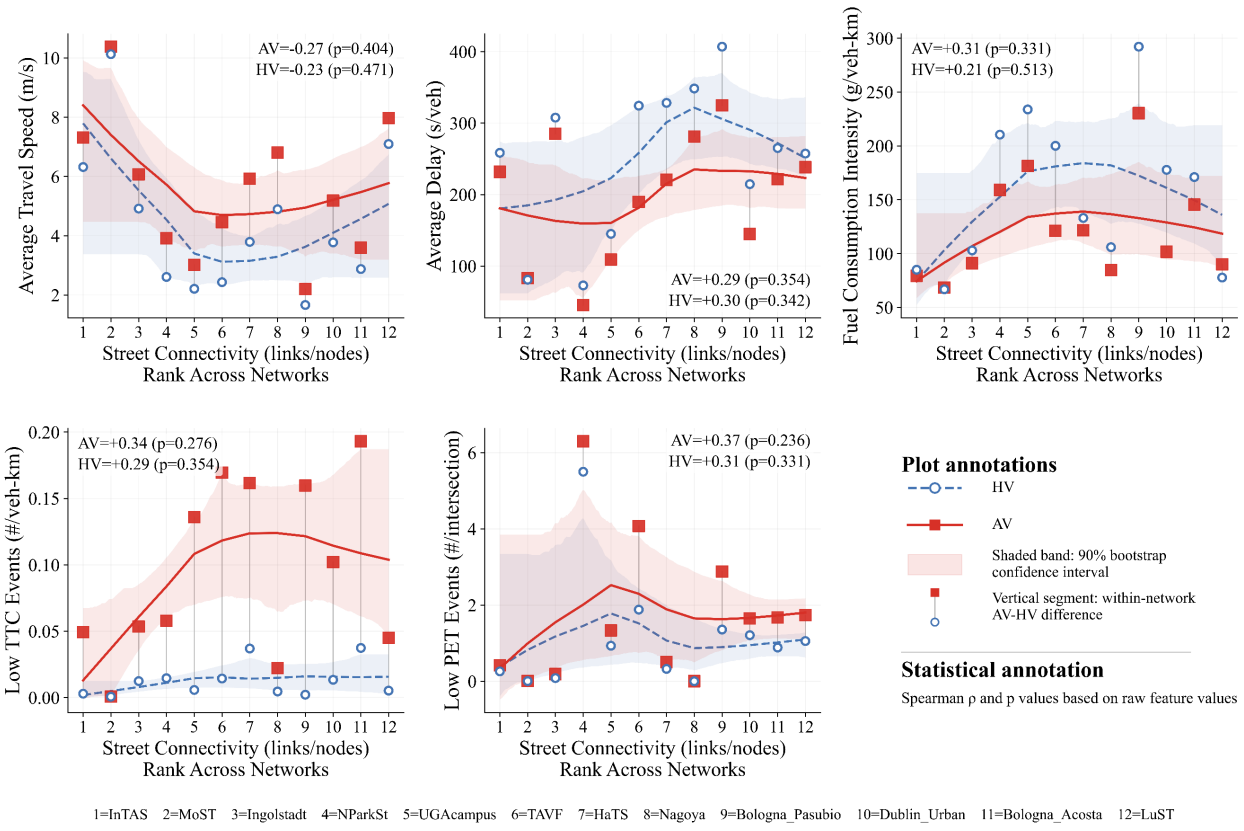


**Figure 4.10. Feature–performance trends across street connectivity under AV and HV.**

In the efficiency and environmental dimensions, AV and HV show broadly similar non-monotonic responses to street connectivity, but the AV curves exhibit smaller local fluctuations in the trend shape. Average travel speed first declines and then rises under HV and AV, with the AV curve remaining generally above HV. Average delay and fuel consumption intensity both reach higher levels in the mid-to-high connectivity range before flattening or declining. Relative to HV, the AV curves for speed, delay, and fuel display weaker local oscillations, indicating that the influence of street connectivity on AV is reflected more in reduced response variation than in a change in overall direction. Unlike the clearer inter-regime separation observed under demand

intensity, road density, and signalized intersection percentage, the AV–HV differences here are more localized in the shape of the non-monotonic curves.

In the surrogate safety dimension, low TTC and low PET again show different response patterns. For low TTC, the AV curve rises rapidly from the low to the moderate connectivity range, then remains elevated with a slight decline toward the upper end, whereas the HV curve stays at a lower level and varies only weakly. For low PET, both AV and HV follow a rise–fall–stabilize pattern, but the AV curve reaches a higher peak in the moderate connectivity range. Overall, the effect of street connectivity on surrogate safety is better characterized by higher exposure in the moderate connectivity range than by continued accumulation at the high-connectivity end.

Taken together, the moderating effect of street connectivity on AV–HV differences is relatively limited. Its role lies less in creating clear directional separation than in producing localized differences in curve shape and smoothness across outcomes. The street connectivity results, therefore, suggest that not all network features regulate AV–HV differences by progressively widening the inter-regime gap; for some, the effect is expressed mainly through local variation in response shape.

## 4.4 Chapter Summary

This chapter examines how network features shape performance differences between AV and HV regimes across heterogeneous urban networks. Based on Spearman correlation analysis and trend analysis, the results show that AV impacts are not a context-independent technological effect, but are jointly conditioned by network structure and operating conditions.

Demand intensity emerged as the primary constraint shaping regime-specific performance differences. In higher-demand networks, AVs showed a more pronounced advantage in fuel consumption intensity, indicating that smoother longitudinal behavior under AV is more readily

translated into environmental benefits under heavier loading. This advantage, however, did not extend to surrogate safety. As demand intensity increased, AV's low TTC exposure rose more steeply than HV's before leveling off at the mid-to-high demand range, and its low PET exposure showed exploratory evidence of a faster rate of increase than HV's. These results indicate that improvements in operational or environmental performance do not necessarily coincide with reductions in surrogate safety exposure.

Road density and signalized intersection percentage revealed more specific moderating patterns. Higher road density and higher signalized intersection percentage generally corresponded to more frequent stop-and-go cycles, denser interactions at the intersection, and more complex local disturbance environments. Under such conditions, AVs tended to show better fuel consumption performance, likely reflecting more stable car-following and more controllable operations, but also higher surrogate safety exposure. Notably, although both demand intensity and signalized intersection percentage amplified AV safety exposure, the most pronounced divergence fell on different indicators and was associated with different behavioral mechanisms. Under demand intensity, regime divergence was most evident in TTC: the AV curve rose more steeply than HV's before leveling off at the mid-to-high demand range. This pattern is more consistent with the spatiotemporal compression of car-following in the road segment under high loading, which made vehicles more likely to reach low-TTC conditions. Under signalized intersection percentage, by contrast, the AV–HV difference in TTC showed no clear directional trend, and the more pronounced divergence appeared in PET, with AV showing a steeper increase in low PET exposure at the high-signalization end. This pattern is more plausibly related to more compact movement execution within signalized intersections, which reduces temporal margins at conflict points. Together, these results suggest that elevated AV safety exposure does not arise

from a single behavioral source, but from distinct behavioral differences at the link and node levels, with different network features activating different layers of safety risk.

Road length showed a different moderating direction. As network length increased, the AV–HV gaps in both low TTC events and low PET events narrowed, indicating that longer and more continuous networks may partially mitigate the relative AV disadvantage in surrogate safety exposure. AV environmental benefits were more evident in shorter networks, but the moderating role of road length was more pronounced in the safety dimension. Street connectivity showed a relatively limited moderating effect, with all Spearman coefficients remaining non-significant. Its influence was expressed mainly through localized differences in response shape rather than progressively widening inter-regime separation, indicating that not all network features regulate AV–HV differences by continuously amplifying the gap between HV and AV.

From a deployment and policy perspective, the results support a network-aware approach to AV assessment. No single network condition produced a uniform AV advantage across the efficiency, environmental, and safety dimensions. AV deployment potential should therefore not be judged by average performance alone but should be assessed against the specific features of the target network. High-demand, dense, and highly signalized urban networks appear more likely to realize substantial AV-related environmental benefits, making them promising contexts for AV energy and emission gains. At the same time, these networks require closer attention to TTC risk in road segments and PET risk in intersections, together with targeted safety monitoring and mitigation strategies. By contrast, longer and more continuous networks may offer conditions under which the relative AV safety disadvantage is less pronounced, suggesting that network continuity may be an important condition for AV safety adaptability. Policy design and

deployment decisions should therefore integrate network type, operating environment, and application context into a unified assessment framework.

Several limitations should be noted in this chapter. First, the network sample remains limited. Although the selected networks cover diverse urban types, their representativeness of a broader range of network forms remains constrained. Second, the pure AV versus pure HV comparison is a stylized design, whereas real-world traffic systems more commonly involve mixed traffic under varying AV penetration rates. Third, low TTC events and low PET events are simulation-based surrogate safety proxies and do not equate to actual crash risk. Fourth, the AV and HV parameters used in the simulation were calibrated from specific datasets, which may not fully represent the broader range of AV and HV driving behaviors observed in practice. Finally, the analysis identifies network-level associations rather than strict causal effects, and the mechanistic interpretations should therefore be treated with appropriate caution.

Future research may extend this work in several directions. Broader network samples are needed to improve geographic and functional coverage. Mixed-traffic scenarios with varying AV penetration rates should be introduced to examine how heterogeneous impacts evolve as technology diffuses. The AV and HV parameters can also be further refined by incorporating data from a wider variety of sources or by statistically deriving representative behavioral parameters that better reflect the broader range of AV and HV behaviors. Richer behavioral models, control strategies, and empirical data should also be incorporated to further validate the surrogate safety findings and refine the interpretation of the underlying mechanisms. Overall, this chapter shows that AV impacts are conditional rather than uniform, and that understanding this heterogeneity is essential for more reliable AV assessment and more targeted deployment strategies.

# 5 URBAN MOBILITY APPLICATIONS DEVELOPMENT

Chapter 4 reveals that AV impacts are strongly moderated by network features, particularly demand intensity, road density, and signalized intersection percentage. However, the network features we observe in real urban systems may not always be ideal for AV performance, and rebuilding roads or redesigning intersections is rarely practical. This raises a complementary question: rather than passively observing how networks shape AV impacts, can we actively use CAV controllability to improve network-level performance? Answering this question requires shifting from a network-aware perspective to a control-oriented perspective, and it motivates the framework developed in this chapter.

CAVs introduce new possibilities for network-level traffic control by enabling coordinated, real-time regulation of vehicle behavior. This chapter develops a macroscopic framework that uses CAVs as mobile traffic control agents for city-level traffic decongestion and energy efficiency improvement. An ArTM, formulated as a macroscopic extension of the CTM, is developed to represent aggregate urban traffic dynamics while explicitly incorporating the MFD. Based on this formulation, a network-level optimal control strategy is proposed in which variable speed limits are applied to regulate traffic states and mitigate congestion propagation. The framework is evaluated through traffic simulation on two real-world urban networks in Madison and Boston, with sensitivity analyses across CAV penetration rates. The results indicate improved network-level performance and reduced energy consumption, supporting the use of macroscopic CAV-enabled control strategies for large-scale urban traffic management.

The remainder of this chapter is organized as follows. Section 5.1 presents the methodological framework, including the formulation of the Area Transmission Model, the macroscopic network representation, and the optimal control strategy for CAV-based variable

speed regulation. Section 5.2 describes the numerical experiment design and reports simulation results for the two real-world urban networks, including analyses of network-level performance and energy consumption across different CAV penetration rates. Section 5.3 concludes the chapter by summarizing the main findings and discussing implications and directions for future research.

## 5.1 Methodology

### 5.1.1 Notation

To facilitate the understanding of macroscopic network modeling, a summary of the notation has been compiled and presented in TABLE 5.1.

**TABLE 5.1 Notation list.**

| | |
|---|---|
| **Parameters** | |
| $\mathcal{I}$ | Set of areas in the studied city, $i \in \{1,2,\cdots,I\}$. |
| $\mathcal{I}_i^-$ | Set of upstream areas of area $i$. |
| $\mathcal{I}_i^+$ | Set of downstream areas of area $i$. |
| $[0,T]$ | Studied time horizons in continuous time. |
| $\mathcal{T}$ | Studied time horizon in a discrete time interval, $t \in \{1,2,\cdots,\mathbb{T}\}$. |
| $\Delta$ | Length of each time interval, $\Delta = T/\mathbb{T}$. |
| $\bar{v}_{it}$ | Average speed in area $i$ at time interval $t$. |
| $v_i^{lim}$ | Design speed limit of area $i$. |
| $l_i$ | Length of area $i$. |
| $\rho_i^c$ | Maximum permitted density under the free flow speed or critical density. |
| $Q_i^M$ | Maximum flow of area $i$ that occurs at critical density $\rho_i^c$. |
| $\rho_i^{jam}$ | Jam density of area $i$. |
| $\overline{\omega}_i$ | Average speed of area $i$ at which congestion waves propagate upstream through the road under fully congested conditions. |
| $\alpha$ | Coefficient to convert energy consumption into cost. |
| $\beta$ | Coefficient to convert time delay into cost. |
| $w_{ii'}$ | Proportion of flow from area $i$ that flows into area $i'$ |
| $q_{it}$ | Average flow rate into area $i$ during the interval $[t, t+1)$, in vehicles per unit time. |
| $\rho_{it}$ | Density of area $i$ at time interval $t$. |
| $\rho_{it}^I$ | Density change caused by internal traffic of area $i$ at time interval $t$. |
| $TC$ | Travel cost. |
| **Intermediate variables** | |
| $s_{it}$ | Maximum flow that can be sent by area $i$ at time $t$. |
| $R_{it}$ | Maximum flow that can be received by area $i$ at time $t$. |
| $e_{it}$ | Energy consumption for all vehicles in area $i$ in time interval $t$. |
| $d_{it}$ | Time delay for all vehicles in area $i$ in time interval $t$. |
| $U_{ii't}$ | Number of vehicles flow from area $i$ to area $i' \in \mathcal{I}_i^+$ at time $t$, |
| **Decision variables** | |
| $v_{it}$ | Controlled speed limit in area $i$ at time interval $t$. |

### 5.1.2 Problem Statement

Consider an urban traffic network partitioned into a finite set of homogeneous areas, indexed by $\mathcal{I} = \{1,2,\cdots,I\}$, as illustrated in Figure 5.1. The study horizon is defined over the continuous time interval $[0,T]$, which is discretized into a set of uniform time steps $\mathcal{T} \coloneqq \{0,1,2,\cdots,\mathbb{T}\}$, and the length of each time step is $\Delta$, where the time index $t \in \mathcal{T}$ maps to continuous time $t\Delta$.

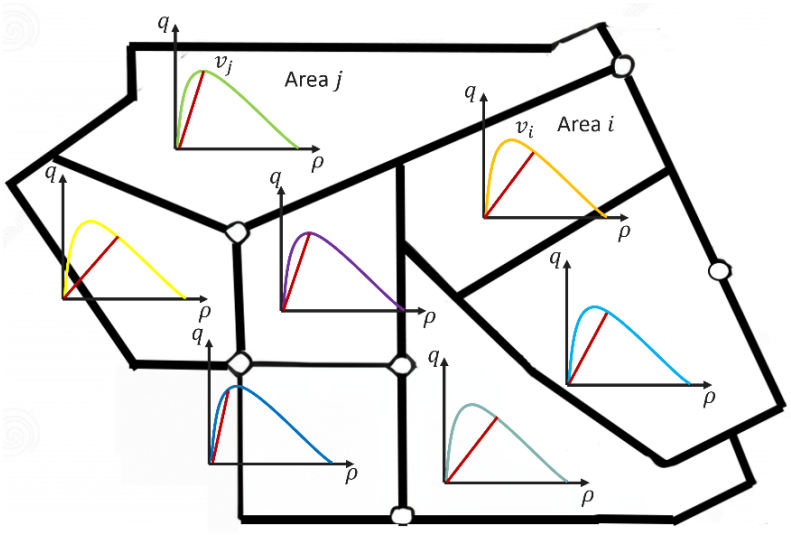


**Figure 5.1. Urban traffic network illustration.**

The urban network is represented as a directed graph at the area level, where each node corresponds to an area $i \in \mathcal{I}$ and directed links represent traffic flow connections between adjacent areas. For each area $i$, let $\mathcal{I}_i^- \subset \mathcal{I}$ and $\mathcal{I}_i^+ \subset \mathcal{I}$ denote the sets of upstream and downstream neighboring areas, respectively. Traffic flows between areas are governed by the sending capacity $s_{it}$ and receiving capacity $R_{it}$ determined by area-level traffic states and macroscopic flow relationships. Vehicles departing from an upstream area enter a downstream area subject to both upstream demand and downstream supply constraints, while boundary areas exchange flows with the external environment through exogenous inflows and outflows.

At each time step $t$ (time $t$ for short), area $i \in \mathcal{I}$ is characterized by macroscopic traffic state variables, including average travel speed $\bar{v}_{it}$, flow rate $q_{it}$, density $\rho_{it}$. Each area is further associated with geometric and traffic-flow parameters, including average traversal length $l_i$, critical density $\rho_i^c$, jam density $\rho_i^{jam}$, backward shockwave speed $\overline{\omega}_i$, and maximum flow $Q_i^M$ at $\rho_i^c$.

Vehicles traveling within each area generate energy consumption and experience travel delay, particularly more significantly under congested conditions. Let $e_{it}$ denote the total energy consumption of vehicles traversing area $i$ during time $t$, which depends on vehicle characteristics such as powertrain type (e.g., internal combustion or electric) and vehicle class (e.g., sedan, SUV). Let $d_{it}$ denote the aggregate travel delay incurred in area $i$ at time $t$ due to congestion effects. To jointly evaluate energy and mobility impacts, weighting coefficients $\alpha$ and $\beta$ are introduced to convert energy consumption and travel delay into comparable cost units. The total travel cost (TC) of the network is defined as the weighted sum of energy consumption and travel delay across all areas and time intervals.

The traffic network consists of a mixture of CAVs and HVs, characterized by a given CAV penetration rate. It is assumed that CAVs fully comply with VSA issued by a centralized traffic control center, whereas HVs respond to prevailing traffic conditions and local driving behavior. Through partial penetration, CAVs influence the aggregate traffic state by regulating their operating speeds, thereby affecting the area-level average speed and contributing to network-level traffic control. The control decision variable is the area-based VSA $v_{it}$, which governs the operating speeds of CAVs within each area at each time step. The objective of this study is to determine the optimal VSA control strategy $\{v_{it}\}_{i\in\mathcal{I},t\in\mathcal{T}}$ that minimizes the total network travel cost, subject to macroscopic traffic dynamics and operational constraints.

### 5.1.3 Area Transmission Model

An ArTM is proposed in this paper as a macroscopic extension of the CTM based on the MFD. While classical CTM is formulated using vehicle conservation at the link or cell level, the proposed ArTM is formulated in terms of area-level density conservation, which is more suitable for capturing aggregate traffic dynamics in large urban networks. Despite this aggregation, the model explicitly represents inter-area vehicle transitions through area-to-area flow variables, allowing vehicles to be consistently tracked as they propagate across the network. This formulation preserves flow continuity and congestion propagation mechanisms while enabling scalable modeling and control at the city level.

The ArTM represents traffic dynamics using area-level macroscopic state variables. The primary state variable is traffic density, which evolves over time as a result of inter-area vehicle flows and internal traffic activity. By adopting density as the system state, the model aligns naturally with MFD-based representations of urban traffic while avoiding the dimensionality associated with link-level formulations.

The temporal evolution of traffic density in each area $i \in \mathcal{I}$ is governed by a discrete-time conservation relationship:

$$\rho_{it} = \rho_{i(t-1)} + \frac{\Delta}{l_i}\left( q_{it} - \sum_{i' \in \mathcal{I}_i^+} U_{ii't} \right) + \rho_{it}^I,$$

where $q_{it}$ denotes the total inflow rate into area $i$ at time $t$, $U_{ii't}$ represents the vehicle flow from area $i$ to the downstream area $i'$, and $\rho_{it}^I$ captures the net density variation associated with internal traffic generation and attraction within the area.

The total inflow rate into area $i$ at time $t$ can be expressed as:

$$q_{it} = min\left(\sum_{i' \in \mathcal{I}_i^-} w_{i'i} S_{i't}\ , R_{it}\right),$$

where $w_{ii'}$ is the proportion of flow from the upstream area $i$ that flows into area $i'$. These proportions represent aggregate routing behavior and satisfy flow conservation across outgoing connections. For a given $i$, $\sum_{i' \in \mathcal{I}_i^+} w_{ii'} = 1$. The value of $w_{ii'}$ for each given $i'$ needs to be calibrated with real-world data. $\sum_{i' \in \mathcal{I}_i^-} w_{ii'} S_{i't}$ is the maximum flow which can be supplied by the upstream areas of area $i$ under free-flow conditions at time $t$. $S_{i't}$ is the flow supplied by upstream area $i'$ at time $t$:

$$S_{i't} = \begin{cases} min\left(min\left(v_{i't}, v_i^{lim}\right)\left(\rho_{i'(t-1)} + \rho_{it}^I\right), Q_{i'}^M\right), \rho_{i'(t-1)} + \rho_{it}^I \le \rho_i^c \\ \gamma Q_{Mi'}, \rho_{i'(t-1)} + \rho_{it}^I > \rho_i^c \end{cases},$$

where $v_i^{lim}$ represents the design speed limit of area $i$, which is determined by road geometry and cannot be modified. $v_{i't}$ is the decision variable and will be introduced later. To avoid unrealistically small sending flows under highly congested conditions (i.e., $\rho_{i'(t-1)} + \rho_{it}^I > \rho_i^c$), the area-level sending function is defined in a regime-dependent manner where $\rho_i^c$ is the critical density for area $i$. In the uncongested regime, sending flow is governed by the speed–density relationship. Once density exceeds the critical density, the sending flow is bounded by the effective discharge capacity of the area, reflecting the fact that a congested area can still release vehicles when downstream supply is available. $\gamma \in (0,1]$ is a congestion discharge factor representing the fraction of the maximum area outflow capacity that remains available under congested conditions.

To explicitly track vehicle propagation, the inter-area flow from area $i$ to downstream area $i' \in \mathcal{I}_i^+$ at time $t$ is denoted as $U_{ii't}$ and defined as

$$U_{ii't} = \begin{cases} w_{ii'}S_{it}, if \sum_{j\in\mathcal{I}_{i'}^-} w_{ji'}\,S_{jt} < R_{i't}, \\ \dfrac{R_{i't}}{\sum_{j\in\mathcal{I}_{i'}^-} w_{ji'}\,S_{jt}} w_{ii'}S_{it}, if \sum_{j\in\mathcal{I}_{i'}^-} w_{ji'}\,S_{jt} \geq R_{i't}. \end{cases}$$

The inter-area flow is determined by the sending capacity of the upstream area and the receiving capacity of the downstream areas. For each area $i$, a fraction $w_{ii'}$ of its sending flow $S_{i,t}$ is assigned to the downstream area $i'$, so that $w_{ii'}S_{i,t}$ represents the sending flow from $i$ to $i'$. If the total requested inflow to area $i'$, given by $\sum_{j\in\mathcal{I}_{i'}^-} w_{ji'}\,S_{jt}$, does not exceed the receiving capacity $R_{i't}$, then all requested flows are admitted. Otherwise, the incoming flows are proportionally scaled so that the total realized inflow equals $R_{i't}$.

$R_{it}$ is the maximum flow that can be received by area $i$ under congested conditions, at the same time interval $t$:

$$R_{it} = min\left(Q_i^M, \bar{\omega}_i\left(\rho_{jam} - \rho_{i'(t-1)} - \rho_{it}^I\right)\right)$$

It can be found that inter-area flows are constrained by area-level sending and receiving capacities, following CTM-style demand-supply logic adapted to the macroscopic scale. With this, vehicle conservation among different areas is modeled.

The objective of our paper, TC, is the summation of traffic energy consumption cost (i.e., $e_{it}$) and travel delay cost (i.e., $d_{it}$). Energy consumption is calculated with the theoretical models developed by Bottero et al. (2014),

$$e_{it} = \frac{T}{\mathbb{T}} q_{(i+1)t} * l_i F'(v_{it})$$

where $F'(v_{it}) = F(v_{it})\left(1 + \varepsilon\frac{\mathbb{T}d_{it}}{T}\right)$ and $F(v_{it}) = \frac{W^* + Z\bar{v}_{it}^2}{\eta}$. $W^*$ denotes the resistance elements that are independent of speed, $Z$ signifies the resistance elements that are contingent upon

the square of the speed, and $\varepsilon$ is a parameter dependent on the Level of Service (LOS) (Bottero et al., 2014). The LOS can be determined by the corresponding density according to the Highway Capacity Manual (HCM, 2022).

To quantify congestion-induced delay within each area, this study adopts the classical bottleneck model proposed by (Vickrey, 1969), which relates traffic delay to the temporal accumulation of vehicles exceeding the area's discharge capacity. Under the proposed ArTM framework, delay arises from the imbalance between inflow and outflow at the area level, as well as from internal traffic generation. Accordingly, the travel delay incurred in area $i$ during time $t$ is computed as:

$$d_{it} = \int_{t}^{t+\Delta} \left( \frac{\Delta}{l_i} \left( q_{it} - \sum\nolimits_{i' \in \mathcal{I}_i^+} U_{ii't} \right) + \rho_{it}^{I} \right) dt,$$

where the integrand represents the instantaneous excess vehicle accumulation within the area over the interval $[t, t + \Delta]$.

With the area-level energy consumption and travel delay defined, the total network TC over the study horizon is computed as,

$$TC \coloneqq \sum_{t=1}^{\mathbb{T}} \sum_{i=1}^{I} (\alpha e_{it} + \beta d_{it})$$

where $e_{it}$ and $d_{it}$ denote the total energy consumption and travel delay, respectively, incurred by vehicles traveling within area $i$ during time $t$. The weighting coefficients $\alpha$ and $\beta$ convert energy consumption and travel delay into comparable cost units.

To relate the control variables to area-level traffic dynamics, this study assumes that each area exhibits a well-defined MFD, enabling the use of aggregate traffic states for network-level control. Under this assumption, the area-level speed-density relationship for area $i$ at time $t$ is modeled as:

$$v_{it}(\rho_{it}) = v_i^{lim} \exp\left(-0.5\left(\frac{\rho_{it}}{\rho_i^c}\right)^2\right)$$

where $v_i^{lim}$ denotes the design speed limit of the area $i$, and $\rho_i^c$ is the critical density corresponding to the optimal operating condition on the MFD.

Based on this relationship, the control strategy determines the optimal set of area-level VSAs, $\{v_{1,t_c}, v_{2,t_c}, \dots, v_{i,t_c}, \dots, v_{j,t_c}, \dots\}$, only at predefined control update times $t_c \subseteq t$, as indicated by the red lines in Figure 5.1. Once computed, each set of area-level speed limits is maintained over the corresponding control interval until the next update. By regulating operating speeds in this periodic manner, the proposed approach influences traffic flow propagation, balances demand across the network, and alleviates congestion, thereby reducing both travel delay and energy consumption.

### 5.1.4 Optimization Framework

Based on the proposed ArTM, the VSA control problem is formulated as a rolling-horizon model predictive control (MPC) problem. At each control update time, the current network state is observed, and a finite-horizon optimization problem is solved to determine the optimal area-level speed limits over the upcoming prediction horizon. Starting from the observed state, the future network evolution is predicted by recursively propagating the ArTM over the horizon under the candidate VSA decisions. In this way, the predicted area densities, inter-area flows, energy consumption, and travel delay are generated step by step through the model equations. The optimization is then repeated at the next control interval using the updated traffic state, allowing the controller to adapt to evolving network conditions.

The decision variables are the area-level speed limits $v_i$. For each MPC step, the objective is to minimize the total predicted network travel cost over the horizon, defined as the weighted

sum of energy consumption and travel delay, together with two regularization terms to improve control practicality and stability. The first is a free-flow deviation penalty, which discourages unnecessarily low speed limits by penalizing deviations from the area's free-flow speed $v_i^{lim}$. The second is a switching penalty, which discourages abrupt changes from the speed limit applied in the previous control step $v_{i(t-1)}$. The resulting objective can be written as

$$obj \coloneqq \min_{v_t} \left[ \sum_{h=t}^{t+H-1} \sum_{i=1}^{I} (\alpha e_{ih} + \beta d_{ih}) + \lambda_1 \sum_{i=1}^{I} \left(v_i^{lim} - v_{it}\right)^2 + \lambda_2 \sum_{i=1}^{I} (v_{it} - v_{it-1})^2 \right], \forall t \in t_c.$$

where $H$ is the prediction horizon, and $\lambda_1$ and $\lambda_2$ are weighting parameters for the free-flow deviation and switching penalties.

The optimization is subject to the area-level traffic dynamics and flow propagation constraints defined by the ArTM, including density evolution, inter-area flow conservation, and sending and receiving capacity constraints. These constraints couple traffic states across areas and time, capturing congestion propagation and spillback effects at the network level, which are summarized as follows:

$$s.t.\ q_{it} = min\left( \sum_{i' \in \mathcal{I}_i^-} w_{i'i} S_{i't}\ , R_{it} \right), \forall i, t$$

$$\rho_{it} = \rho_{i(t-1)} + \frac{\Delta}{l_i} \left( q_{it} - \sum_{i' \in \mathcal{I}_i^+} U_{ii't} \right) + \rho_{it}^I, \forall i, t$$

$$S_{it} = \begin{cases} min\left(min\left(v_{\mathrm{it}}, v_i^{lim}\right)\left(\rho_{i(t-1)} + \rho_{it}^I\right), Q_i^M\right), \rho_{i(t-1)} + \rho_{it}^I \le \rho_i^c \\ \gamma Q_i^M, \rho_{i(t-1)} + \rho_{it}^I > \rho_i^c \end{cases}, \forall i, t$$

$$R_{it} = min\left(Q_i^M, \bar{\omega}_i\left(\rho_i^{jam} - \rho_{i(t-1)} - \rho_{it}^I\right)\right), \forall i, t$$

$$U_{ii't} = \begin{cases} w_{ii'}S_{it}, if \ \sum_{j\in\mathcal{I}_{i'}^-} w_{ji'}\, S_{jt} < R_{i't}, \\ \dfrac{R_{i't}}{\sum_{j\in\mathcal{I}_{i'}^-} w_{ji'}\, S_{jt}} w_{ii'}S_{it}, if \ \sum_{j\in\mathcal{I}_{i'}^-} w_{ji'}\, S_{jt} \geq R_{i't}, \end{cases} \forall i,t$$

$$d_{it} = \frac{\Delta^2}{l_i}\left(q_{it} - \sum_{i'\in\mathcal{I}_i^+} U_{ii't}\right) + \Delta\rho_{it}^I, \forall i,t$$

Due to the nonlinear speed-density relationship and the min-max structure embedded in the sending and receiving flow formulations, the resulting problem is a nonlinear programming problem. In this study, the optimization problem is solved using the commercial solver Gurobi, which can handle the nonlinearities present in the formulation.

## 5.2 Numerical Experiments

### 5.2.1 Toy Experiment for Model Validation

A toy experiment was conducted to validate the proposed network modeling framework described in Section 2. The simulation was implemented in Python and executed on a desktop computer equipped with an AMD Ryzen 7 5700G processor and 64 GB of RAM.

The experiment was performed on a simplified network based on the City of Madison, a relatively small urban area, as illustrated in Figure 5.2. The downtown area, which includes the State Capitol and the University of Wisconsin–Madison, serves as the primary activity center. For this experiment, the city was partitioned into 20 areas according to the Alder District boundaries (https://cityofmadison.maps.arcgis.com/). Among these areas, nine were designated as origin areas generating traffic inflow (Areas 8, 9, 10, 11, 13, 16, 17, 19, and 20), while Area 5, representing the central business district (CBD), was treated as the primary destination area.

TABLE 5.2 summarizes the parameter settings for the toy experiment. Parameter values were selected from literature-supported ranges for urban macroscopic traffic modeling and then

adjusted within those ranges to produce a plausible peak-period loading scenario (Geroliminis & Daganzo, 2008; Knoop, 2017; Kuhne & Michalopoulos, 2017).

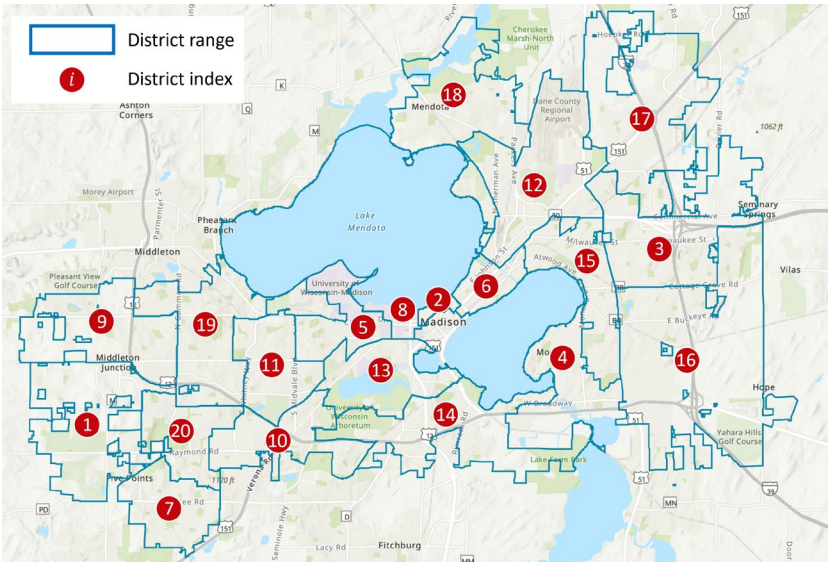


**Figure 5.2. City of Madison area partitions illustration.**

**TABLE 5.2 Summary of simulation settings.**

| Parameter | Value | Parameter | Value |
|---|---|---|---|
| Simulation duration | 150 minutes | Jam density | 150 vehicle/km |
| Number of areas | 20 | Free-flow speed by area | See area-specific settings |
| Number of origin areas | 9 | Shockwave speed | 4.5 m/s |
| Inflow rate (origin) | 0.12 veh/s | Inflow duration | 60 minutes |
| Number of destination areas | 1 | Optimal VSA interval | 10 minutes |
| Outflow rate (destination) | 0.35 veh/s | Critical density | 40 veh/km |
| Time step | 1 min | Maximum flow | 0.5 veh/s |
| $\alpha$ | \$3.668/gallon | $\beta$ | \$17.9/person-hour |
| $\lambda_1$ | 1 | $\lambda_2$ | 0.5 |
| $H$ | 10 minutes | | |

The simulation horizon was 150 min (2.5 hours). The external inflow at each origin area was set to 0.12 veh/s, and the destination discharge rate was set to 0.35 veh/s to represent trip completion and vehicle exit from the system. The jam density, free-flow speed, backward shockwave speed, critical density, and maximum flow were set to 150 veh/km, 13.4 m/s, 4.5 m/s, 40 veh/km, and 0.5 veh/s, respectively, according to (Shi et al., 2021). Energy consumption and

travel delay were converted into monetary values using local gas prices and average personal income (U.S. DOT, 2023). Demand loading was applied during the first hour only, so that the subsequent simulation period could be used to examine congestion dissipation and network recovery. The simulation time step was 1 min. In the controlled case, the optimal VSA was updated at 10-min intervals.

**TABLE 5.3 Area-level free-speed settings.**

| Illustration area ID | Free-flow speed (mph) | Illustration area ID | Free-flow speed (mph) |
|---|---|---|---|
| 1 | 45 | 11 | 25 |
| 2 | 25 | 12 | 40 |
| 3 | 35 | 13 | 30 |
| 4 | 40 | 14 | 30 |
| 5 | 25 | 15 | 35 |
| 6 | 25 | 16 | 45 |
| 7 | 45 | 17 | 45 |
| 8 | 35 | 18 | 45 |
| 9 | 45 | 19 | 30 |
| 10 | 30 | 20 | 30 |

The free-speed parameter for each area was assigned using a zone-based approximation to reflect local posted-speed patterns under the City of Madison's regulations. Specifically, lower free speeds were assigned to the central urban core, moderate values to the surrounding inner-ring areas, and higher values to the peripheral areas. This yields an area-level representation of spatially varying free-flow conditions that is broadly consistent with the spatial distribution of urban street speed limits in Madison. The assigned free-flow speeds for all areas are reported in TABLE 5.3. The simulations were then conducted, and the state variables of each area were recorded throughout the simulation for subsequent analysis.

5.2.1.1 Without VSA Control

Figure 5.3 shows the spatial distribution of traffic states at selected time steps prior to the application of VSA control. Area-level traffic density with colors ranging from green for low

density to red for high density. The results indicate that congestion first emerges in the early stage of demand loading and then propagates progressively from upstream origin areas toward the inner areas of the network. As inflows accumulate toward the common destination, bottleneck effects become increasingly significant in the central areas. By approximately the 30th minute, severe congestion is observed in the CBD and its adjacent areas, indicating that the proposed model captures the directional buildup of peak-period traffic and the associated spatial propagation of congestion.

After the 60th minute, the network evolves under a pure dissipation regime because no further inflow is introduced. Under these conditions, vehicle accumulation decreases gradually as traffic continues to discharge toward the destination and exit the system. The simulated congestion correspondingly weakens over time. At the end of the simulation time, congestion can only be observed in area 5, and the areas immediately connected to area 5. This experiment shows that the proposed ArTM reproduces the fundamental dynamic patterns expected in an urban network, including congestion formation under concentrated demand, spatial spillback across connected areas, and gradual recovery after demand cessation.

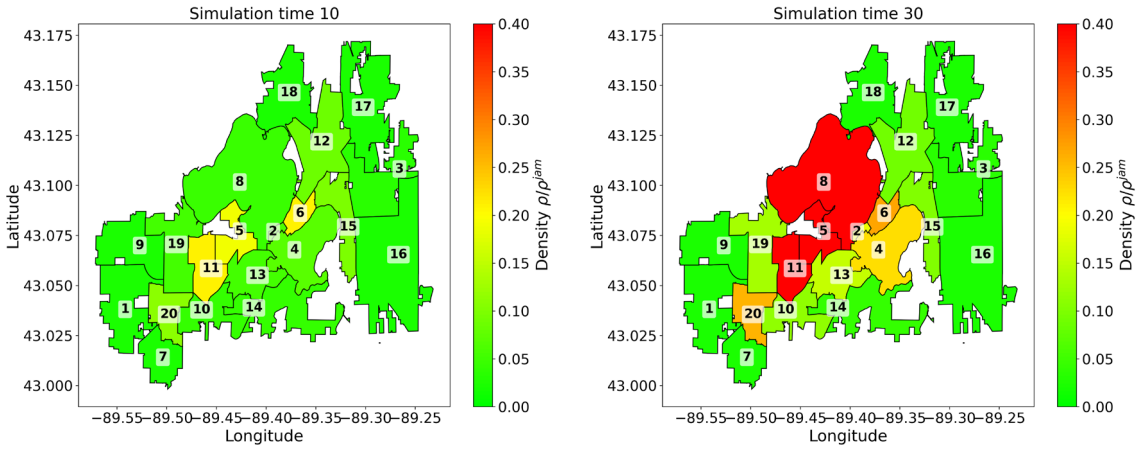

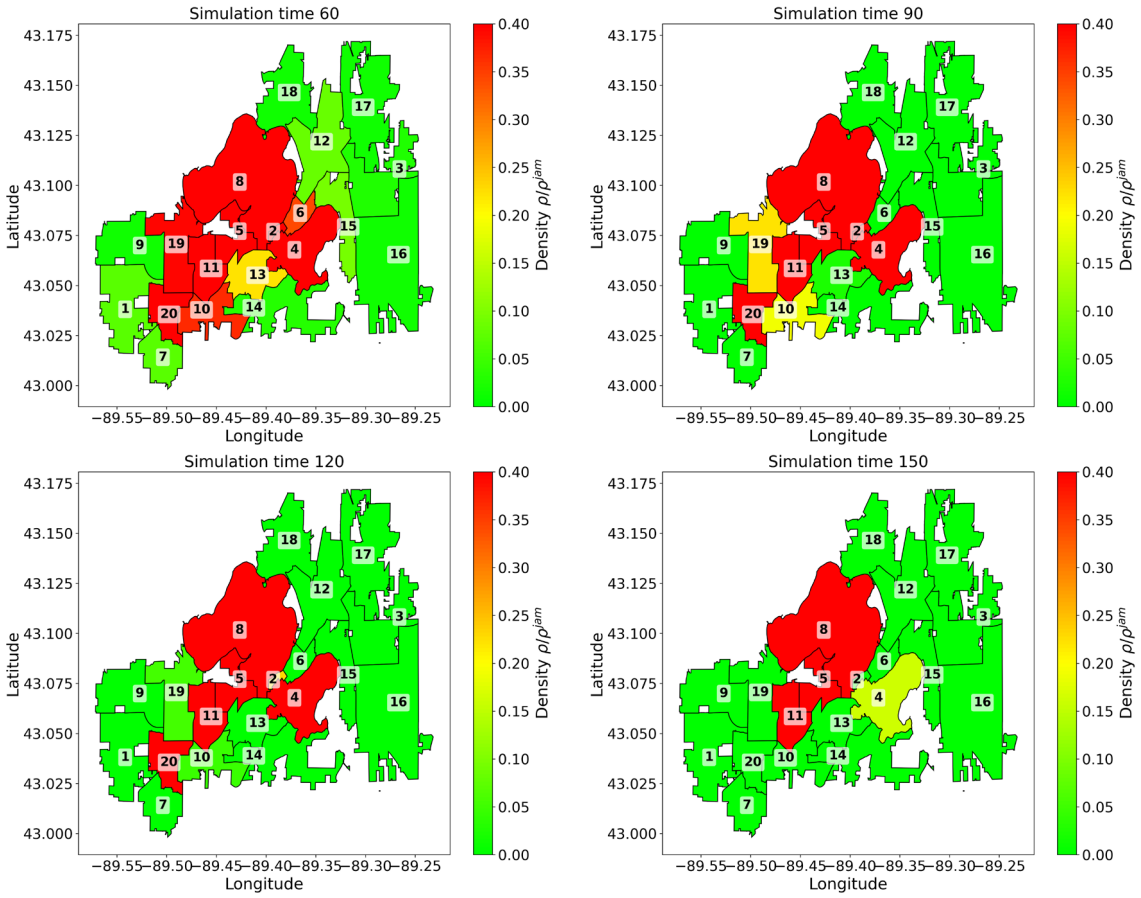


**Figure 5.3. Simulation results at different stages without VSA.**

5.2.1.2 With VSA Control

The proposed VSA-based optimal control strategy was then applied to the same simulation setting. The resulting optimization problem was solved using the commercial solver Gurobi, and the computed optimal VSAs were used as the speed inputs for CAVs in the simulation.

Figure 5.4 presents the spatial distribution of traffic states at selected time steps under VSA control, using the same network configuration and demand settings as in the uncontrolled toy experiment. The primary difference is that CAV speeds are regulated according to the optimized area-level VSAs. Relative to the uncontrolled case shown in Figure 5.3, the controlled results exhibit a substantial reduction in congestion formation, particularly during the period of heaviest demand loading. In particular, the significant congestion previously observed around the 30th

minute was postponed to around the 60th minute, indicating that the proposed control strategy effectively regulates traffic propagation from peripheral areas to the inner network and prevents excessive vehicle accumulation in critical areas.

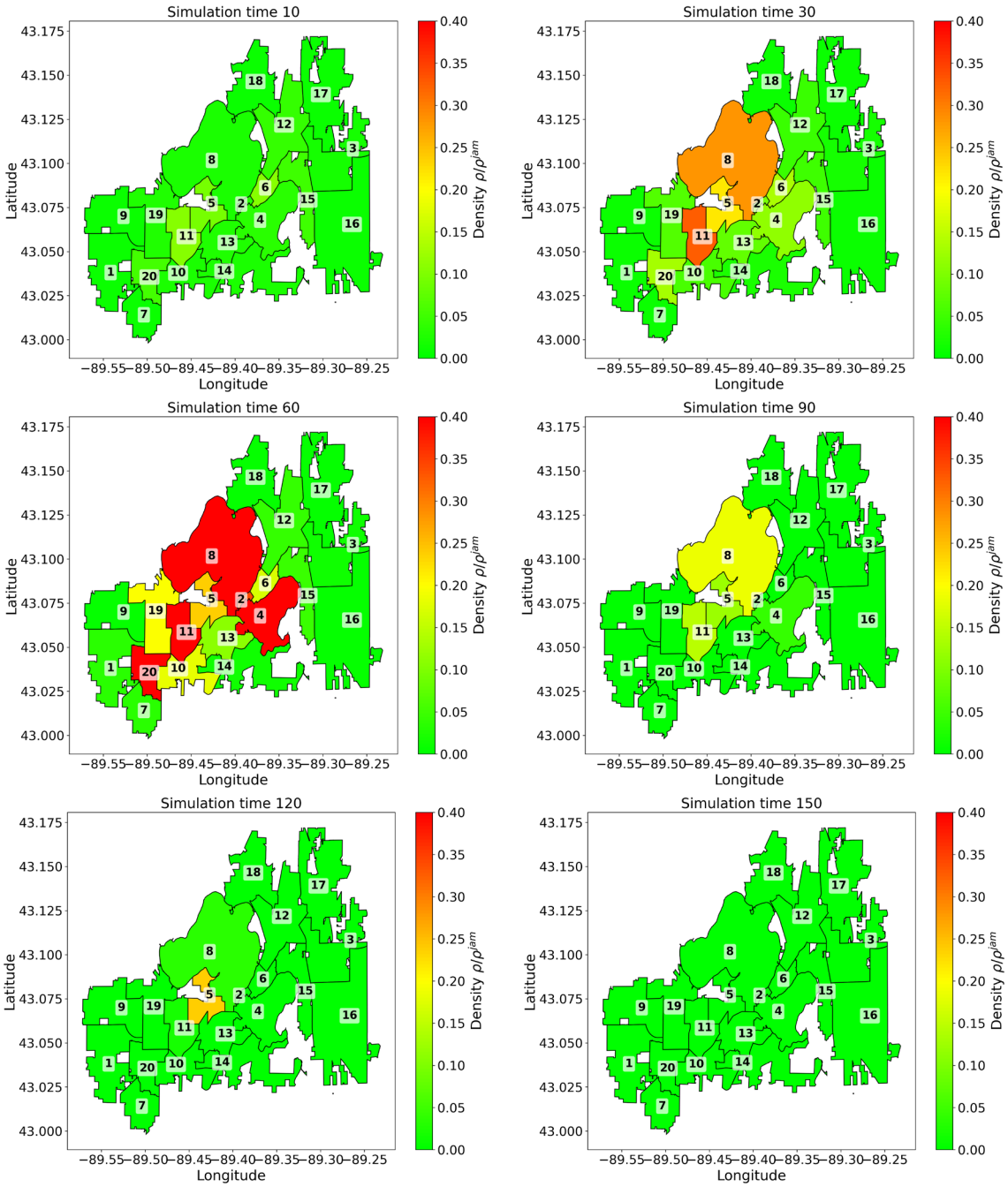


**Figure 5.4. Simulation results at different stages with the optimal VSA.**

A closer examination shows that the most congested condition under VSA control occurs around the 60th minute, after which traffic accumulation begins to decline steadily. By approximately the 120th minute, congestion has largely dissipated across the network. In contrast, under the uncontrolled scenario, significant congestion persists. These results indicate that the proposed VSA strategy substantially accelerates network recovery and improves the spatial-temporal evolution of traffic states. Overall, the controlled simulation demonstrates that area-level VSA regulation can effectively suppress congestion buildup, maintain more balanced density distributions across areas, and reduce the time required for the network to return to uncongested conditions.

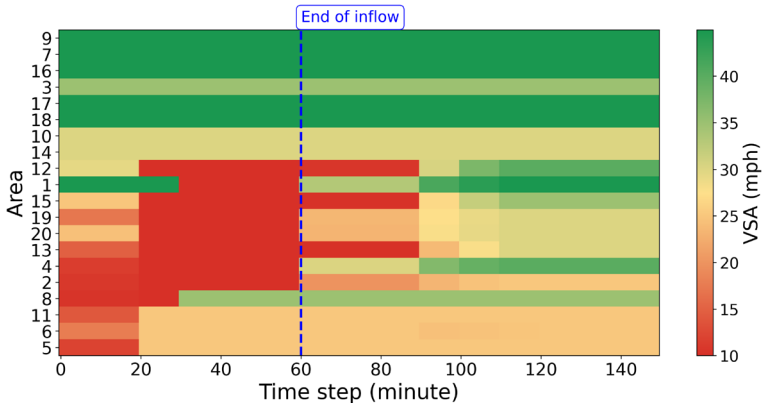


**Figure 5.5. Spatiotemporal heatmap of VSA settings across areas (peripheral areas ordered first and then inner areas).**

Figure 5.5 shows the spatiotemporal distribution of VSA settings across areas, with peripheral areas listed first and inner areas listed second. A clear temporal transition is observed around the dashed blue line marking the end of inflow: during the inflow period, active speed control is applied mainly in selected inner areas, whereas most peripheral areas remain at relatively high speed limits; after inflow ends, VSA values in many previously controlled inner areas gradually return toward their original levels, consistent with the objective function term that discourages unnecessary control once inflow pressure is removed. Overall, the figure shows that

the VSA strategy is both spatially selective and temporally dynamic: spatially, it targets the more congestion-sensitive inner areas rather than the peripheral ones; temporally, the strongest interventions occur during the inflow period and then ease after inflow ends. This pattern is consistent with the intended role of VSA in protecting the congested urban core by regulating approach speeds and mitigating congestion propagation into the most critical parts of the network.

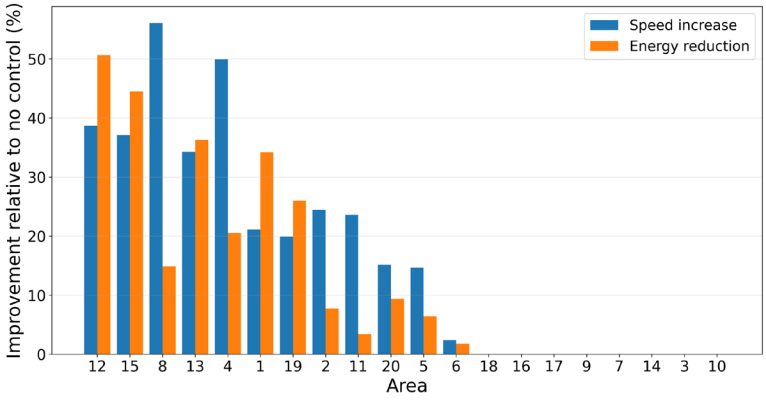


**Figure 5.6. Area-level percentage benefits of VSA control relative to the no-control scenario, ranked by combined improvement.**

Figure 5.6 compares the percentage improvement under VSA control relative to the no-control scenario in terms of speed increase and energy reduction. The results show a clear spatial pattern: the benefits are concentrated mainly in the inner areas, while the peripheral areas (i.e., origin areas) exhibit limited improvement. This suggests that VSA is more effective in the central, congestion-sensitive parts of the network, where smoothing traffic flow and regulating inflow can more effectively reduce stop-and-go conditions. Although Area 5, the CBD area, also benefits from control, its improvement is less significant than that of several other inner areas. A likely reason is that traffic conditions in the CBD are constrained more by severe local bottlenecks, dense interactions, and capacity limitations than by speed regulation alone. In addition, part of the VSA benefit may be realized upstream, as regulating inflows into the CBD can improve conditions in surrounding inner areas more noticeably than within the saturated CBD core itself.

TABLE 5.4 presents a comparative summary of network-level performance with and without the optimal VSA strategy. The comparison includes key indicators of operational efficiency, energy use, congestion, and overall system cost. Under the 150-min simulation horizon, the optimal VSA strategy reduces total energy consumption from 1,369.4 to 1,209.7 gallons, corresponding to an 11.7% reduction. Total travel delay decreases from 3,597,775.1 to 2,745,102.3 vehicle-seconds, a reduction of 23.7%. Using the adopted conversion factors for fuel consumption and delay, the TC decreases from $22,911.5 to $18,083.2, corresponding to a 21.1% reduction. In addition, the average network speed increases from 24.4 to 27.7 mph, while the maximum network density decreases from 60 to 51 veh/km, indicating that congestion accumulation is effectively mitigated under control. The traffic clear time is also shortened to 124 min, whereas the uncontrolled case does not fully clear within the 150-min simulation period.

**TABLE 5.4 Comparison between with and without optimal VSA of the toy experiment.**

| | Without optimal VSA | With optimal VSA | Relative change |
|---|---|---|---|
| Energy Consumption (gallon) | 1,369.4 | 1,209.7 | -11.7% |
| Travel Delay (veh·s) | 3,597,775.1 | 2,745,102.3 | -23.7% |
| Total Travel Cost ($) | 22,911.5 | 18,083.2 | -21.1% |
| Network Speed (m/s) | 24.4 | 27.7 | +13.5% |
| Max Network Density (veh/km) | 60 | 51 | -15.0% |
| Traffic Clear Time (minutes) | >150 | 124 | Cleared |

These results are consistent with the qualitative patterns observed in the previous figures. The higher network speed, lower maximum density, and shorter clearance time together indicate that the proposed VSA strategy improves traffic progression and accelerates congestion dissipation at the network level. At the same time, the reductions in energy consumption and TC suggest that these operational improvements also translate into broader system-level benefits.

Overall, the toy experiment provides an initial validation of the proposed framework by demonstrating its internal consistency and control effectiveness in a simplified urban setting.

Because the scenario is based on hypothetical simulation settings, the results are not intended to reproduce real-world traffic conditions. Rather, the experiment is designed to test whether the proposed model can capture the essential dynamics of urban traffic, including congestion formation, propagation, and dissipation, and whether the VSA-based control strategy can effectively mitigate these dynamics under controlled conditions.

### 5.2.2 Large-Scale Urban Network Case Study

Building on the validation results presented in Section 5.2.1, this section extends the proposed framework to a large-scale case study based on the Boston urban network as shown in Figure 5.7, with the aim of further evaluating its applicability, scalability, and robustness under more realistic and operationally complex traffic conditions. Compared with the benchmark setting, the Boston case involves a substantially larger network, richer spatial heterogeneity, and more intricate congestion propagation patterns, thereby providing a more demanding test of the proposed area-level control strategy.

The Boston road network geometry, traffic demand inputs, and baseline scenario settings were adopted from (Ambühl et al., 2023). In addition, several default network and simulation parameters were retained from the same source to preserve consistency with the original Boston case configuration. All simulations were conducted in SUMO using the same computing platform to maintain computational consistency. Within SUMO, CAV speeds were regulated online through the TraCI interface, which enabled dynamic implementation of the proposed control logic during simulation. To support area-level state estimation and control deployment, the network was partitioned according to Transportation Analysis Zones (TAZs) defined by the Boston Region MPO (Boston Region MPO, 2026), with each TAZ treated as a control unit for aggregating traffic states and updating speed guidance.

At each control update, area-level traffic states (e.g., $S_{it}, R_{it}, \rho_{it}$) were aggregated from the simulation, and advisory speeds for CAVs were updated accordingly. The control interval was set to 10 min, such that the controller recomputed speed guidance every 10 min in response to evolving network conditions. This update frequency was chosen as a compromise between responsiveness and practical implementability, allowing the controller to capture meaningful changes in congestion while avoiding overly frequent interventions. Different control interval values will be discussed in Section 5.2.3 Sensitivity Analysis.

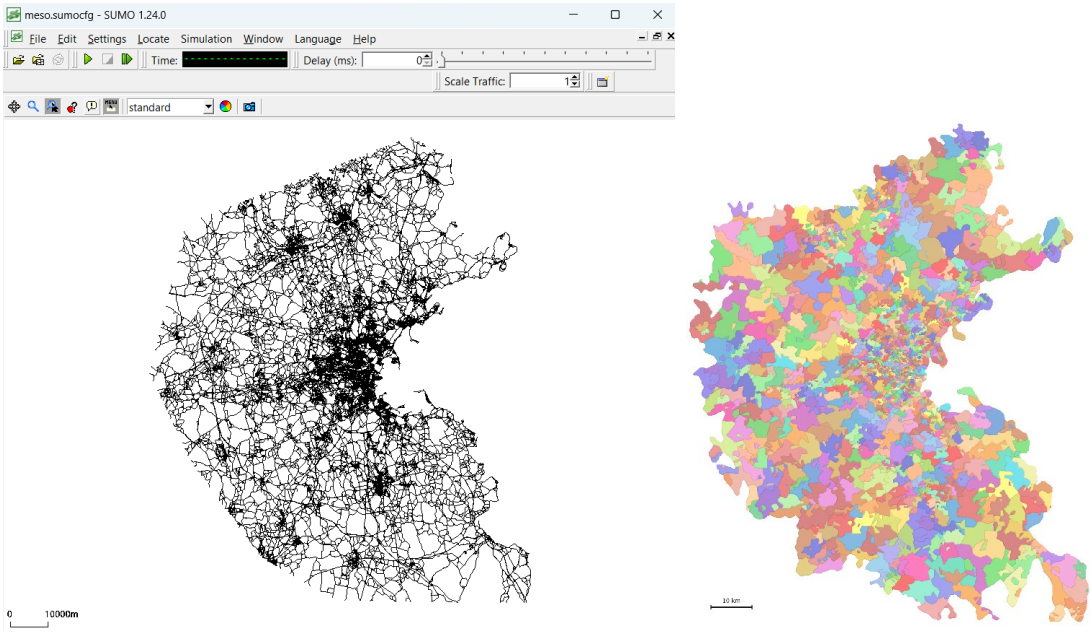


(a) network in SUMO (b) TAZ partition

**Figure 5.7. Boston network in SUMO and corresponding TAZ partition.**

To evaluate the performance of the proposed VSA strategy, a set of network-level metrics was considered from operational, energy, and throughput perspectives. Average network speed and average network density were used to characterize the overall traffic state. Average delay per inserted vehicle was used to reflect the travel time burden experienced by vehicles that successfully entered the network. Average energy per vehicle mile traveled (VMT) was used as a distance-normalized measure of energy consumption. In addition, inserted vehicles, estimated finished

vehicles, and the network clearance ratio were reported to describe network loading, network discharge, and the proportion of entered demand that was cleared within the simulation horizon. For the controlled case, the mean advisory speed was also reported to summarize the overall level of the implemented speed intervention.

TABLE 5.5 presents the comparison between the scenarios with and without optimal VSA. Overall, the results show that the proposed control improved network performance in the large-scale urban setting. Average network speed increased from 7.6 to 10.7 m/s, corresponding to a 40.8% increase, while average network density decreased from 6.0 to 3.4 veh/km, a reduction of 43.3%. These changes indicate that the controlled scenario maintained a less congested network state over the simulation period.

**TABLE 5.5 Comparison between with and without optimal VSA of the Boston case study.**

| Metric | Without optimal VSA | With optimal VSA | Relative change |
|---|---|---|---|
| Average network speed (m/s) | 7.6 | 10.7 | +40.8% |
| Average network density (veh/km) | 6.0 | 3.4 | -43.3% |
| Average delay per inserted vehicle (s/veh) | 457.0 | 46.7 | -89.8% |
| Average energy per VMT (gallon) | 0.0746 | 0.0619 | -17.0% |
| Inserted vehicles | 2,495,139 | 2,499,418 | +0.2% |
| Estimated finished vehicles | 2,270,009 | 2,415,608 | +6.4% |
| Network clearance ratio | 0.91 | 0.97 | +6.6% |
| Mean advisory speed (m/s) | — | 24 mph | — |
| Energy Consumption (gallon) | 991,582.0 | 1,105,769.5 | +11.5% |
| Travel Delay (veh-s) | 1,140,253,571.6 | 116,722,820.6 | -89.8% |
| Total Travel Cost ($) | 9,306,717.0 | 4,636,334.4 | -50.2% |

The delay metric shows an even larger improvement under control. Average delay per inserted vehicle decreased from 457.0 to 46.7 s/veh, corresponding to an 89.8% reduction. This result suggests that the proposed area-level VSA strategy substantially reduced the time vehicles spent under congested conditions. Together with the increase in average network speed and the

reduction in average density, this finding indicates that the control strategy improved traffic progression and mitigated queue accumulation at the network level.

The energy metric also improved under the controlled scenario. Average energy per VMT decreased from 0.0746 to 0.0619 gallons, corresponding to a 17.0% reduction. This result suggests that the smoother traffic conditions achieved under VSA control were accompanied by lower energy consumption per unit distance traveled.

The throughput-related metrics further support the effectiveness of the proposed strategy. The number of inserted vehicles remained nearly unchanged between the two scenarios, increasing only slightly from 2,495,139 to 2,499,418 (+0.2%), which indicates that the comparison was conducted under essentially the same demand level. By contrast, the number of estimated finished vehicles increased from 2,270,009 to 2,415,608 (+6.4%), and the network clearance ratio increased from 0.91 to 0.97. This indicates that, under comparable demand input, the controlled network discharged a larger share of vehicles within the same simulation period.

The mean advisory speed in the optimal VSA scenario was 24.0 mph. This suggests that the observed improvements were achieved through moderate speed regulation rather than uniformly restrictive control.

Overall, the Boston case shows that the proposed framework remains effective when extended to a larger and more heterogeneous urban network, and that it can improve traffic state, reduce delay, lower energy consumption, and increase network clearance under large-scale operating conditions.

### 5.2.3 Sensitivity Analysis of the Model

Figure 5.8 compares network-level travel delay and energy consumption under different control update intervals, ranging from 600 s to 3600 s. The results show that shorter update

intervals generally lead to lower delay and lower energy consumption. Both metrics are minimized at 600 s and deteriorate as the update interval increases, although energy consumption exhibits some non-monotonic variation at intermediate intervals. This finding indicates that more frequent updates improve the controller's ability to track evolving traffic conditions, whereas infrequent updates reduce control responsiveness and lead to poorer system performance. As a result, the 600 s interval was selected for the main experiments as a setting that maintains the best control performance.

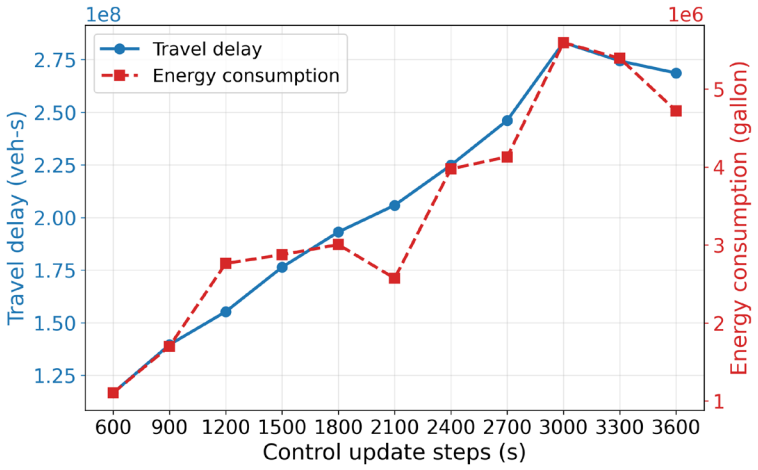


**Figure 5.8. Effects of control update interval on network delay and energy consumption.**

Figure 5.9 compares TC, network-level travel delay, and network energy consumption under different combinations of $\lambda_1$ and $\lambda_2$. Here, $\lambda_1$ controls the extent to which the optimized speed remains close to the free-flow speed, whereas $\lambda_2$ controls the smoothness of the speed trajectory across consecutive control intervals. The results indicate that $\lambda_1$ is the main driver of system performance. Larger $\lambda_1$ values generally reduce TC and energy consumption, implying that preventing overly conservative speed control improves overall network operation. However, the lowest delay is obtained at smaller to moderate $\lambda_1$ values, suggesting that some departure from free-flow speed is still necessary to regulate congestion effectively. By contrast, $\lambda_2$ mainly acts as

a damping term: a small value helps stabilize the control, whereas a large value can over-smooth the response and reduce its effectiveness. These findings suggest that effective tuning should rely primarily on $\lambda_1$ to set the control intensity, with $\lambda_2$ chosen as a small regularization term to improve implementability without sacrificing responsiveness.

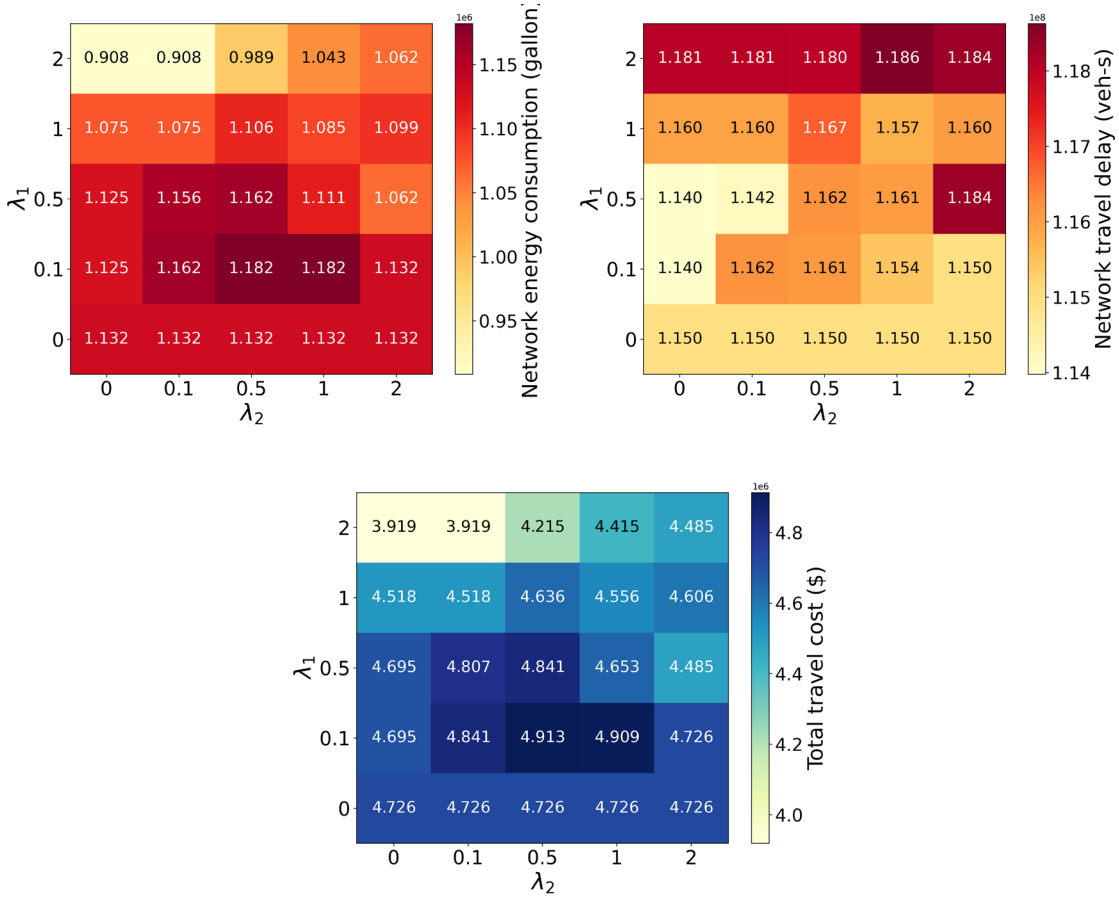


**Figure 5.9. Effects of the control weighting parameters $\lambda_1$ and $\lambda_2$ on network energy consumption, travel delay, and total travel cost.**

### 5.2.4 MFD with Different CAV Penetration Rates

It is important to note that although the scenario with fully CAVs offers promising insights, it remains a distant reality. In the foreseeable future, roadways will predominantly feature mixed traffic composed of both HVs and CAVs. Therefore, it is essential to evaluate the performance of the proposed model, the MFD, under varying CAV penetration rates.

In mixed traffic environments, Shi and Li (2021) categorize vehicle-following interactions into four distinct types: a CAV following another CAV, an HV following a CAV, a CAV following an HV, and an HV following another HV. Due to the presence of high-performance onboard computation and rapid-response sensing technologies, CAVs can maintain significantly shorter headways compared to HVs, particularly when following HVs. Moreover, when a CAV follows another CAV, V2V communication facilitates platooning, thereby enabling even smaller inter-vehicle spacing and enhancing traffic throughput efficiency. Figure 5.10 illustrates the Vehicle-Following Interactions in Mixed Traffic Scenarios.

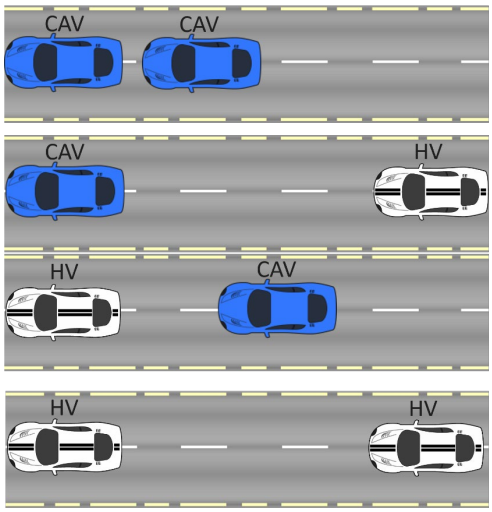


**Figure 5.10. Illustration of vehicle-following interactions in mixed traffic scenarios.**

Based on these heterogeneous interaction patterns and vehicle capabilities, we model the MFD under mixed traffic conditions with different CAV penetration rates using the following equation from Shi and Li (2021):

$$q(k) = \begin{cases} \bar{v}k, & k \in [0, R]; \\ \dfrac{1 - k\sum_{j\in\mathcal{J}} w_j\,\alpha_j/q_j^0}{\sum_{j\in\mathcal{J}} \alpha_j/q_j^0}, & k \in \left[R, \dfrac{1}{\sum_{j\in\mathcal{J}} w_j\,\alpha_j/q_j^0}\right], \end{cases}$$

where $R = 1/(\sum_{j\in\mathcal{J}}(\bar{v} + w_j)\alpha_j/q_j^0)$, $\alpha_j$ is the penetration rate of type-$j$ vehicles.

Figure 5.11 presents the MFDs under varying levels of CAV penetrations. TABLE 5.6 shows the MFD-based capacity and density summary by CAV penetration level. The underlying assumptions for this analysis are that CAVs and HVs are randomly distributed within the traffic stream and that both vehicle types share an identical stopping distance. Consequently, the jam density remains constant across all scenarios.

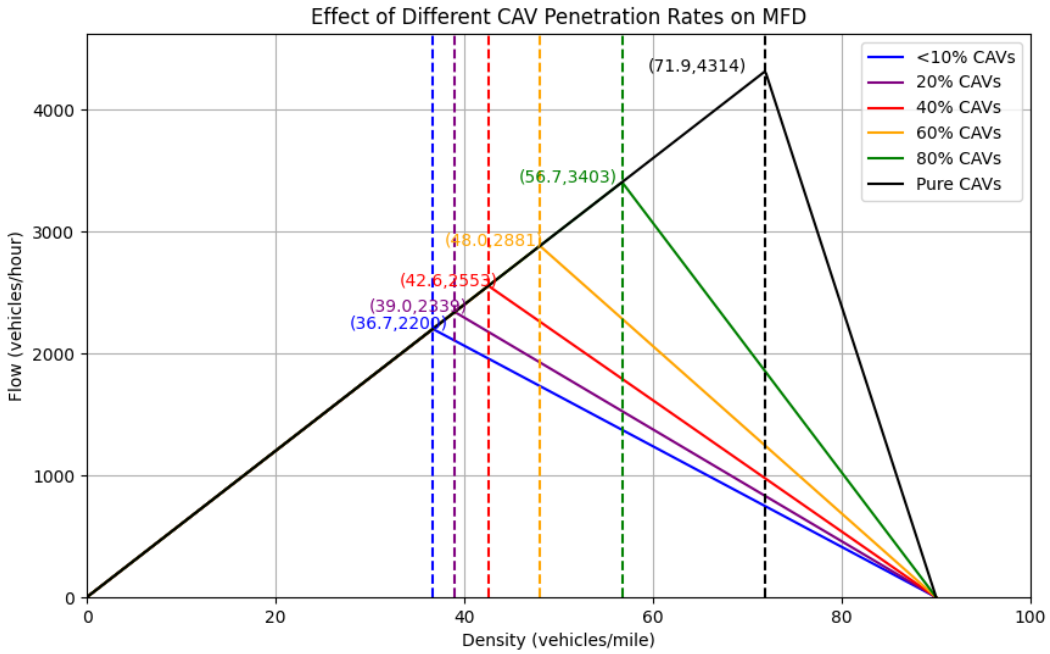


**Figure 5.11. MFD under varying CAV penetration rates.**

**TABLE 5.6 MFD-based capacity and density summary by CAV penetration level.**

| CAV Penetration Rates | Density (vehicles/mile) | Capacity (vehicles/hour) | Improvement |
|---|---|---|---|
| <10% CAVs | 36.7 | 2200 | 10% |
| 20% CAVs | 39.1 | 2345 | 17.3% |
| 40% CAVs | 43.2 | 2582 | 29.1% |
| 60% CAVs | 49.4 | 2965 | 48.3% |
| 80% CAVs | 60.3 | 3618 | 80.9% |
| Pure CAVs | 81.5 | 4889 | 144.5% |

In the graph, each curve corresponds to a distinct CAV penetration level: the blue curve represents less than 10% penetration, followed by purple (20%), red (40%), yellow (60%), green (80%), and black indicating 100% (pure CAV) traffic. It is evident that as the proportion of CAVs

increases, the roadway capacity—measured by the maximum achievable flow—also increases. This improvement stems from the ability of CAVs to maintain shorter following distances compared to HVs.

In the scenario of full CAV adoption, the roadway capacity reaches approximately 5,000 vehicles per hour, representing a 2.5-fold increase relative to the capacity under human-driven conditions (~2,000 vehicles per hour, Shi et al., 2021). This result highlights the potential of CAV technology to significantly enhance traffic throughput and mitigate congestion using existing infrastructure.

## 5.3 Chapter Summary

This study proposed an ArTM based on MFD theory and integrated it with a rolling-horizon VSA optimization framework for large-scale urban network control. The main contribution lies in providing a computationally tractable and scalable method for network-level congestion management that jointly addresses traffic efficiency and energy performance. By formulating speed guidance at the area level, the proposed framework extends macroscopic traffic control toward practical large-network applications.

The case studies in Madison and Boston demonstrate the effectiveness of the proposed approach across networks of substantially different scales and demand conditions. In Madison, optimal VSA reduced energy consumption by 11.7%, travel delay by 23.7%, and TC by 21.1%, while increasing network speed by 13.8%, lowering the maximum network density by 15.0%, and shortening traffic clear time from more than 150 minutes to 124 minutes. In Boston, the benefits were even more pronounced at the system level: average network speed increased by 40.8%, average network density decreased by 43.3%, average delay per inserted vehicle decreased by 89.8%, and average energy per VMT decreased by 17.0%. The estimated number of finished

vehicles increased by 6.4%, and the network clearance ratio improved from 0.91 to 0.97. At the aggregate level, total travel delay decreased by 89.8% and TC decreased by 50.2%. Although total energy consumption increased in the Boston case, this result reflects the substantial increase in completed travel and total VMT under control; importantly, the energy intensity per VMT still decreased, indicating improved operating efficiency.

The additional analyses further support the robustness and practical relevance of the framework. Sensitivity analysis showed that control performance depends on the update interval and parameter settings, indicating a tradeoff between responsiveness and implementation practicality. While shorter update intervals generally improved performance, the 600s setting provided a balanced choice for the main experiments. The CAV penetration analysis further showed that the potential network benefits increase substantially as fleet automation rises, with estimated capacity improvement ranging from 10% at very low CAV penetration to 144.5% under a pure CAV scenario. This suggests that the proposed framework is well-suited not only for current mixed-traffic conditions but also for future traffic systems with higher levels of automation.

Overall, the results demonstrate that the proposed ArTM-VSA framework is an effective and scalable strategy for large-scale urban traffic management. It improves mobility, reduces congestion-related delay, and enhances energy efficiency, while remaining adaptable to varying network conditions and future fleet compositions. Future research can extend this framework by incorporating stochastic demand variation, more detailed behavioral responses, and real-time field implementation considerations, as well as by exploring its integration with CAV control in mixed-traffic environments.

# 6 CONCLUSION

## 6.1 Summary of Chapters

Chapter 1 introduces the background of AV deployment across different scales, identifying the research objectives, scope of work, and key contributions of this dissertation.

Chapter 2 reviews the existing literature on AV technical readiness, network-level impacts of AVs, and urban mobility applications enabled by AVs. It discusses the strengths and limitations of previous studies and highlights the research gaps that motivate this dissertation.

Chapter 3 presents an empirical evaluation of AV driving features in 6 production vehicles under real-world driving conditions. Six categories of AV driving features are tested, including ACC, Collision Avoidance Assist, Lane Markings Detection, Static Message Sign Detection, Traffic Light Awareness, and FSD. The results reveal that production AV driving features are not uniformly reliable, and that their performance depends strongly on sensing technology and driving environment. Camera-only features are sensitive to low visibility, unclear markings, fading, and obstruction, while radar-based features, such as blind-spot and rear cross-traffic detection, remain stable across lighting conditions. Up-to-date digital maps can compensate for perception limitations in degraded conditions, as observed in Tesla's map fusion, while commercial V2I traffic-light functions still show timing errors and remain immature. Based on these findings, recommendations are provided for vehicle manufacturers and infrastructure stakeholders to improve AV driving feature reliability on both the vehicle side and the infrastructure side.

Chapter 4 extends the vehicle-level evaluation to the network level by examining how network features shape AV impacts. A cross-network simulation analysis is conducted on 12 urban networks in SUMO under pure AV and pure HV regimes, using movement-specific AV/HV parameterization for ca-following in road vehicle-signal interactions at the intersection. Five

network features, demand intensity, road length, road density, street connectivity, and signalized intersection percentage, are evaluated against operational, environmental, and surrogate safety performance measures through correlation and trend analyses. The results show that AV impacts vary with network features rather than appearing uniformly across networks. AV fuel benefits are more likely to be realized in high-demand, high-density, and highly signalized urban networks, while AV-HV surrogate safety profiles are more favorable in longer, more continuous networks. At the same time, TTC and PET indicators require closer monitoring in high-demand, high-density, and highly signalized networks, with TTC gaps appearing mainly on road segments under demand intensity and PET gaps appearing mainly at signalized intersections. These findings highlight the need for a network-aware perspective in AV deployment and assessment, so that AV evaluation reflects target network features rather than average performance alone.

Chapter 5 develops a macroscopic control framework that uses AVs as mobile traffic control agents to actively improve network-level performance. An ArTM is proposed as a macroscopic extension of the CTM, capturing aggregate urban traffic dynamics through the MFD and enabling large-scale traffic control for congested urban networks. Based on this formulation, a rolling-horizon optimal control strategy is developed in which AVs deliver area-level VSAs as real-time mobile controllers to regulate traffic states and mitigate congestion. The framework is validated through traffic simulation on two real-world urban networks in Madison and Boston, with sensitivity analyses across control update intervals, control weights, and AV penetration rates. The results demonstrate that the proposed framework improves network mobility and reduces energy consumption, and that performance changes in a clear pattern with these settings, supporting the use of AV-enabled macroscopic control strategies for large-scale urban traffic management.

## 6.2 Future Research Directions

Future research can extend this work in several directions.

The empirical evaluation in Chapter 3 identified key environmental and operational factors that affect AV driving feature performance, but the assessment was largely qualitative. Future research can build on these findings by conducting more detailed, quantitative evaluations. For example, testing the retroreflectivity of lane markings and static message signs may help determine infrastructure requirements for reliable AV driving feature operation. Measuring system performance across varying ambient light levels, camera glare conditions, and adverse weather such as rain, snow, and fog could further reveal the sensitivity of different sensing modalities. Investigation of glare effects from headlights, sunlight reflections, and other visual interferences would also contribute to the continued refinement of connected and automated driving technologies.

The cross-network analysis in Chapter 4 was based on 12 well-documented urban networks, which limits the geographic and functional coverage of the findings. A clear direction for future work is to expand the scope and diversity of study networks. One promising approach is to build more realistic networks directly from OpenStreetMap and to pair them with real demand and routing patterns obtained from telematics data sources such as StreetLight, TomTom, or Compass. This would provide a larger and more diverse set of urban networks with more realistic traffic patterns, which would substantially strengthen the cross-network analysis and improve the generalizability of the findings.

The ArTM-VSA framework developed in Chapter 5 assumes that all vehicles have communication capability and follow the speed advisory. This will not be the case for a long time. At the vehicle level, a real mixed-traffic environment consists of four types of vehicles, including

HVs, AVs, Connected Vehicles (CVs), and CAVs, and only some of them can receive and follow the VSA. HVs and non-connected AVs cannot receive advisories at all, while CVs can receive them but may not always comply. The refined control model should therefore handle both the information gaps and the partial compliance across different vehicle types. At the system level, traffic demand is also uncertain and varies over time, and this stochastic variation should be incorporated into the optimization. Together, these extensions would make the control framework more realistic and more directly applicable to real-world mixed-traffic deployment.

# 7 REFERENCES


Abdel-Aty, M., Dilmore, J., & Dhindsa, A. (2006). Evaluation of variable speed limits for real-time freeway safety improvement. Accident Analysis and Prevention, 38(2), 335–345. https://doi.org/10.1016/j.aap.2005.10.010

Aboudolas, K., & Geroliminis, N. (2013). Perimeter and boundary flow control in multi-reservoir heterogeneous networks. Transportation Research Part B: Methodological, 55, 265–281. https://doi.org/10.1016/j.trb.2013.07.003

Akandwanaho, E., & Nakamura, H. (2020a). Analysis of Travel Speed on 4-Lane Signalized Arterials. Transportation Research Procedia, 48(2018), 890–903. https://doi.org/10.1016/j.trpro.2020.08.106

Akandwanaho, E., & Nakamura, H. (2020b). Analysis of Travel Speed on 4-Lane Signalized Arterials. Transportation Research Procedia, 48, 890–903. https://doi.org/10.1016/j.trpro.2020.08.106

Allen, E., Costello, S. B., & Henning, T. F. (2024). Contribution of Network Redundancy to Reducing Criticality of Road Links. Transportation Research Record, 2678(12), 1574–1590. https://doi.org/10.1177/03611981241252767

Ambühl, L., Menendez, M., & González, M. C. (2023). Understanding congestion propagation by combining percolation theory with the macroscopic fundamental diagram. Communications Physics, 6(1), 26. https://doi.org/10.1038/s42005-023-01144-w

American Planning Association. (2024). Principles for Autonomous Vehicle Policy. https://www.planning.org/policy/principles/av/

Ardekani, S. A., Williams, J. C., & Bhat, Sudarshana. (1992). Influence of Urban Network Features on Quality of Traffic Service. Transportation Research Record, 1358, 6–12. http://onlinepubs.trb.org/Onlinepubs/trr/1992/1358/1358-002.pdf

Audi. (2023). OWNER'S MANUAL.

Audi Newsroom. (2024). Audi expands Traffic Light Information - now includes speed recommendations to minimize stops. https://media.audiusa.com/en-us/releases/301

AVIA. (2025). 2025 State of AV Report. [Online]. Available: Https://Theavindustry.Org/Newsroom/Press- Releases/Avia-Releases-2025-State-of-Av.

Begg, D. (2014). A 2050 Vision for London : What are the implications of driversless transport. Report Commissioned by Clear Channel, 1–65. https://www.transporttimes.co.uk/Admin/uploads/64165-transport-times_a-2050-vision-for-london_aw-web-ready.pdf%0Ahttp://www.transporttimes.co.uk/Admin/uploads/64165-Transport-Times_A-2050-Vision-for-London_AW-WEB-READY.pdf

Bieker, L., Krajzewicz, D., Morra, A., & Michelacci, C. (2014). Traffic simulation for all: a real world traffic scenario from the city of Bologna. Modeling Mobility with Open Data, 47–60.

Binshuang, Z., Jiaying, C., Runmin, Z., & Xiaoming, H. (2019). Skid resistance demands of asphalt pavement during the braking process of autonomous vehicles. MATEC Web of Conferences, 275(201 9), 04002. https://doi.org/10.1051/matecconf/201927504002

Boggs, A. M., Arvin, R., & Khattak, A. J. (2020). Exploring the who , what , when , where , and why of automated vehicle disengagements. Accident Analysis and Prevention, 136(July 2019), 105406. https://doi.org/10.1016/j.aap.2019.105406

Boston Region MPO. (2026). Boston Region Metropolitan Planning Organization. https://www.ctps.org/mpo

Bottero, M., Dalla Chiara, B., Deflorio, F., Franco, G., & Spessa, E. (2014). Model-based approach for estimating energy used by traffic flows on motorways with ITS. IET Intelligent Transport Systems, 8(7), 598–607. https://doi.org/10.1049/iet-its.2013.0132

Bronco, F. (2022). Owner's Manual.

Chen, C., Guo, J., Guo, C., Chen, C., Zhang, Y., & Wang, J. (2021). Adaptive cruise control for cut-in scenarios based on model predictive control algorithm. Applied Sciences (Switzerland), 11(11). https://doi.org/10.3390/app11115293

Choi, D., & Ewing, R. (2021). Effect of street network design on traffic congestion and traffic safety. Journal of Transport Geography, 94(April), 103094. https://doi.org/10.1016/j.jtrangeo.2021.103200

Chu, K. F., Lam, A. Y. S., & Li, V. O. K. (2020). Dynamic Lane Reversal Routing and Scheduling for Connected and Autonomous Vehicles: Formulation and Distributed Algorithm. IEEE Transactions on Intelligent Transportation Systems, 21(6), 2557–2570. https://doi.org/10.1109/TITS.2019.2920674

Codecá, L., Frank, R., & Engel, T. (2015). Luxembourg sumo traffic (lust) scenario: 24 hours of mobility for vehicular networking research. Proceedings of the 7th IEEE Vehicular Networking Conference (VNC15), 2157–9865. https://doi.org/10.1109/VNC.2015.7385539

Codecá, L., & Härri, J. (2017). Towards Multimodal Mobility Simulation of C-ITS : The Monaco SUMO Traffic Scenario. IEEE Vehicular Networking Conference, 97–100.

Coyner, K., & Bittner, J. (2021). Automated Vehicles and Infrastructure Enablers: Pavement Markings and Signs. In SAE Technical Paper. https://doi.org/10.4271/EPR2022011

Daganzo, C. F. (2005). Improving City Mobility through Gridlock Control: an Approach and Some Ideas. Working Paper, 1–32. https://www.escholarship.org/uc/item/7w6232wq.pdf;origin=repeccitec

Daganzo, C. F. (2007). Urban gridlock: Macroscopic modeling and mitigation approaches.

Transportation Research Part B: Methodological, 41(1), 49–62. https://doi.org/10.1016/j.trb.2006.03.001

Daganzo, C. F., & Geroliminis, N. (2008). An analytical approximation for the macroscopic fundamental diagram of urban traffic. Transportation Research Part B: Methodological, 42(9), 771–781. https://doi.org/10.1016/j.trb.2008.06.008

David, H., & Plötz, P. (2020). Test track for automated and connected driving in Hamburg ( TAVF-HH ). In Virtual ITS European Congress, November, ITS-TP2213.

De Jong, D., Knoop, V. L., & Hoogendoorn, S. P. (2013). The effect of signal settings on the macroscopic fundamental diagram and its applicability in traffic signal driven perimeter control strategies. IEEE Conference on Intelligent Transportation Systems, Proceedings, ITSC, Itsc, 1010–1015. https://doi.org/10.1109/ITSC.2013.6728364

Desai, V., Degadwala, S., & Vyas, D. (2023). Multi-Categories Vehicle Detection For Urban Traffic Management. Proceedings of the 2023 2nd International Conference on Electronics and Renewable Systems, ICEARS 2023, 1486–1490. https://doi.org/10.1109/ICEARS56392.2023.10085376

Di, X., & Shi, R. (2021). A survey on autonomous vehicle control in the era of mixed-autonomy: From physics-based to AI-guided driving policy learning. Transportation Research Part C: Emerging Technologies, 125(March), 103008. https://doi.org/10.1016/j.trc.2021.103008

Ding, H., Wang, S., Cao, Y., Fu, X., Fu, H., Yuan, Q., Chen, T., Wang, S. C., Cao, Y., & Connect, J. I. (2025). What patterns contribute to autonomous vehicle crashes? A study of Level 2 and 4 automation via association rule analysis. Journal of Intelligent and Connected Vehicles, 8(3), 9210065. https://doi.org/10.26599/JICV.2025.9210065

Dongchedi. (2025). 216 crashes, 36 cars closed-highway ADAS test [Video]. YouTube. https://www.youtube.com/watch?v=0xumyEf-WRI

Duarte, F., & Ratti, C. (2018). The Impact of Autonomous Vehicles on Cities: A Review. Journal of Urban Technology, 25(4), 3–18. https://doi.org/10.1080/10630732.2018.1493883

Essamlali, I., Nhaila, H., & Khaili, M. El. (2025). Transportation Research Interdisciplinary Perspectives Impact of urban block shape on traffic and air quality : A SUMO-based comparative study of rectangular , radial , and triangular forms. Transportation Research Interdisciplinary Perspectives, 31(March 2024), 101413. https://doi.org/10.1016/j.trip.2025.101413

Farah, H., Erkens, S. M. J. G., Alkim, T., & van Arem, B. (2018). Infrastructure for Automated and Connected Driving: State of the Art and Future Research Directions. 187–197. https://doi.org/10.1007/978-3-319-60934-8_16

Fayyaz, M., González-González, E., & Nogués, S. (2022). Autonomous Mobility: A Potential Opportunity to Reclaim Public Spaces for People. Sustainability (Switzerland), 14(3). https://doi.org/10.3390/su14031568

Federal Highway Administration. (2021). FHWA-HRT-21-015: Impacts of Automated Vehicles on Highway Infrastructure (Issue March). https://rosap.ntl.bts.gov/view/dot/55710

Federal Highway Administration (FHWA). (2023). Manual on Uniform Traffic Control Devices (11th ed., p. 1161). U.S. Department of Transportation. https://mutcd.fhwa.dot.gov/pdfs/11th_Edition/mutcd11thedition.pdf

Fei, Y., Shi, P., Liu, Y., & Wang, L. (2024). Critical roles of control engineering in the development of intelligent and connected vehicles. Journal of Intelligent and Connected Vehicles, 7(2), 79–85.

Geroliminis, N., & Daganzo, C. F. (2008). Existence of urban-scale macroscopic fundamental diagrams: Some experimental findings. Transportation Research Part B: Methodological, 42(9), 759–770. https://doi.org/10.1016/j.trb.2008.02.002

Geroliminis, N., Haddad, J., & Ramezani, M. (2013). Optimal perimeter control for two urban regions with macroscopic fundamental diagrams: A model predictive approach. IEEE Transactions on Intelligent Transportation Systems, 14(1), 348–359. https://doi.org/10.1109/TITS.2012.2216877

Gettman, D., Pu, L., & Sayed, Tarek, Shelby, S. G. (2008). Surrogate Safety Assessment Model and Validation (No. FHWA-HRT-08-051). In Turner-Fairbank Highway Research Center (Issue June).

Glancy, D. J., Peterson, R. W., & Graham, K. F. (2016). A Look at the Legal Environment for Driverless Vehicles. Transportation Research Board. https://doi.org/10.17226/23453

González-Aliste, P., Derpich, I., & López, M. (2023). Reducing Urban Traffic Congestion via Charging Price. Sustainability (Switzerland), 15(3). https://doi.org/10.3390/su15032086

Gouda, M., & El-Basyouny, K. (2022). Safety Assessment of Lane Marking for Autonomous Vehicles Using Light Detection and Ranging (Lidar) Data. SSRN Electronic Journal, 1–47. https://doi.org/10.2139/ssrn.4107155

Grand View Research. (2024). Autonomous Vehicle Market Size, Share & Trends Analysis Report, 2025–2030. [Online]. Available: Https://Www.Grandviewresearch.Com/Industry-Analysis/Autonomous-Vehicles-Market.

Guériau, M., & Dusparic, I. (2020). Quantifying the impact of connected and autonomous vehicles on traffic efficiency and safety in mixed traffic. In 2020 IEEE 23rd International Conference on Intelligent Transportation Systems (ITSC), 1–8. https://doi.org/10.1109/ITSC45102.2020.9294174

Haddad, J., Mirkin, B., & Assor, K. (2021). Traffic flow modeling and feedback control for future Low-Altitude Air city Transport: An MFD-based approach. Transportation Research Part C: Emerging Technologies, 133(December 2020), 103380. https://doi.org/10.1016/j.trc.2021.103380

Hajiahmadi, M., Haddad, J., De Schutter, B., & Geroliminis, N. (2013). Optimal hybrid macroscopic traffic control for urban regions: Perimeter and switching signal plans controllers. 2013 European Control Conference, ECC 2013, 3500–3505. https://doi.org/10.23919/ecc.2013.6669572

Hallmark, S., Veneziano, D., & Litteral, T. (2019). Preparing local agencies for the future of connected and autonomous vehicles (No. MN/RC 2019-18). Minnesota Department of Transportation Research Services and Library, September.

Haris, M., & Hou, J. (2020). Obstacle detection and safely navigate the autonomous vehicle from unexpected obstacles on the driving lane. Sensors (Switzerland), 20(17), 1–22. https://doi.org/10.3390/s20174719

Harper, C. D., Hendrickson, C. T., Mangones, S., & Samaras, C. (2016). Estimating potential increases in travel with autonomous vehicles for the non-driving, elderly and people with travel-restrictive medical conditions. Transportation Research Part C: Emerging Technologies, 72, 1–9. https://doi.org/10.1016/j.trc.2016.09.003

Harth, M., Langer, M., & Bogenberger, K. (2021). Automated Calibration of Traffic Demand and Traffic Lights in SUMO Using Real-World Observations. SUMO Conference Proceedings, 133–148. https://doi.org/10.52825/scp.v2i.120

HCM. (2022). The Highway Capacity Manual 7th Edition. In National Academies of Sciences, Engineering, and Medicine. http://trid.trb.org/view.aspx?id=475202

He, Y., Liu, Y., Yang, L., & Qu, X. (2024). Deep Adaptive Control: Deep Reinforcement Learning-Based Adaptive Vehicle Trajectory Control Algorithms for Different Risk Levels. IEEE Transactions on Intelligent Vehicles, 9(1), 1654–1666. https://doi.org/10.1109/TIV.2023.3303408

He, Y., & Zeng, A. (2024). Expanding bottlenecks reveals hidden bottlenecks and leads to more congested city centers. Physica A: Statistical Mechanics and Its Applications, 640(March), 129707. https://doi.org/10.1016/j.physa.2024.129707

Hegyi, A., De Schutter, B., & Hellendoorn, J. (2003). Optimal Coordination of Variable Speed Limits to Suppress Shock Waves. Transportation Research Record, 6(1852), 167–174. https://doi.org/10.3141/1852-21

Higuchi, T., Zhong, L., & Onishi, R. (2024). NUMo: Nagoya Urban Mobility Scenario for City-Scale V2X Simulations. 2024 IEEE Vehicular Networking Conference (VNC), 17–24. https://doi.org/10.1109/VNC61989.2024.10575975

Honda. (2022). Honda Accord Owner ' s Manual.

Hu, X., Zheng, Z., Chen, D., & Sun, J. (2023). Autonomous Vehicle's Impact on Traffic: Empirical Evidence From Waymo Open Dataset and Implications From Modelling. IEEE Transactions on Intelligent Transportation Systems, 24(6), 6711–6724. https://doi.org/10.1109/TITS.2023.3258145

Hyundai. (2022). Hyundai.pdf. Hyundai SmartSense. https://www.hyundaiusa.com/us/en/safety

Ingole, D., Mariotte, G., & Leclercq, L. (2020). Perimeter gating control and citywide dynamic user equilibrium: A macroscopic modeling framework. Transportation Research Part C: Emerging Technologies, 111(August 2019), 22–49. https://doi.org/10.1016/j.trc.2019.11.016

Jang, H., Kim, I., Park, S. H., & Jang, K. (2023). Analyzing the Impact of Autonomous Vehicles on Urban Traffic Flow at the Large Scale Network Using Real-World Data. IEEE Conference on Intelligent Transportation Systems, Proceedings, ITSC, September, 5530–5535. https://doi.org/10.1109/ITSC57777.2023.10421991

Jia, Y., Wang, S., Peng, J., Gao, Y., Hu, D., & Zhao, X. (2022). Evaluation of Pavement Rutting Based on Driving Safety of Vehicles. International Journal of Pavement Research and Technology, 15(2), 457–469. https://doi.org/10.1007/s42947-021-00032-2

Johnson, C. (2017). Readiness of the road network for connected and autonomous vehicles. RAC Foundation -Royal Automobile Club for Motoring Ltd, April, 1–42. www.racfoundation.org

Khatab, E., Onsy, A., Varley, M., & Abouelfarag, A. (2021). Vulnerable objects detection for autonomous driving: A review. Integration, 78(March 2020), 36–48. https://doi.org/10.1016/j.vlsi.2021.01.002

Khondaker, B., & Kattan, L. (2015). Variable speed limit: An overview. Transportation Letters, 7(5), 264–278. https://doi.org/10.1179/1942787514Y.0000000053

Khoury, J., Amine, K., & Saad, R. A. (2019). An Initial Investigation of the Effects of a Fully Automated Vehicle Fleet on Geometric Design. Journal of Advanced Transportation, 2019. https://doi.org/10.1155/2019/6126408

Kmiotek, P., & Ruichek, Y. (2008). Multisensor fusion based tracking of coalescing objects in urban environment for an autonomous vehicle navigation. IEEE International Conference on Multisensor Fusion and Integration for Intelligent Systems, 52–57. https://doi.org/10.1109/MFI.2008.4648107

Knoop, V. L. (2017). Introduction to Traffic Flow Theory: An introduction with exercises.

Kouvelas, A., Saeedmanesh, M., & Geroliminis, N. (2017). Enhancing model-based feedback perimeter control with data-driven online adaptive optimization. Transportation Research Part B: Methodological, 96, 26–45. https://doi.org/10.1016/j.trb.2016.10.011

Kuang, S., Liu, Y., Wang, X., Wu, X., & Wei, Y. (2024). Harnessing multimodal large language models for traffic knowledge graph generation and decision-making. Communications in Transportation Research, 4, 100146. https://doi.org/10.1016/j.commtr.2024.100146

Kuhne, B. Y. R., & Michalopoulos, P. (2017). CONTINUUM FLOW MODELS. In Revised Monograph on Traffic Flow Theory.

Lakshminarasimhan, V., & Knoll, A. (2020). C-V2X Resource Deployment Architecture Based

on Moving Network Convoys. 2020 IEEE 91st Vehicular Technology Conference (VTC2020-Spring), 2020-May, 1–6. https://doi.org/10.1109/VTC2020-Spring48590.2020.9128410

Le, S., Zolfaghari, A., & Polak, J. (2015). Autonomous cars : The tension between occupant experience and intersection capacity. TRANSPORTATION RESEARCH PART C, 52, 1–14. https://doi.org/10.1016/j.trc.2015.01.002

Lei, T., Hou, Z., & Ren, Y. (2020). Data-Driven Model Free Adaptive Perimeter Control for Multi-Region Urban Traffic Networks with Route Choice. IEEE Transactions on Intelligent Transportation Systems, 21(7), 2894–2905. https://doi.org/10.1109/TITS.2019.2921381

Levin, M. W., Fritz, H., & Boyles, S. D. (2017). On Optimizing Reservation-Based Intersection Controls. IEEE Transactions on Intelligent Transportation Systems, 18(3), 505–515. https://doi.org/10.1109/TITS.2016.2574948

Li, Q., Zhang, P., Yao, H., Chen, Z., & Li, X. (2024). Online learning-based model predictive trajectory control for connected and autonomous vehicles : Modeling and physical tests. Journal of Intelligent and Connected Vehicles, 7(2), 86–96.

Li, Z., Bao, Z., Meng, H., Shi, H., Li, Q., & Yao, H. (2025). Interaction dataset of autonomous vehicles with traffic lights and signs. Communications in Transportation Research, 5(August), 100201. https://doi.org/10.1016/j.commtr.2025.100201

Li, Z., Li, Y., Li, Q., Yao, H., Li, X., Hourdos, J., & McHale, G. (2026). Behavioral Analysis and Impact Assessment of Automated Driving Systems' Interaction with Traffic Lights. Transportation Research Part D: Transport and Environment, under Review.

Li, Z., Zhang, P., Liang, S., Zhou, H., Ma, C., & Yao, H. (2025). Benchmarking Tesla' s Traffic Light and Stop Sign Control: Field Dataset and Behavior Insights.

Lin, Y., Tiwari, A., Fabien, B., Ban, X., & Devasia, S. (2023). Increasing traffic capacity of mixed traffic at signalized traffic intersections using delayed self reinforcement. Transportation Research Part C, 157(April), 104403. https://doi.org/10.1016/j.trc.2023.104403

Liu, Y., Tight, M., Sun, Q., & Kang, R. (2019). A systematic review: Road infrastructure requirement for Connected and Autonomous Vehicles (CAVs). Journal of Physics: Conference Series, 1187(4). https://doi.org/10.1088/1742-6596/1187/4/042073

Lobo, S., Neumeier, S., Fernandez, E. M. G., & Facchi, C. (2020). InTAS - The Ingolstadt Traffic Scenario for SUMO. SUMO User Conference Proceedings, 2750–4425, 1–20. https://doi.org/10.52825/scp.v1i

Loder, A., Ambühl, L., Menendez, M., & Axhausen, K. W. (2019). Understanding traffic capacity of urban networks. Scientific Reports, 9(1), 16283. https://doi.org/10.1038/s41598-019-51539-5

Lu, J., Li, B., Li, H., & Al-Barakani, A. (2021). Expansion of city scale, traffic modes, traffic

congestion, and air pollution. Cities, 108(February 2019). https://doi.org/10.1016/j.cities.2020.102974

Lu, Q., Tettamanti, T., Hörcher, D., Varga, I., & Lu, Q. (2020). The impact of autonomous vehicles on urban traffic network capacity : an experimental analysis by microscopic traffic simulation experimental analysis by microscopic tra ffi c simulation. Transportation Letters, 12(8), 540–549. https://doi.org/10.1080/19427867.2019.1662561

Ma, K., & Wang, H. (2019). Influence of Exclusive Lanes for Connected and Autonomous Vehicles on Freeway Traffic Flow. IEEE Access, 7, 50168–50178. https://doi.org/10.1109/ACCESS.2019.2910833

Mahdinia, I., Mohammadnazar, A., Arvin, R., & Khattak, A. J. (2021). Integration of automated vehicles in mixed traffic: Evaluating changes in performance of following human-driven vehicles. Accident Analysis and Prevention, 152(February), 106006. https://doi.org/10.1016/j.aap.2021.106006

Malinverno, M., Avino, G., Casetti, C., Chiasserini, C. F., Malandrino, F., & Scarpina, S. (2018). Performance Analysis of C-V2I-Based Automotive Collision Avoidance. 19th IEEE International Symposium on a World of Wireless, Mobile and Multimedia Networks, WoWMoM 2018, 1–9. https://doi.org/10.1109/WoWMoM.2018.8449772

Manivasakan, H., Kalra, R., O'Hern, S., Fang, Y., Xi, Y., & Zheng, N. (2021). Infrastructure requirement for autonomous vehicle integration for future urban and suburban roads – Current practice and a case study of Melbourne, Australia. Transportation Research Part A: Policy and Practice, 152(September 2020), 36–53. https://doi.org/10.1016/j.tra.2021.07.012

Marshall, W., & Garrick, N. W. (2011). Does street network design affect traffic safety ? Accident Analysis and Prevention, 43(3), 769–781. https://doi.org/10.1016/j.aap.2010.10.024

Martinez-Diaz, M., Al-Haddad, C., Soriguera, F., & Antoniou, C. (2021). Platooning of connected automated vehicles on freeways: A bird's eye view. Transportation Research Procedia, 58(2019), 479–486. https://doi.org/10.1016/j.trpro.2021.11.064

McDonald, S. S., & Rodier, C. (2015). Envisioning Automated Vehicles within the Built Environment: 2020, 2035, and 2050. In Lecture Notes in Mobility (pp. 225–233). https://doi.org/10.1007/978-3-319-19078-5_20

Miller, S. A., & Heard, B. R. (2016). The Environmental Impact of Autonomous Vehicles Depends on Adoption Patterns. Environmental Science and Technology, 50(12), 6119–6121. https://doi.org/10.1021/acs.est.6b02490

Mirbakhsh, A., Lee, J., & Besenski, D. (2023). Development of a Signal-Free Intersection Control System for CAVs and Corridor Level Impact Assessment. Future Transportation, 3(2), 552–567. https://doi.org/10.3390/futuretransp3020032

Morando, M. M., Tian, Q., Truong, L. T., & Vu, H. L. (2018). Studying the Safety Impact of Autonomous Vehicles Using Simulation-Based Surrogate Safety Measures. Journal of

Advanced Transportation, 1, 11. https://doi.org/10.1155/2018/6135183

Neumeister, D., & Pape, D. (2019). Automated Vehicles and Adverse Weather. Federal Highway Administration, June, 82.

NHTSA. (2025). NHTSA Automated Vehicle Framework. [Online]. Available: Https://Www.Transportation.Gov/Briefing-Room/Trumps-Transportation-Secretary-Sean-p-Duffy- Unveils-New-Automated-Vehicle-Framework.

Nitsche, P., Mocanu, I., & Reinthaler, M. (2014). Requirements on tomorrow's road infrastructure for highly automated driving. 2014 International Conference on Connected Vehicles and Expo, ICCVE 2014 - Proceedings, 939–940. https://doi.org/10.1109/ICCVE.2014.7297694

Ostendorf, N., Garlichs, K., & C. Wolf, L. (2025). HaTS - Hanover Traffic Scenario for SUMO. SUMO Conference Proceedings. https://doi.org/10.52825/scp.v6i.2605

Othman, K. (2021). Impact of autonomous vehicles on the physical infrastructure: Changes and challenges. Designs, 5(3). https://doi.org/10.3390/designs5030040

Pandian, S., Gokhale, S., & Kumar, A. (2009). Evaluating effects of traffic and vehicle characteristics on vehicular emissions near traffic intersections. Transportation Research Part D, 14(3), 180–196. https://doi.org/10.1016/j.trd.2008.12.001

Papadoulis, A., Quddus, M., & Imprialou, M. (2019). Evaluating the safety impact of connected and autonomous vehicles on motorways. Accident Analysis and Prevention, 124(September 2018), 12–22. https://doi.org/10.1016/j.aap.2018.12.019

Pillai, P. S., Kinnal, B., Pattanashetty, V., & Iyer, N. C. (2023). Traffic Sign Detection and Recognition. Lecture Notes in Networks and Systems, 400, 175–184. https://doi.org/10.1007/978-981-19-0095-2_18

Qian, G., Guo, M., Zhang, L., Wang, Y., Hu, S., & Wang, D. (2021). Traffic scheduling and control in fully connected and automated networks. Transportation Research Part C: Emerging Technologies, 126(February), 103011. https://doi.org/10.1016/j.trc.2021.103011

Rahman, M. M., & Thill, J. C. (2023). Impacts of connected and autonomous vehicles on urban transportation and environment: A comprehensive review. Sustainable Cities and Society, 96(May), 104649. https://doi.org/10.1016/j.scs.2023.104649

Rakha, H. A., Chen, H., Almannaa, M. H., Kamalanathsharma, R. K., El-Shawarby, I., Loulizi, A., Institute, V. T. T., Center, C. V. U. T., & Administration, R. and I. T. (2016). Field Testing of Eco-Speed Control Using V2I Communication. 45p. http://cvi-utc.org/wp-content/uploads/2015/10/Rakha_Field-Testing-of-Eco-Speed-Control-Using-V2I-Communication_Final.pdf%0Ahttps://trid.trb.org/view/1418192

Ramezani, M., & Ye, E. (2019). Lane density optimisation of automated vehicles for highway congestion control. Transportmetrica B, 7(1), 1096–1116. https://doi.org/10.1080/21680566.2019.1568925

Ravindran, R., Santora, M. J., & Jamali, M. M. (2022). Camera, LiDAR, and Radar Sensor Fusion Based on Bayesian Neural Network (CLR-BNN). IEEE Sensors Journal, 22(7), 6964–6974. https://doi.org/10.1109/JSEN.2022.3154980

Ren, T., Xie, Y., & Jiang, L. (2020). Cooperative Highway Work Zone Merge Control Based on Reinforcement Learning in a Connected and Automated Environment. Transportation Research Record, 2674(10), 363–374. https://doi.org/10.1177/0361198120935873

Ren, Y., Hou, Z., Sirmatel, I. I., & Geroliminis, N. (2020). Data driven model free adaptive iterative learning perimeter control for large-scale urban road networks. Transportation Research Part C: Emerging Technologies, 115(March), 102618. https://doi.org/10.1016/j.trc.2020.102618

Rosca, M. A., Burciu, S., Oprea, F. C., Dragu, V., Dinu, O. M., & Costea, I. (2025). Evaluating the Impact of Automated Vehicle Penetration on Intersection Traffic Flow : A Microsimulation-Based Approach. Systems, 13(9), 751.

Sadid, H., & Antoniou, C. (2024). A simulation-based impact assessment of autonomous vehicles in urban networks. IET Intelligent Transport Systems, 18(9), 1677–1696. https://doi.org/10.1049/itr2.12537

Saeed, T. U., Alabi, B. N. T., & Labi, S. (2021). Preparing Road Infrastructure to Accommodate Connected and Automated Vehicles: System-Level Perspective. Journal of Infrastructure Systems, 27(1), 2–4. https://doi.org/10.1061/(asce)is.1943-555x.0000593

Sanusi, F., Choi, J., & Moses, R. (2022). A Multiyear Infrastructure Planning Framework for Connected and Automated Vehicles. In Lecture Notes in Civil Engineering (Vol. 250). Springer Nature Singapore. https://doi.org/10.1007/978-981-19-1065-4_54

Seuwou, P., Banissi, E., & Ubakanma, G. (2020). The Future of Mobility with Connected and Autonomous Vehicles in Smart Cities. Internet of Things, 37–52. https://doi.org/10.1007/978-3-030-18732-3_3

Shi, X., & Li, X. (2021a). Constructing a fundamental diagram for traffic flow with automated vehicles: Methodology and demonstration. Transportation Research Part B: Methodological, 150, 279–292. https://doi.org/10.1016/j.trb.2021.06.011

Shi, X., & Li, X. (2021b). Empirical study on car-following characteristics of commercial automated vehicles with different headway settings. Transportation Research Part C: Emerging Technologies, 128(April), 103134. https://doi.org/10.1016/j.trc.2021.103134

Shi, X., Zhao, D., Yao, H., Li, X., Hale, D. K., & Ghiasi, A. (2021). Video-based trajectory extraction with deep learning for High-Granularity Highway Simulation (HIGH-SIM). Communications in Transportation Research, 1(November), 100014. https://doi.org/10.1016/j.commtr.2021.100014

Sirmatel, I. I., & Yildirimoglu, M. (2023). Nonlinear model predictive control of large-scale urban road networks via average speed control. Transportation Research Part C: Emerging

Technologies, 156(August), 104338. https://doi.org/10.1016/j.trc.2023.104338

Stogios, C., Kasraian, D., Roorda, M. J., & Hatzopoulou, M. (2019). Simulating impacts of automated driving behavior and tra ffi c conditions on vehicle emissions. Transportation Research Part D, 76(October), 176–192. https://doi.org/10.1016/j.trd.2019.09.020

Sun, X., Yu, F. R., & Zhang, P. (2022). A Survey on Cyber-Security of Connected and Autonomous Vehicles (CAVs). IEEE Transactions on Intelligent Transportation Systems, 23(7), 6240–6259. https://doi.org/10.1109/TITS.2021.3085297

Tafidis, P., Farah, H., Brijs, T., & Pirdavani, A. (2021). "Everything somewhere" or "something everywhere": Examining the implications of automated vehicles' deployment strategies. Sustainability (Switzerland), 13(17). https://doi.org/10.3390/su13179750

Taillanter, E., Schadschneider, A., & Barthelemy, M. (2024). Structure of road networks and the shape of the macroscopic fundamental diagram. Physical Review E, 109(014314), 1–9. https://doi.org/10.1103/PhysRevE.109.014314

Talebpour, A., & Mahmassani, H. S. (2016). Influence of connected and autonomous vehicles on traffic flow stability and throughput. Transportation Research Part C, 71, 143–163. https://doi.org/10.1016/j.trc.2016.07.007

Tang, X., Yang, M., Wen, T., Jia, P., Cui, L., & Luo, M. (2025). PriorFusion : Unified integration of priors for robust road perception in autonomous driving. Communications in Transportation Research, 5(June), 100229. https://doi.org/10.1016/j.commtr.2025.100229

Tengilimoglu, O., Carsten, O., & Wadud, Z. (2023). Infrastructure requirements for the safe operation of automated vehicles: Opinions from experts and stakeholders. Transport Policy, 133, 209–222. https://doi.org/10.1016/j.tranpol.2023.02.001

Tesla. (2024). Model Y Owner's Manual. https://www.tesla.com/ownersmanual/modely/en_us/

Toyota. (2022). toyota.pdf. Toyota Safety Sense. https://www.toyota.com/safety-sense/

Trubia, S., Giuffrè, T., Canale, A., & Severino, A. (2017). Automated Vehicle: a Review of Road Safety Implications as Driver of Change. Proceedings of the 27th CARSP Conference, 16. https://www.researchgate.net/publication/321110582

U.S. DOT. (2023). Benefit-Cost Analysis Guidance for Discretionary Grant Programs (Issue 63).

UNECE. (2021). UN Regulation No. 157 – Uniform Provisions Concerning the Approval of Vehicles with Regard to Automated Lane Keeping Systems. Addendum 156, World Forum for Harmonization of Vehicle Regulations. [Online]. Available: Https://Unece.Org/Transport/Documents/2021/03/Standards/Un-Regulation-No-157-Automated-Lane-Keeping-Systems-Alks.

Vickrey, W. S. . (1969). Congestion Theory and Transport Investment William S . Vickrey The American Economic Review , Vol . 59 , No . 2 , Papers and Proceedings of the Eighty-first

Annual Meeting of the American Economic Association . ( May , 1969 ), pp . 251-260 . 59(2), 251–260. https://matthewturner.org/ec2410/readings/Vickrey_AER_1969.pdf

Wan, C., Shan, X., Hao, P., & Wu, G. (2024). Multi-objective coordinated control strategy for mixed traffic with partially connected and automated vehicles in urban corridors. Physica A: Statistical Mechanics and Its Applications, 635(December 2023), 129485. https://doi.org/10.1016/j.physa.2023.129485

Wang, J., Zhang, L., Huang, Y., & Zhao, J. (2020). Safety of Autonomous Vehicles. Journal of Advanced Transportation, 2020(1), 8867757. https://doi.org/10.1155/2020/8867757

Wang, M., Hoogendoorn, S. P., Daamen, W., Arem, B. Van, & Happee, R. (2015). Game theoretic approach for predictive lane-changing and car-following control. Transportation Research Part C, 58, 73–92. https://doi.org/10.1016/j.trc.2015.07.009

Wang, P., McKeever, B., & Chan, C. Y. (2022). Automated Vehicles Industry Survey of Transportation Infrastructure Needs. Transportation Research Record, 2676(7), 554–569. https://doi.org/10.1177/03611981221080135

Wang, Q., Zhang, Q., Liang, X., Wang, Y., Zhou, C., & Mikulovich, V. I. (2022). Traffic lights detection and recognition method based on the improved yolov4 algorithm. Sensors, 22(1), 1–20. https://doi.org/10.3390/s22010200

Wang, S., Shang, M., Levin, M. W., & Stern, R. (2023). A general approach to smoothing nonlinear mixed traffic via control of autonomous vehicles. Transportation Research Part C, 146(November 2022), 103967. https://doi.org/10.1016/j.trc.2022.103967

Wang, S., Yu, D., Kwan, M., Zheng, L., & Miao, H. (2020). The impacts of road network density on motor vehicle travel : An empirical study of Chinese cities based on network theory. Transportation Research Part A, 132(April 2019), 144–156. https://doi.org/10.1016/j.tra.2019.11.012

Wang, Y., Cai, P., & Lu, G. (2020). Cooperative autonomous traffic organization method for connected automated vehicles in multi-intersection road networks. Transportation Research Part C: Emerging Technologies, 111(December 2019), 458–476. https://doi.org/10.1016/j.trc.2019.12.018

Wang, Y., Farah, H., Yu, R., Qiu, S., & Arem, B. Van. (2023). Characterizing Behavioral Differences of Autonomous Vehicles and Human-Driven Vehicles at Signalized Intersections Based on Waymo Open Dataset. Transportation Research Record, 2677(11), 324–337. https://doi.org/10.1177/03611981231165783

Wang, Y., Zhang, D., Li, Y., Shuai, L., Tang, Z., Hou, Y., Zhang, D. F., Li, Y. Q., & Connect, J. I. (2025). Safety-critical scenario test for intelligent vehicles via hybrid participation of natural and adversarial agents. Journal of Intelligent and Connected Vehicles, 8(3), 9210066–1. https://doi.org/10.26599/JICV.2025.9210066

Waymo. (2025). Scaling our fleet through U.S. manufacturing. Waymo Blog. [Online]. Available:

Https://Waymo.Com/Blog/2025/05/Scaling-Our-Fleet-through-Us-Manufacturing/.

Wong, W., Wong, S. C., & Liu, H. X. (2021). Network topological effects on the macroscopic fundamental Diagram. Transportmetrica B: Transport Dynamics, 9(1), 376–398. https://doi.org/10.1080/21680566.2020.1865850

Yang, K., Zheng, N., & Menendez, M. (2018). Multi-scale perimeter control approach in a connected-vehicle environment. Transportation Research Part C: Emerging Technologies, 94, 32–49. https://doi.org/10.1016/j.trc.2017.08.014

Yigitcanlar, T., Wilson, M., & Kamruzzaman, M. (2019). Disruptive impacts of automated driving systems on the built environment and land use: An urban planner's perspective. Journal of Open Innovation: Technology, Market, and Complexity, 5(2). https://doi.org/10.3390/joitmc5020024

Yu, C., Feng, Y., Liu, H. X., Ma, W., & Yang, X. (2019). Corridor level cooperative trajectory optimization with connected and automated vehicles. Transportation Research Part C: Emerging Technologies, 105(November 2018), 405–421. https://doi.org/10.1016/j.trc.2019.06.002

Yu, L., & Wang, R. (2022). Researches on Adaptive Cruise Control system: A state of the art review. Proceedings of the Institution of Mechanical Engineers, Part D: Journal of Automobile Engineering, 236(2–3), 211–240. https://doi.org/10.1177/09544070211019254

Zhang, L., Garoni, T. M., & Gier, J. De. (2013). A comparative study of Macroscopic Fundamental Diagrams of arterial road networks governed by adaptive traffic signal systems. Transportation Research Part B, 49, 1–23. https://doi.org/10.1016/j.trb.2012.12.002

Zhang, M., Li, Z., Si, H., Cheng, L., Zhou, X., & Wang, B. (2023). Urban travel time and residential location choice: The impacts of traffic congestion. Sustainable Cities and Society, 99(September), 104975. https://doi.org/10.1016/j.scs.2023.104975

Zhang, T., & Gao, K. (2020). Will Autonomous Vehicles Improve Traffic Efficiency and Safety in Urban Road Bottlenecks? The Penetration Rate Matters. 2020 IEEE 5th International Conference on Intelligent Transportation Engineering, ICITE 2020, 366–370. https://doi.org/10.1109/ICITE50838.2020.9231360

Zhao, Y., Bai, L., Lyu, Y., & Huang, X. (2019). Camera-based blind spot detection with a general purpose lightweight neural network. Electronics (Switzerland), 8(2). https://doi.org/10.3390/electronics8020233

Zhou, W., Weng, J., Li, T., Fan, B., & Bian, Y. (2024). Modeling the road network capacity in a mixed HV and CAV environment. Physica A: Statistical Mechanics and Its Applications, 636(January), 129526. https://doi.org/10.1016/j.physa.2024.129526

Zhu, B., Sun, Y., Zhao, J., Han, J., Zhang, P., & Fan, T. (2023). A Critical Scenario Search Method for Intelligent Vehicle Testing Based on the Social Cognitive Optimization Algorithm. IEEE Transactions on Intelligent Transportation Systems, 24(8), 7974–7986.

https://doi.org/10.1109/TITS.2023.3268324

Zhu, F., & Ukkusuri, S. V. (2015). A linear programming formulation for autonomous intersection control within a dynamic traffic assignment and connected vehicle environment. Transportation Research Part C: Emerging Technologies, 55(2015), 363–378. https://doi.org/10.1016/j.trc.2015.01.006

Zhuang, Y., Liu, P., Yang, H., Zhang, K., Wang, Y., & Pu, Z. (2025). Few-shot learning for novel object detection in autonomous driving. Communications in Transportation Research, 5(July), 100194. https://doi.org/10.1016/j.commtr.2025.100194

Zlatkovic, M., Zlatkovic, S., Sullivan, T., Bjornstad, J., & Seyed Kiavash Fayyaz Shahandashti. (2019). Assessment of effects of street connectivity on traffic performance and sustainability within communities and neighborhoods through traffic simulation. Sustainable Cities and Society, 46(December 2018), 101409. https://doi.org/10.1016/j.scs.2018.12.037